A Detailed Analysis of Radial Turbines

Svensson, Erik

2014

Citation for published version (APA):
Svensson, E. (2014, May 3). A Detailed Analysis of Radial Turbines. Lund University, Lund Institute of Technology.

Total number of authors:
1

A DETAILED ANALYSIS OF

RADIAL TURBINES

Erik Svensson

Master of Science Thesis
Official report

Division of Thermal Power Engineering
Department of Energy Sciences
Lund University
Lund, Sweden 2014

A Detailed Analysis Of Radial Turbines

Thesis for the Degree of Master of Science
Division of Thermal Power Engineering
Department of Energy Sciences
By

Erik Svensson

May 2014
Master Thesis
Department of Energy Sciences
Lund Institute of Technology
Lund University, Sweden

Abstract

The field of radial turbines is wide and radial turbines of today find applications in areas as diverse as small gas turbines; turbochargers for cars, buses, and trucks, railway locomotives, and diesel power generators; cryogenic and process expanders; rocket engine turbopumps; and specialty steam turbines, [12]. The three-dimensional flow inside a radial turbine is complex and ever since the radial turbine was introduced on the market, a desire to model this flow with simple correlations and loss models has existed.

This master thesis consist of two studies. In the first study two radial turbines are modeled on a mean-line basis and the performance of different operating conditions are simulated. The results are compared to test data to evaluate the accuracy of the simulations. In the second and final study an aerodynamic design of a radial turbine is conducted. Initially a preliminary design is considered. This design is evaluated with the same mean-line tool which were used to simulate the two turbines already mentioned and additionally a blade-to-blade tool. The preliminary design is revised, based on the evaluations, to a detailed design. The detailed design is evaluated with the same tools as the preliminary design and changed until it meets the requirements stated.

The results from the simulations show good agreement with the test data and it can, therefore, be concluded that it would be possible to evaluate a new design using the mean-line tool used in this thesis. It is, however, naive to think that a mean-line analysis is able to predict the flow completely and thus the mean-line analysis should be viewed as a tool which is able to speed up the design process. It is difficult to judge the aerodynamic design from the second study because it would require for the turbine to be manufactured and tested. However, the design shows promise according to the one- and two-dimensional analyses preformed.

Acknowledgments

Contents

Nomenclature

α Absolute flow angle

α' Relative flow angle

β Blade angle

Δh_{0s} Isentropic heat drop

δ Boundary layer thickness

δ^* Boundary layer displacement thickness

$\dot{m}$ Mass flow

η Efficiency

γ Ratio of specific heats

κ Curvature

μ Dynamic viscosity

ϕ Flow coefficient

ψ Stage loading

ρ Density

σ Slip factor

θ Boundary layer momentum thickness

ξ Enthalpy loss coefficient

A Area

a Speed of sound

c Absolute velocity

c Chord

c_f Skin friction coefficient

c_m Meridional velocity

c_p Specific heat at constant pressure

c_θ Tangential velocity

c_θ Tangential velocity

D Diameter

D_s Specific diameter

e Surface roughness

H Shape factor

h Static enthalpy

h_0 Total enthalpy

I Rothalpy

i Incidence

K Metal blockage

L Velocity loss coefficient

M Mach number

m Meridional coordinate

N Shaft speed

N_N Number of nozzle blades

N_R Number of rotor blades

N_s Specific speed

o Throat

P Power

p Static pressure

p_0 Total pressure

R Degree of reaction

R Gas constant

r Radius

r Radius

s Pitch

t Thickness

T_0 Total temperature

U Blade speed

u Boundary layer velocity

w Relative velocity

Y Pressure loss coefficient

z Axial coordinate

1. Introduction

The three-dimensional flow of radial turbines is extremely complex. Since the turbine was introduced great effort has been invested into modeling this flow and trying to predict the turbine's performance. Computational fluid dynamics are used extensively throughout the industry, however, more time efficient methods are required. The one-dimensional meanline analysis is one such method.

1.1. Background

Turbines are a group of turbomachines which recover energy from a fluid and in turn transform this energy to work. The work can be of various forms, e.g. electrical or mechanical. Turbines exist in different types, such as steam turbines, gas turbines, water turbines, wind turbines or turbochargers. The type used depends greatly on the application and the state of the fluid, which can be either compressible or incompressible. The work is extracted from a fluid at high pressure and temperature and is allowed to expand to a lower pressure level. The expansion ratios can be relatively small or extremely large.

Most turbines are composed of several stages and each stage comprises two major parts. A stator,[1] and a rotor[2]. The stator is a fixed section of vanes used to guide the fluid and accelerate it. An acceleration is always followed by an expansion and hence some expansion will always occur in the stator. The rotor is also composed of vanes, however, unlike in the stator they are connected to a shaft. In the rotor the fluid is accelerated, now in the rotating plane, and expanded causing the shaft to rotate. From the shaft it is then possible to extract the work, e.g. by connecting the shaft to a generator and thus producing electricity. While it is possible to design a turbine without a stator, it would undoubtedly lead to a lower thermal efficiency.

A further classification of turbines can be done in respect to the amount of expansion occurring in the stator. This concept used is termed reaction and it is defined below. The subscript $1, 2$ and 3 are taken as the inlet, the station between stator and rotor and

---

[1]The stator is often called a nozzle or guide vanes.
[2]When discussing radial turbines the rotor is sometimes referred to as the impeller.

1

the outlet respectively.

$$R = \frac{h_2 - h_3}{h_1 - h_3} \approx \frac{p_2 - p_3}{p_1 - p_3} \qquad (1.1)$$

The degree of reaction, defined in equation (1.1), is taken as the enthalpy drop in the rotor to the enthalpy drop of the whole stage. If the fluid is incompressible and the expansion is taken as reversible, then equation (1.1) can be approximated with the ratio of the pressure drop in the rotor to that of the pressure drop of the whole stage. Most often the criterion of incompressible fluid and irreversible expansion is disregarded and the approximation is used anyway. It is therefore important to state which definition is used. In turbines of impulse type all the expansion takes place in the stator. It can be seen from the definition of reaction that these turbines have zero reaction. In practice it is not possible to design a turbine of impulse type and a compromise is often required to be made which lets the reaction be above zero. Common gas turbine practice for axial turbines is to have a reaction of five percent closest to the shaft [personal communication, Magnus Genrup, 2014].

1.2. Objective

The main objective of this study has been to investigate a mean-line analysis tool for radial turbines. Furthermore, a blade-to-blade analysis tool was used. This has been conducted in two parts.

- Modeling and simulations of two radial turbines.

- Aerodynamic design of a radial turbine.

1.3. Limitations

The work presented in this thesis has the following limitations.

- The presented theory is focused in mean-line analysis.

- "TurbAero" has been used as the main simulation tool.

- The calculation methods in "TurbAero" are one- and two-dimensional.

1.4. Methodology

This work is based mainly on the theory presented by R.H. Aungier, [2], and all the modeling and simulations are performed with his tool "TurbAero"[3]. The theory included in this thesis governs performance analyses on a mean-line basis. Also some examples and guidelines for preliminary design are presented.

The program "RIFT" is used for all performance simulations. Every component of the radial turbine is modeled using geometry from three stations on a mean-line basis. Calculations are performed on every station which yield the flow conditions.

The program "RIFTSIZE" is used in chapter five to develop a preliminary stage design for the aerodynamic design. It uses empirical correlations together with one-dimensional physical equations.

The program "TDB2B" is used to perform blade-to-blade analyses. It is mainly used as an evaluation tool for the detailed design.

1.5. Outline

Chapter one gives a brief introduction to the subject. In chapter two more information about radial turbines in general is given together with an explanation of the different strategies for design which exist.

The work is divided into a theory part and an objective part. Chapter three is focused on the theory and here are the equations and models which are used in the programs explained. This is done because it makes it possible to realize the limitations of the programs and to better understand how the results appear. In the section which concerns the aerodynamic design of a radial turbine, programs will be handled which make use of two-dimensional theory. Because those programs are used to a very small extent, the two-dimensional theory governing them is not investigated in this thesis.

The objective part consists of two chapters. The fourth chapter of this thesis presents the simulations which are performed on two different radial turbines, designed by Volvo Powertrain AB. The simulations aim to predict the off-design performance of the turbines. The fifth chapter presents an aerodynamical design of a radial turbine. Initially a preliminary design is produced using simple correlations. This design is revised to a detailed design which is analyzed using a blade-to-blade tool. Although, it was not meant

---

[3]"TurbAero" includes a number of programs. It is an aerodynamic design and analysis software system for axial-flow and radial-inflow turbines.

as an objective in the beginning, a simple tool for preliminary design was developed at the end. The program is presented in the appendix.

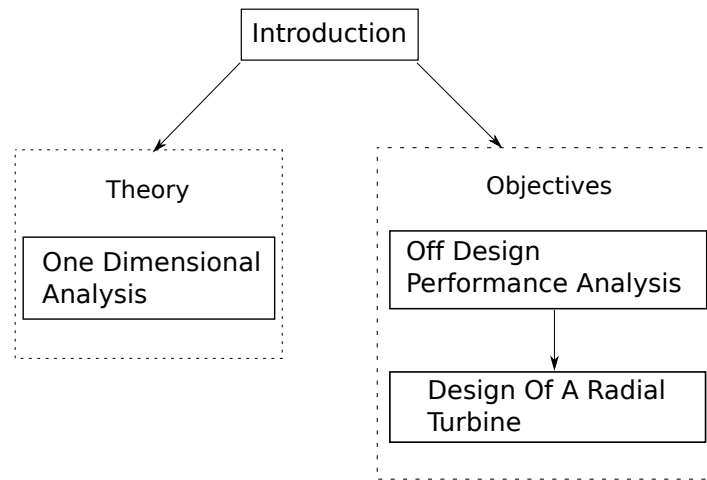**Figure 1.1.: The report presenting the work which has been conducted during this master thesis is divided into four major parts. In the introduction the reader is given some background knowledge on the subject. The theory which this thesis concerns is presented in chapter 3. The real work of the thesis is then presented in chapter four and five which concern off design performance analyses and aerodynamical design respectively.**

2. Radial turbines

While nowadays most radial turbines are run with compressible fluids, the first radial turbines worked with water as the flow medium. "Today the compressible flow radial turbine finds applications in areas as diverse as small gas turbines; turbochargers for cars, buses and trucks, railway locomotives, and diesel power generators; cryogenic and process expanders; rocket engine turbopumps; and specialty steam turbines, [12]". Turbochargers are small turbomachines consisting of a centrifugal compressor and a radial turbine (might be axial) which make use of the exhaust gases in piston engines. This increases the power and sometimes even the efficiency. The fluid in a radial turbine undergoes a dramatic change in direction when it is turned ninety degrees from a radial direction to an axial one. This process can be seen in figure 2.1, which shows a cross section of a radial turbine. The figure shows only one stage, however, a radial turbine can be composed of several stages which can be interconnected via pipes or ducts. Due to the fact that the fluid is turned from a radial direction to an axial direction it is convenient to employ a cylindrical coordinate system. The coordinate system is shown in figure 2.2.
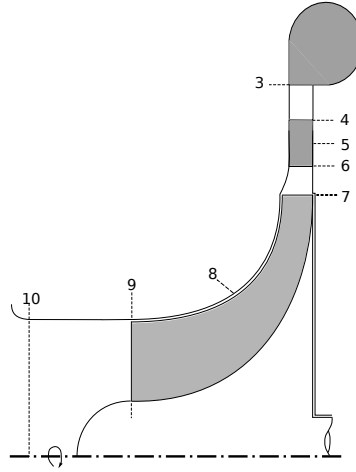

Figure 2.1.: A cross sectional view and the notations which are used in this report are shown in this figure.

The radial turbine stage can be composed of a stator and a rotor or the rotor alone. The stator is often made up of an inlet scroll, generally called a volute, and a nozzled
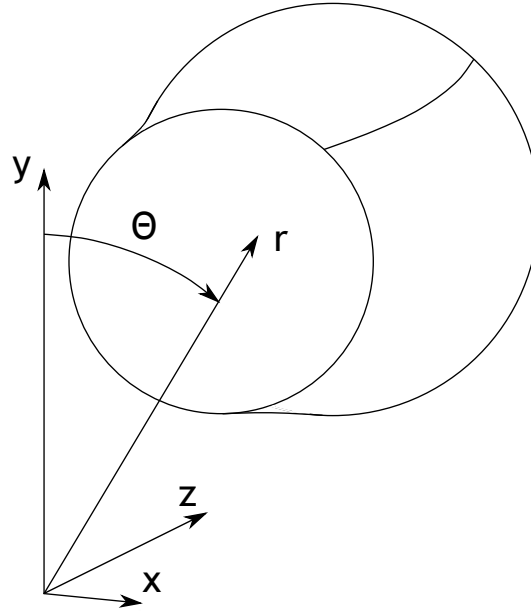
Figure 2.2.: It is convenient to apply a cylindrical coordinate system when describing the geometry of a radial turbine, since the impeller is rotating about an axis.

vane row. It is in the rotor, usually called the impeller, where the fluid is turned while expanding and thereby exerting work on the blades which forces the shaft to rotate. From inlet to outlet there is a dramatic change in radius and that is, together with the turning, what signifies the radial turbine.

The fluid enters the radial turbine through the volute (inlet scroll) in a direction which is perpendicular to the rotor vanes and is distributed equally around the perphery. The purpose of the volute is to turn the flow toward the rotor vanes. Ideally, this is done while maintaining a uniform static pressure and mass flow at the volute exit, otherwise the impeller might be exposed to unsteady radial loading. The volute can be of double entry type, which means that instead of being distributed around a perphery of 360°, two streams contributes 180° each. Ultimately, there will be some fluid which recirculates and mixes with the incoming fluid.

From the volute, the fluid is approaching the stator vanes[1]. The nozzle vanes are distributed around the periphery in an annular ring which encloses the rotor and they are used to continue the turning started in the volute. The shape of the nozzle vanes can differ but generally they can be divided into three common groups based on the blade camber angle. The vanes can be designed with no camber (straight blades), with negative camber (yielding concave blades) and with positive camber (yielding convex blade).

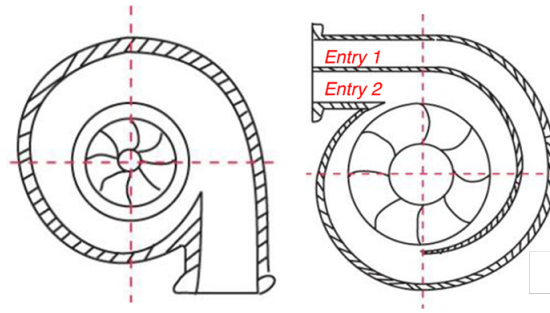[1]The stator vanes are often referred to as nozzle vanes

Figure 2.3.: The volute can be designed with a single entry or multiple entries. This figure shows how, for a single entry type, the fluid is circulated 360° around the periphery and 180° for a double entry type. The figure is adapted from [17].

Maki H. and Mori Y. studied the difference in pressure coefficient for the different types and their conclusion was, a bit unexpectedly, that the smoothest pressure distribution is obtained with concave blades [11]. Leaving the nozzle vanes the flow most likely does not follow the trailing edge, this is term deviation. N.C. Baines describes this phenomenon as a combination of two events. As the fluid leaves the trailing edge, an expansion occurs due to the finite difference which the thickness at the trailing edge forms. This causes the flow to overturn due to a decrease of the radial component of the velocity. On the other hand the vanes do not give perfect guidance which causes the flow to underturn. The vanes do not give perfect guidance because this would require an infinite number of blades (or at least, a high number of blades) which would increase the wet surface and cause friction losses.

The vaneless space between the nozzle vanes' trailing edge and the leading edge of the impeller must be given special attention when designing the radial turbine (this would also apply on a radial turbine lacking nozzle vanes, then the vaneless space would exist between the volue exit and impeller inlet). If the vaneless space is too small, wakes which forms at the trailing edge of the nozzle vanes are not allowed to be mixed out and the flow approaching the impeller will not be uniform. It is also possible for the stator and impeller to be mechanically coupled which could excite blade resonances. If instead the vaneless space is made to large the wet surface, which induces friction, could lead to extreme pressure losses and also it would make the overall size of the turbine unnecessary big.

The use of radial turbines in turbochargers is widely spread. A turbocharger will work with large variations in inlet pressure and mass flow and this leads to poor performance. A common implemented solution has been to incorporate variable nozzle vanes. They are variable in the sense that they can shift their angle, making the throat smaller or bigger. There will arise a void (or clearance) at the end walls and this will lead to the leakage of some of the fluid which will not be turned in the nozzle vanes but instead
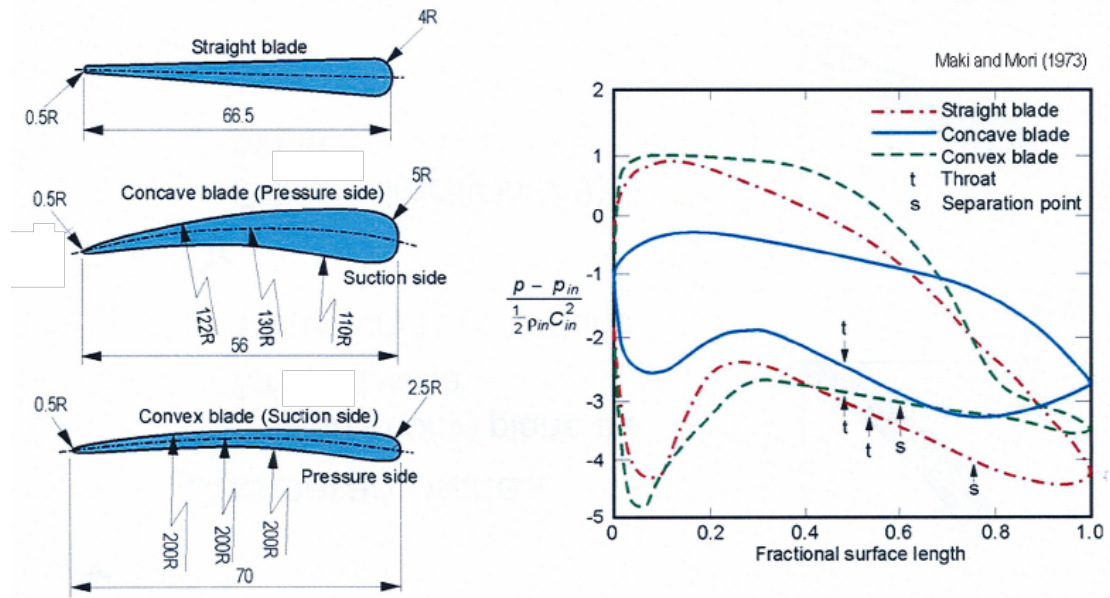
Figure 2.4.: Maki H. and Mori Y. studied the difference in pressure coefficient for the different types of camber angle and their conclusion was, a bit unexpectedly, that the smoothest pressure distribution is obtained with concave blades, [11]. The figure is adapted from [12].

keep its radial velocity component.
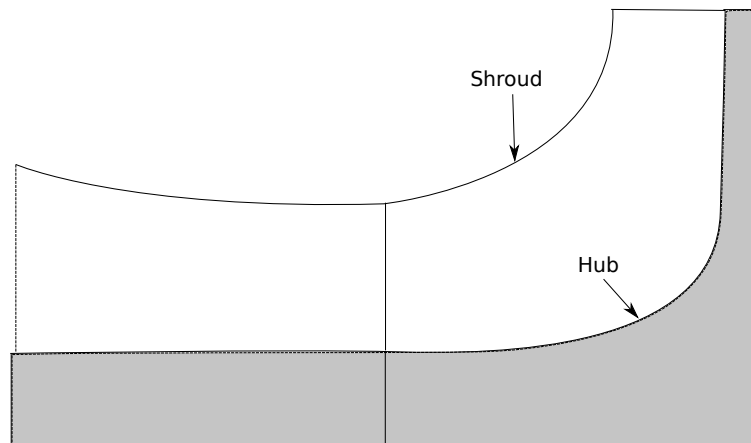
Figure 2.5.: The impeller cross section can be described with the two end walls, hub and shroud..

The impeller is consisting of vanes attached around an axis. The end walls are often called the hub and the shroud. The hub is attached to the axis and is rotating with it. The shroud can be defined in two different ways. Either it is defined as the tip of
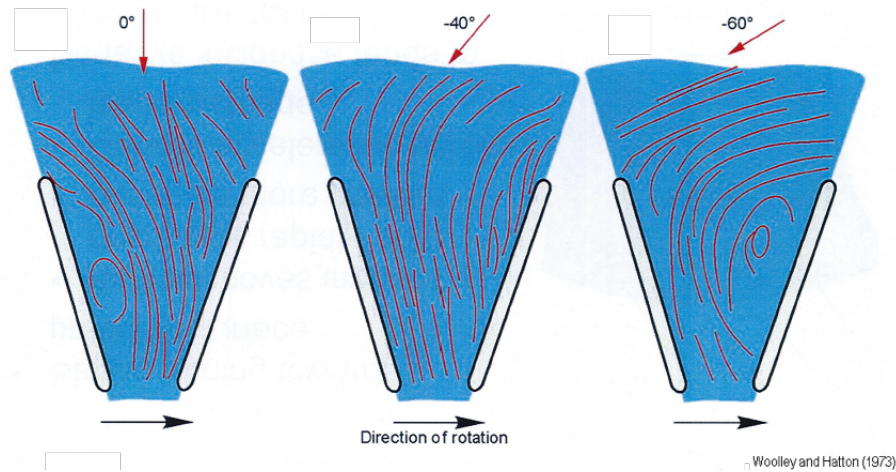
Figure 2.6.: Studies have shown that the best performance of the radial turbine's impeller is obtained when the flow enters the inducer with a negative incidence of -20° to -40°. At other angles of incidence the flow will separate. This phenomenon is shown in this figure which is adapted from [**12**].
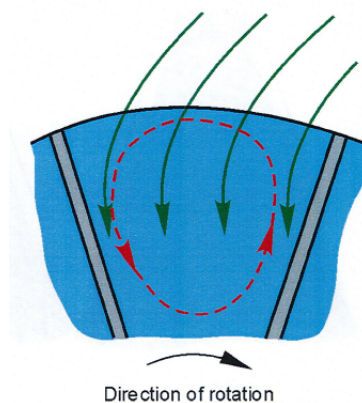
Figure 2.7.: Studies have shown that the best performance of the radial turbine's impeller is obtained when the flow enters the inducer with a negative incidence of -20° to -40°. This is partly due to the circulation arising in the inducer of the impeller. This phenomenon is shown in this figure which is adapted from [**12**].

blades which means that the shroud is also rotating with the blades, however, it can also be defined as the cover which encloses the impeller, thus it does not rotate. The flow enters the inducer[2] of the impeller with a meridional velocity component which is largely radial. It has been found that the best performance of the impeller is achieved

---

[2]The inlet of the impeller is often called "the inducer"

when the flow is approaching the tip with a negative incidence. It can be found in the literature that, highest efficiency is obtained with an incidence of -20° to -40°, [12]. This phenomenon can be explained on the basis of the figures 2.6 and 2.7. While the fluid is entering the inducer, angular momentum is conserved which increases the tangential velocity, however, the blade speed is decreasing at a faster rate. This forces the fluid to move toward the pressure surface. In addition to this effect there is the Coriolis acceleration, which, however, diminishes with radius. The effect of these events is that at the tip the fluid is forced toward the suction surface, however, this force is not matched at lower radius and as a consequence the fluid is pressed toward the pressure surface, causing some flow to circulate. At large negative incidence angles the circulation will be extensive and cause the flow to separate on the pressure surface. The contrary will happen at small negative or positive incidence angles, the flow will then separate on the suction surface.

The outlet of the impeller, often called the exducer or the exducer region, represents the part of the impeller where the fluid is mainly axial and has a large component of swirl (large tangential component). Because of the large component of swirl, a Coriolis acceleration will arise but unlike in the inducer, this Coriolis acceleration will act in the radial direction which will direct the flow from hub to shroud. As a consequence of the change in tangential velocity in the impeller, another force will arise which acts between the blade surfaces. Finally there are secondary flows resulting from these forces.

To recover some of the static pressure after the impeller, a diffusor might be incorporated in which the flow is allowed to expand due to an increase in flow area. The diffusor is not always incorporated and in fact, while it will help recover static pressure it will ultimately cause losses in total pressure and total efficiency.

2.1. Strategies for design and performance analysis of radial turbines

The course of action when designing a radial turbine is quite different from the one conducted when running a performance analysis. The design procedure attempts to develop a geometry which is going to meet certain performance parameter, (e.g. mass flow, efficiency, power and expansion ratio), at one operating point. The turbine will, however, work at multiple running points which do not match the design point, this is called off-design. The performance analysis is used to predict the performance of the turbine at operating points and while the geometry is the product developed from the design stage, the geometry is used as input in the performance analysis.

The process of aerodynamically designing a radial turbine involves several steps. Preferably the steps can be divided into one-, two- and three-dimensional design (other steps

are possible). When the aerodynamic analysis is performed, structural simulation reviewing the mechanical and thermal stresses that the turbine will be exposed to has to be performed. This analysis is just as important as the aerodynamic analysis and can often force the designer to rethink and change the design. Finally the auxiliary systems needs to be incorporated. These can for example consist of systems for cooling, valves and ducts. It should be stressed that these systems together with the structural analysis can form obstacles which might be impossible for the designer to overcome. This results in the process having to be restarted. In this thesis only the aerodynamic analysis is reviewed and the theory presented concerns only that part of the design process.

In the one-dimensional stage, performance analysis are conducted at the inlet and outlet of each component (volute, nozzle, impeller, diffusor and vaneless spaces). This analysis is made using thermodynamic and aerodynamic principles and relations and to some extent models to predict the losses which occurs. The outcome from this simple analysis are predictions of some geometrical parameters, such as radii, blade angles, section width and axial length, at the inlet and outlet for the various components. It is also possible to determine the flow conditions at one certain design point and to some extent predict performance at points dissimilar from the design point. The one-dimensional analysis is performed on a single streamline, a mean-line, situated in the center as can be seen in figure 2.8.
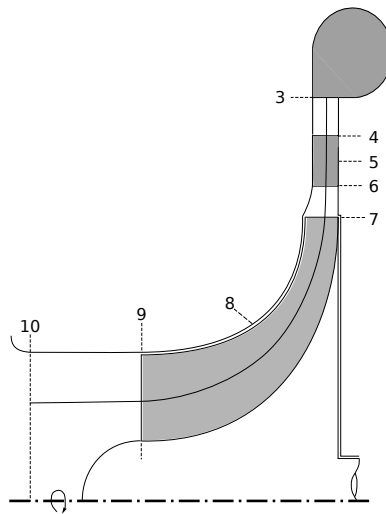
Figure 2.8.: In one-dimensional analyses a mean streamline is used. Calculations are performed on this streamline at the inlet and outlet of each component

A two-dimensional approach includes several streamlines. This is often called a blade-to-blade analysis. Even though the flow in a radial turbine is strongly affected by three-dimensional effects a blade-to-blade analysis helps in understanding the basic aerodynamics of the flow. It can be used to analyze flow condition in a range not far away

from the design point. Here the approximation of the blade loading and blade angle distribution can be very precise. Both inviscid and viscous solvers exists. In the inviscid solvers a boundary layer analysis can be performed to predict viscous losses. A significant advantage of blade-to-blade analysis is the possibility to construct blade loading diagram which shows the velocity distribution, or pressure distribution, on the pressure and suction surface of the blade. Such a diagram can be viewed in figure 2.9. Here the velocity distribution is shown for the hub and shroud but similar plots can be made for other sections across the hub and shroud. The area between the lines representing the velocity distributions on the suction and pressure surfaces respectively in these diagrams is proportional to the power which is possible to extract from this section of the stage. The use of two-dimensional blade-to-blade analysis is widely spread in the industry and used as an important tool in the design process. This is because the computational effort is very small and simulations can be run in the frame of a few seconds. However it can not be used when the flow is separating. It is highly likely that this will be the situation far away from the design point. When conditions like that needs to be examined viscous three dimensional solvers have to be used.
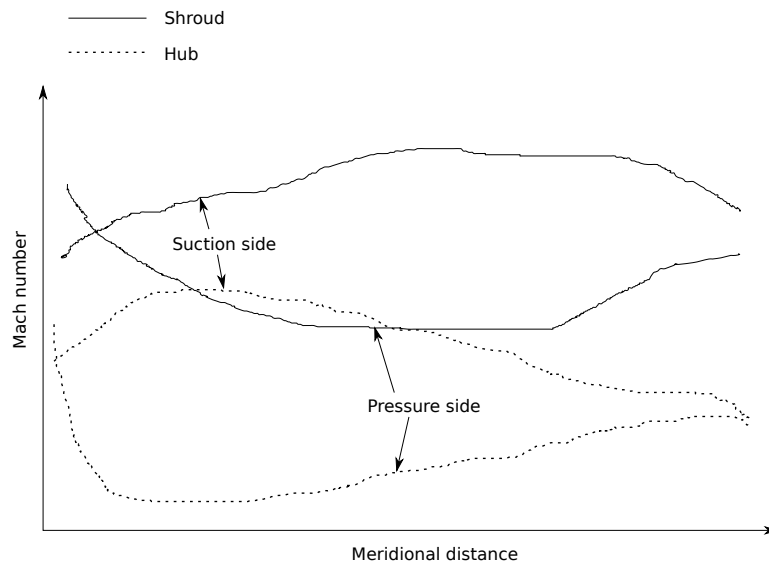
Figure 2.9.: **Blade loading diagrams resulting from two-dimensional blade-to-blade analyses helps the designer to evaluate the velocity distribution and spot defects. They should not be trusted at flow conditions far away from the design point because the flow might be separating. The separation phenomenon will most likely not be captured by the blade-to-blade analysis.**

When designers need to understand the three-dimensional aspects of the flow they usually turn to "CFD". CFD, **C**omputational **F**luid **D**ynamics, is used to solve the Navier Stokes equations, either in their full form or in various simplified forms. This is done

by discretizing the equations and solving them at grid points which cover the flow field. Different turbulence models are applied to capture the small variations in the flow parameters. The results are presented in colorful plots showing the different flow variables, such as pressure, temperature and velocity. CFD is mainly an evaluation tool. While the development of faster computers is preceding as strongly as ever, it is still not possible to run a full CFD-analysis of the flow in radial turbine in as a short time as would be preferable. This means that the developers of radial turbines still need to employ one- and two-dimensional tools.
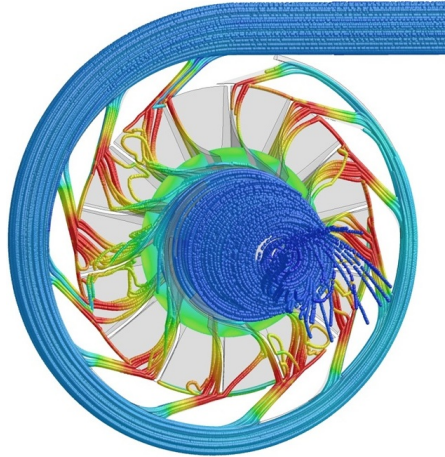
Figure 2.10.: Computational fluid dynamics are used to analyze the flow through a radial turbine in three dimensions. The results are presented in colorful plots showing the different flow variables, such as pressure, temperature and velocity.

3. One-dimensional Analysis

The preliminary design of a radial turbine is an efficient way of determining the basic component geometry and it gives a primary prediction of the performance of the turbine at the design point. If needed, this performance analysis can be extended to generate off-design maps which can be used to predict the performance at conditions dissimilar from the design point. The iterative process of designing a radial turbine often returns to the preliminary design. It speeds the process of designing the turbine because without it, or if it is done badly, an extensive trial and error procedure might arise.

A preliminary design can be carried out in different ways, some requiring less input data than others. According to N.C. Baines there are three different ways in which a mean-line analysis can be conducted [12].

1. Scaling according to similitude from an existing design.

2. The use of the basic conservation principles and simple stage or component correlations.

3. The use of fundamental physical models.

As reported by Baines, there is no right or wrong approach and which method is used is dependent on the information provided to the designer [12].

3.1. Scaling

Scaling is used when a turbine application which is going to operate at conditions similar to an existing turbine is desired. Instead of designing a new turbine, the existing turbine is scaled in accordance with non dimensional groups. This will reduce the cost and effort and thereby the time used in developing the turbine. The non dimensional groups are made up by parameters describing the turbine, the fluid used and the flow conditions. One group is a function of one or more of the other groups, e.g.

$$\Pi_1 = f(\Pi_2, \Pi_3, \Pi_4, \Pi_5) \tag{3.1}$$

The groups used when working with turbo machines handling compressible fluids can be found in basic textbooks about turbo machinery. Here those in [7] are recited.

$$\frac{\Delta h_{0s}}{a_{01}^2}, \eta, \frac{P}{\rho_{01} a_{01}^3 D^2} = f\left\{\frac{\dot{m}}{\rho_{01} a_{01} D^2}, \frac{\rho_{01} a_{01} D}{\mu}, \frac{ND}{a_{01}}, \gamma\right\} \tag{3.2}$$

When the machine is run with a perfect gas some alterations to the groups stated above can be made. This simplifies the situation. The derivation can be found in Dixon, [7]. Here, just the results are presented.

$$\frac{p_{01}}{p_{010}}, \eta, \frac{\Delta T_0}{T_{01}} = f\left\{\frac{\dot{m}\sqrt{\gamma R T_{01}}}{D^2 p_{01}}, \frac{ND}{\sqrt{\gamma R T_{01}}}, Re, \gamma\right\} \tag{3.3}$$

The groups in equation (3.3) are readily used when running experiments on a turbomachine because the inlet and outlet conditions are determined in a simple manner. If the machine under observation is running with only one gas, the ratio of specific heats, γ, can be excluded from equation (3.3) and if the machine works only at high Reynolds number, this group can also be omitted. The results is shown below.

$$\frac{p_{01}}{p_{010}}, \eta, \frac{\Delta T_0}{T_{01}} = f\left\{\frac{\dot{m}\sqrt{c_p T_{01}}}{D^2 p_{01}}, \frac{ND}{\sqrt{\gamma R T_{01}}}\right\} \tag{3.4}$$

In the industry working with turbomachines is has become praxis to delete R, γ, c_p and D from equation (3.4). This further simplifies the situation.

$$\frac{p_{01}}{p_{010}}, \; \eta, \; \frac{\Delta T_0}{T_{01}} \; = \; f\left\{\frac{\dot{m}\sqrt{T_{01}}}{p_{01}}, \; \frac{N}{\sqrt{T_{01}}}\right\} \tag{3.5}$$

The parameters on the left hand side of equation (3.5) are then plotted against $\dot{m}\sqrt{T_{01}}/p_{01}$, which is also known as the corrected mass flow, with $N/\sqrt{T_{01}}$ as a parameter. $N/\sqrt{T_{01}}$ is termed the corrected shaft speed. For a radial turbine such plots can look something like those in figure 3.1. Figure 3.1 shows that at a certain pressure ratio the turbine flow chokes and thereby makes it independent of the shaft speed.
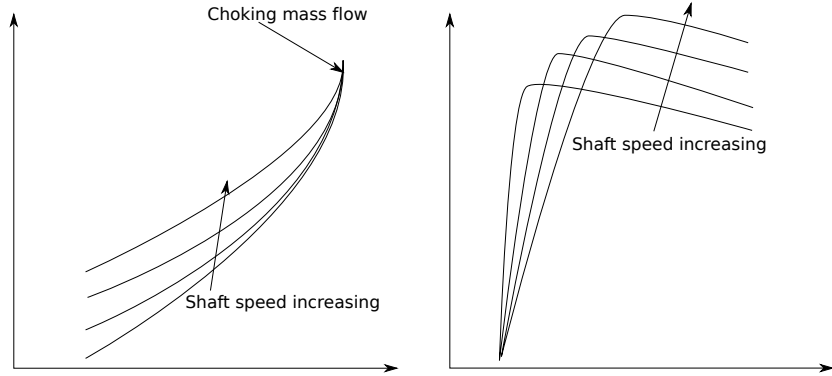

Figure 3.1.: The dimensional groups are plotted against each other. The figure shows, on the left hand side, p_{01}/p_{010} as a function of $\dot{m}\sqrt{T_{01}}/p_{01}$ with $N/\sqrt{T_{01}}$ as different parameters and, on the right hand side, the efficiency η as a function of $\dot{m}\sqrt{T_{01}}/p_{01}$ with $N/\sqrt{T_{01}}$ as different parameters.

3.1.1. Correlations for radial turbines

The equations derived previously can be applied on all turbomachines. For radial turbines additional correlations have been proven useful to derive a starting point for a new design.

The **Flow Coefficient** is defined as the ratio of meridional velocity and blade speed.

$$\text{Flow coefficient}: \quad \phi = \frac{c_m}{U} = f\left\{\frac{\dot{m}\sqrt{c_p T_{01}}}{D^2 p_{01}}, \frac{ND}{\sqrt{\gamma R T_{01}}}\right\} \tag{3.6}$$

The **Stage loading** is defined as.

$$\text{Stage loading}: \quad \psi = \frac{\Delta h_0}{U^2} = f\left\{\frac{\dot{m}\sqrt{c_p T_{01}}}{D^2 p_{01}}, \frac{ND}{\sqrt{\gamma R T_{01}}}\right\} \tag{3.7}$$

The derivation of equations (3.6) and (3.7) can be found in e.g. [7]. The stage loading and flow coefficient have been used to correlate efficiency for radial turbines. N. Baines presents one such diagram in [3]. From that diagram it can be noted that an increase of the flow coefficient from 0.3 to 0.4 gives a decrease in efficiency by almost a $\frac{1}{10}$th. To achieve a low flow coefficient either the speed or the area (thereby decreasing the meridional velocity) needs to increase.
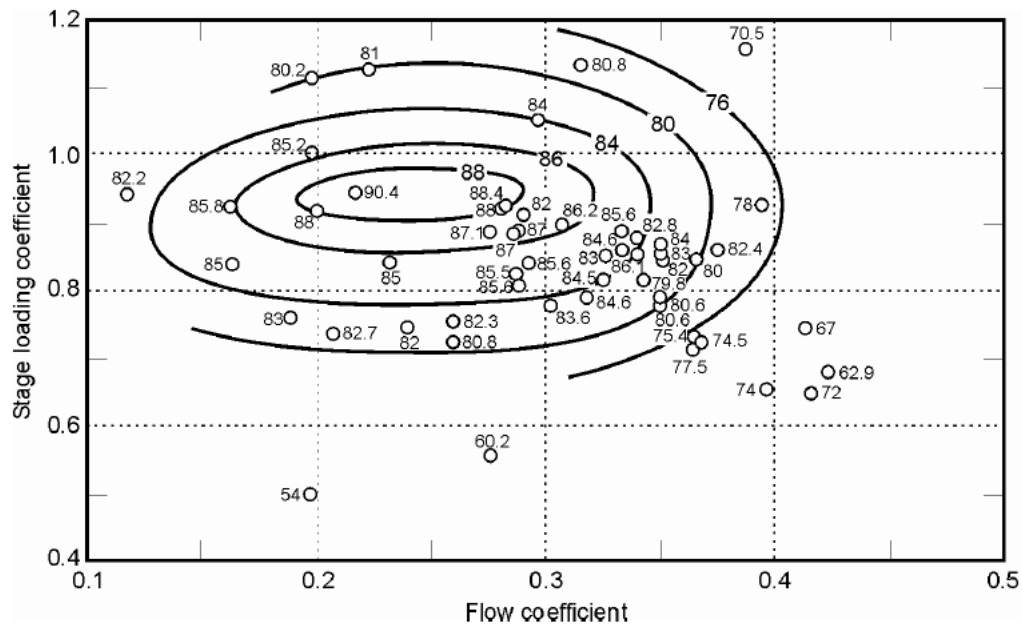
Figure 3.2.: N. Baines presents a chart which correlates the flow and stage loading coefficients with efficiency lines as parameters. Figure taken from [3].

Two other parameters which are often mentioned when discussing radial turbines are the **Specific Speed** and the **Specific diameter**. Specific speed is a function of rotational speed, volume flow and power. This means that there is no parameter that describes the geometry of the turbine. A remedy for this is to introduce the specific diameter which has the desired features. They are strongly linked to the flow coefficient and stage loading which is shown in equations (3.8) and (3.9). Figure 3.3 shows a relationship correlating the specific speed and specific diameter.

$$\text{Specific speed}: \ N_s \ = \ \frac{\phi^{\frac{1}{2}}}{\psi^{\frac{3}{4}}} \ = \ \frac{\omega\sqrt{Q}}{\Delta h_0^{3/4}} \tag{3.8}$$

$$\text{Specific diameter}: \ D_s \ = \ \frac{\psi^{\frac{1}{4}}}{\phi^{\frac{1}{2}}} \ = \ \frac{D\Delta h_0^{1/4}}{\sqrt{Q}} \tag{3.9}$$

Figure 3.3.: The well known correlation parameters specific speed and specific diameter used in preliminary design of radial turbines can be plotted to generate the curve shown in this figure. The theoretical curve, assuming ideal conditions, is situated somewhat lower than the experimental values. The figure is taken from [12].

18

3.2. Mean-line analysis according to physical relations and equations

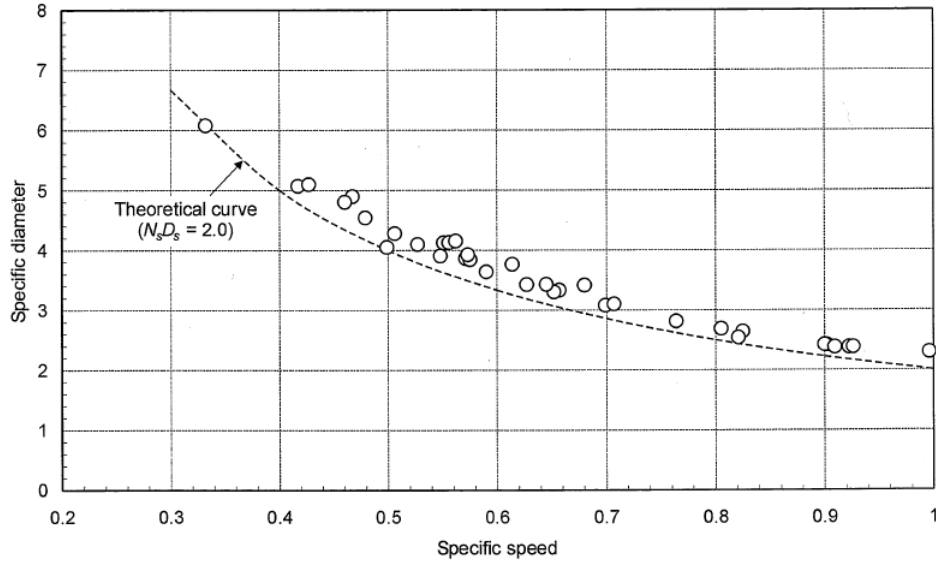A full mean-line analysis is used to predict the performance at the design point. This analysis is based entirely on physical laws and correlations and the input data needed to perform it is extensive in comparison with the two analysis methods described earlier.

This section serves as an investigation of the different equations in the program called "RIFT"[1]. Additional equations found in the literature used for loss modeling are also presented. Examples of equations governing simple designing can be found in appendix where a simple design program is developed.

Examples of input parameters which are used in a performance analysis are shown in table 3.1 below. It is readily understood that an insufficient number of input parameters will not yield a solution. However, it is not certain that a solution is met if too many parameters are specified. That is because the geometry is already set when conducting a performance analysis and this geometry is most often not able to meet all the specifications at once.

Table 3.1.: Performance analyses can be conducted with different set of input variables. Three possible set are presented in this table.

	Case one	Case two	Case three
Input	$\dot{m}$, N, T_{01}, p_{01}	N, T_{01}, p_{01}, p_9	$\dot{m}$, N, T_{01}, p_9
parameters	All geometry	All geometry	All geometry

In the table 3.1, there are three different sets of input variables. If the first set is chosen a direct solution can be obtained. The second requires an iteration where the mass flow is chosen and the exit pressure is calculated. If the calculated exit pressure deviates from the specified, the mass flow is adjusted and the procedure proceeds until it converges on the exit pressure. The third case requires a similar iteration procedure, however, this procedure converges on the inlet total pressure.

It is possible to run the analysis with different stator configurations. Generally they can be summed up into four alternatives, shown in table 3.2.

---

[1]"RIFT" is used in this thesis to run performance analyses in chapter 4 and is based on chapter nine in the book written by R.H. Aungier [2]

Table 3.2.: There are in general four stator configurations fitting a radial turbine. They are presented in this table.

1.	No stator
2.	Nozzle
3.	Volute
4.	Nozzle + Volute

In figure 3.1 it can be seen that the flow is choking at a certain pressure ratio. Expanding further will not give an increase in mass flow as it would if the turbine was not choking. In light of this it can be realized that to get a solution when the turbine is choking, another constraint must be set.

The second option in table 3.1 will most often generate an unstable numerical solution. This is because the chosen mass flow can take values, during the iteration, which are higher than the choked mass flow. A simple solution to this problem is shown in figure 3.4.

Given: N, T01, p01, p9
All geometry
Guess: Pressure at each station

For each component, calculate
mass flow rate m based on
expansion ratio across component

Check component mass flows;
adjust station pressures until
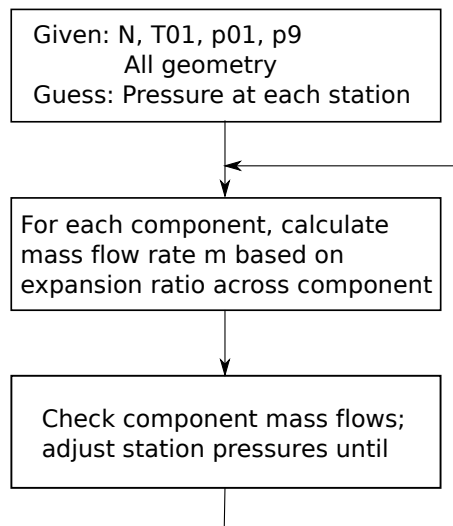
Figure 3.4.: When the mass flow is not given as an input variable a numerical solution might become unstable. A solution to this problem is presented in this figure. Adapted from [12].

One-dimensional performance analyses often only need the geometry to be specified at three different points, the inlet, the exit and somewhere in between. The analysis aims to predict the losses. This can be done by dividing the losses into different groups. It is possible to define the losses as loss in pressure or in enthalpy and corresponding loss coefficients emerge from this. The pressure loss and enthalpy loss coefficients are often

defined as.

$$Y = \frac{p_{0,inlet} - p_{0,exit}}{p_{0,exit} - p_{exit}} \tag{3.10}$$

$$\xi = \frac{h_{exit} - h_{exit,s}}{h_{0,exit} - h_{exit}} = \frac{c_{exit}^2}{c_{exit,s}^2} \tag{3.11}$$

In equation (3.11), $h_{exit,s}$ is the exit static enthalpy which would be attained in an isentropic expansion. The enthalpy loss can be modified and described as a velocity loss coefficient given by.

$$L = c_{exit,s}^2 - c_{exit}^2 \tag{3.12}$$

This subchapter presents different ways of modeling the various losses surrounding the flow in a radial turbine. It is however naive to think that a one-dimensional analysis can be able to completely predict the nature of the flow. Initially the volute is concerned, it is followed by the nozzle, the impeller and finally the diffusor and vaneless spaces but before going into the different components, the theory of profile loss which is defined in [2] and used extensively of Aungier is presented.

Boundary layer analysis

When performing a mean-line analysis of a radial turbine it is convenient to use a simple one-dimensional boundary layer model. This can help predict the profile and viscous losses in the various components of the radial turbine. In a radial turbine the flow is accelerating in each component, except for the diffusor. This results in a decrease in both total and static pressure which, unlike in compressors where the flow is decelerating and give rise to an adverse pressure gradient, provides thin boundary layers. The flow is also more unlikely to separate because of the thin boundary layers that this accelerating flow give rise to. According to Aungier [2], the model takes extensive use of four parameters namely the boundary layer thickness, δ, the boundary layer displacement thickness, δ^*, the boundary layer momentum thickness θ and the skin friction coefficient, c_f. These parameters are well defined in most elementary textbooks on fluid mechanics, for example in reference [8]. The boundary layer thickness is defined in figure 3.5.

The boundary layer momentum thickness is defined as.

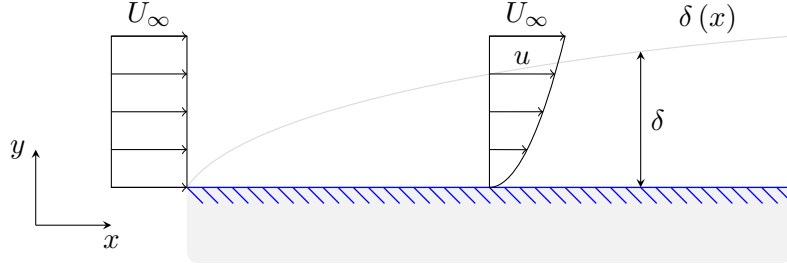$$\rho_e u_e^2 \theta = \int_0^\delta \rho u[u_e - u]dy \tag{3.13}$$

Figure 3.5.: The boundary layer on a flat plate. Acknowledgment of Marcus Thern.

Where ρ_e and u_e is the inviscid density and velocity respectively at the boundary layer edge. This can be rewritten according to [14] and [15] which is cited in [2] .

$$\theta = \frac{c_f}{2u_e^n} \int_0^L u_e^n dx \tag{3.14}$$

Where u_e is the boundary edge velocity, L is the flow path length through the component. Depending on the nature of the flow (i.e. if it is accelerating or defusing) the exponent n can be varied. Pai makes no variation and says that $n = 5$ provides a general solution, this is cited in [2]. Aungier makes use of the following approximation of equation (3.14) which describes the boundary layer momentum thickness at the discharge station.

$$\theta = c_f \rho_{ave} \left[\left(\frac{u_1}{u_3} \right)^5 + 2 \left(\frac{u_2}{u_3} \right)^5 + 1 \right] \frac{L}{8\rho_3} \tag{3.15}$$

$$\rho_{ave} = \frac{\rho_1 + 2\rho_2 + \rho_3}{4} \tag{3.16}$$

The density average value is included to model the compressible effects. The velocities are taken as the absolute velocities in a stationary coordinate system and as the relative velocities in a rotational one.

The boundary layer displacement thickness is derived from the definition of shape factor, H.

$$\delta^* = H\theta \tag{3.17}$$

From the $\frac{1}{7}$th power-law and for turbulent flow at discharge it can be shown that, [2].

$$H = 1.2857 \tag{3.18}$$

The skin friction coefficient is modeled according to Aungier's empirical model, quoted below.

Skin friction c_f

The reynolds number for all components of the radial turbine will be based on the discharge density ρ_3, velocity u_3 and dynamic viscosity. Since it is on the annular end walls in all the radial turbine components, except the volute, that the boundary layers occur, it is natural to base the reynolds number on the width, b_3 between these end walls as non-dimensional length instead of the usual, the diameter, d. In the volute the dimensional length will be taken as the equivalent diameter, D_{eq}, of the section which is under observation. This gives.

$$Re_d \rightarrow \frac{\rho_3 u_3 b_3}{\mu} \tag{3.19}$$

$$Re_d \rightarrow \frac{\rho_3 u_3 D_{eq}}{\mu} \tag{3.20}$$

This assumes that the boundary layers are fully turbulent, which according to Aungier is not completely true. However, he says that this does not flaw the model because the skin friction coefficient is not strongly a function of the reynolds number. Aungier cites Nikuradse's model [13] of pipe skin friction coefficient and says that this can be used in this case. The flow is considered to be laminar if the reynolds number does not exceed 2000.

$$Re_d < 2000 \tag{3.21}$$

The skin friction coefficient is then given by the laminar skin friction coefficient.

$$c_f = c_{fl} = \frac{16}{Re_d} \tag{3.22}$$

When the flow is turbulent, care most be taken to examine if the peak-to-valley surface roughness, e, will yield a rough wall skin friction coefficient, c_{ftr}, or a smooth wall skin friction coefficient, c_{fts}.

$$\frac{1}{\sqrt{4c_{fts}}} = -2\log_{10}\left[\frac{2.51}{Re_d\sqrt{4c_{fts}}}\right] \tag{3.23}$$

$$\frac{1}{\sqrt{4c_{ftr}}} = -2\log_{10}\left[\frac{e}{3.71d}\right] \tag{3.24}$$

The actual (peak-to-valley) surface roughness, e, is estimated by assuming a sin-wave form, [2].

$$e = \frac{e_{rms}}{0.3535} \tag{3.25}$$

To determine if the smooth wall or the rough wall skin friction coefficient should be used the definition of a surface roughness reynolds number can be applied.

$$Re_e = (Re_d - 2000)\frac{e}{d} \tag{3.26}$$

If Re_e is less than or equal to 60 the turbulent skin friction coefficient is approximated with the smooth wall skin friction coefficient, otherwise it is approximated with a weighted value of c_{ftr} and c_{fts}.

$$c_{ft} = c_{fts}; \quad Re_e \leq 60 \tag{3.27}$$

$$c_{ft} = c_{fts} + (c_{ftr} - c_{fts})\left(1 - \frac{60}{Re_e}\right); \quad Re_e > 60 \tag{3.28}$$

For the case when the reynolds number is in transition between laminar and turbulent a weighted average is used.

$$c_f = c_{fl} + (c_{ft} - c_{fl})\left(\frac{Re_d}{2000} - 1\right) \tag{3.29}$$

Assuming that fluid of the mainstream and the boundary layer are instantly mixed and that the mass and momentum are conserved the pressure loss for radial turbine components can be approximated according to Lieblein and Roudebush [10], cited in [2]. While it is applicable to the volute and the vaneless spaces, the nozzle rows and the impeller need some further evaluation. This is described within the chapters covering the nozzle and impeller respectively.

$$Y_p = \frac{\Delta p_0}{p_{03,is} - p_3} = \frac{2\Theta + \Delta^2}{(1-\Delta)^2} + \sum \Delta Y \tag{3.30}$$

$$\Theta = \sum \theta/b \tag{3.31}$$

$$\Delta = \sum \delta^*/b \tag{3.32}$$

The last term in (3.30) is different for the various components and is described in the respective chapters. When a volute or a vaneless space is under consideration the Θ and Δ in equations (3.31) and (3.32) can be used directly. The blade surface boundary layer which arises on the nozzle and the impeller blades also needs to be taken into account when the component under consideration is a nozzle row or an impeller. This is modeled

by the following relationship.

$$\Theta = 1 - \left(1 - \sum \frac{\theta_w}{b_w}\right)\left(1 - \sum \frac{\theta_b}{b_b}\right) \tag{3.33}$$

$$\Delta = 1 - \left(1 - \sum \frac{\delta_w}{b_w}\right)\left(1 - \sum \frac{\delta_b}{b_b}\right) \tag{3.34}$$

The subscripts w and b indicates the boundary layers on the end walls and the blade surfaces respectively.

The Volute

A performance analysis can be performed with the volute divided into two sections which yield three stations where the geometry is specified, as in figure 3.6. The geometry needed is presented in table 3.3.

Table 3.3.: The geometrical parameters which are needed to conduct the performance analysis.

Inlet radius	r_1
Inlet area	A_1
Mid passage radius	r_2
Mid passage area	A_2
Exit radius	r_3
Exit width	b_3
Surface finish	e_{rms}

Since this is the first component of the turbine all the inlet conditions are available. From a mass balance at the inlet station together with the fact that the velocity is in general entirely tangential, the flow conditions can be calculated. Assuming that the velocity is still entirely tangential at the mid passage and that half of the mass flow has turned off toward the nozzle blades a similar analysis can be conducted at this station. The tangential velocity at the exit station is estimated assuming that the angular momentum is conserved between the mid passage and exit.

$$c_{3\theta} = c_2 \frac{r_2}{r_3} \tag{3.35}$$

The volute is exposed to two types of losses. The profile loss is determined using the relations in chapter 3.2. The second type Aungier terms "circumferential distortion loss" [2]. This loss occurs due to the fact that the angular momentum is in fact not conserved and the flow is thereby mixed, hence mixing losses result. The loss coefficient for this
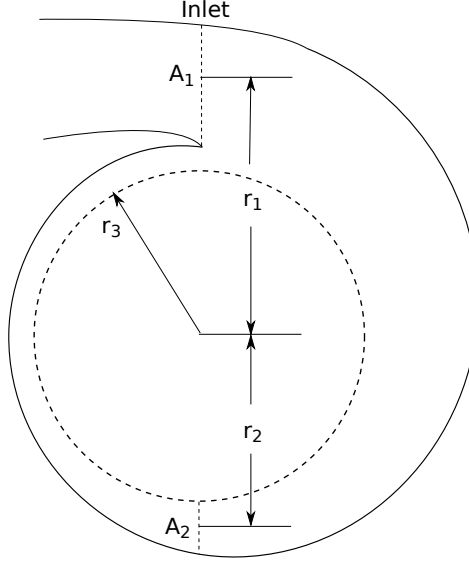
Figure 3.6.: The sections in a simplified model of the volute.

loss is given by.

$$Y_\theta = \left(\frac{\frac{r_1}{r_3} c_1 - c_{3\theta}}{c_3} \right)^2 \tag{3.36}$$

The total loss coefficient is given by.

$$Y = Y_p + Y_\theta = \frac{p_{01} - p_{03}}{p_{03} - p_3} \tag{3.37}$$

Since the total enthalpy is constant through this component the exit total enthalpy together with the exit total pressure and a mass balance yields all other flow variables. When performing the mass balance, caution must be taken to include the boundary layer thickness. This is done by.

$$\dot{m} = A_3 \rho_3 c_{3m} (1 - \Delta) \tag{3.38}$$

The meridional velocity takes into account both the radial component and the axial component of velocity according to.

$$c_m^2 = c_r^2 + c_z^2 \tag{3.39}$$

The blockage can be determined using the boundary layer analysis described previously. Baines presents a different correlation in [12].

$$\Delta = 0.04 \Delta L Re_{\Delta L}^{-1/7} \tag{3.40}$$

$$Re_{\Delta L} = \frac{\rho c \Delta L}{\mu} \tag{3.41}$$

Baines also presents a way of determining the total pressure loss.

$$\Delta p_0 = C_f (\Delta L / D) \frac{1}{2} \rho c^2 \tag{3.42}$$

$$\tag{3.43}$$

In the equation above, C_f is the skin friction coefficient. It can either be calculated using the relations presented previously or by using a Moody chart. Baines, however, recommends that a skin friction coefficient slightly bigger than the one taken from a Moody chart should be used. He argues that this should be done because of the additional curvature effects in the volute.

The Nozzle

The main purpose of the nozzle blades is to lead the flow while creating swirl. This is optimally done without any loss in total pressure. In a real situation however losses will occur. This sub section serves as a demonstration of how the losses can be modeled.

According to Augnier the pressure losses are a combination of two parts. The first part includes the profile losses while the second includes losses derived from the fact that the flow does not follow the blade at the inlet, these are called incidence losses. The incidence phenomenon is demonstrated in figure 3.7.

$$Y = Y_p + Y_{inc} = \frac{p_{04} - p_{06}}{p_{06} - p_6} \tag{3.44}$$

$$p_{06} = \frac{p_{04} + Y_{p6}}{1 + Y} \tag{3.45}$$

$$i = \alpha - \beta \tag{3.46}$$
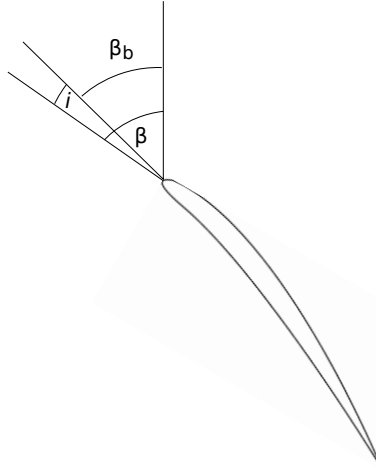
Figure 3.7.: The incidence phenomenon.

The performance analysis, described in [2], begins with the nozzle blades being divided into two sections yielding three stations. An inlet station, an exit station and one in between. At all of these stations the radius, r, the axial coordinate, z, the passage width, b, the blade angle, β and blade thickness, t, are specified. Additionally the number of blades, the surface finish and the throat length and width, o and b_{th} are specified.

Figure 3.8.: The nozzle row geometry. Adapted from Aungier [2].

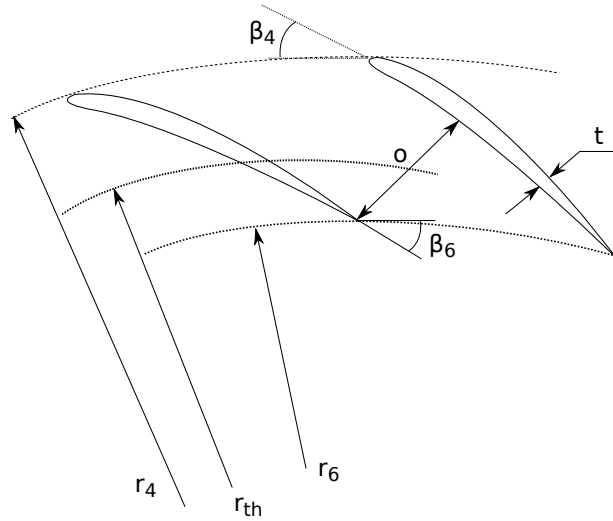The meridional distances can then be calculated by a numerical integration.

$$m^2 = \int_0^m dr^2 + dz^2 \tag{3.47}$$

The throat radius can then be estimated. Aungier [2] derives an expression which is recited here.

$$r_{th} = r_6 - \left(\frac{\partial r}{\partial m}\right)_6 \frac{o^2}{2s_6} \tag{3.48}$$

In the equation above s_6 corresponds to the exit nozzle pitch. The first derivative of r with respect to m can be approximated, according to Aungier, as follows.

$$\left(\frac{\partial r}{\partial m}\right)_6 = \frac{m_6(r_6 - r_5)}{m_5(m_6 - m_5)} - \frac{(m_6 - m_5)(r_6 - r_4)}{m_5 m_6} \tag{3.49}$$

The pitch at every station is defined as.

$$s = \frac{2\pi r}{N_N} \tag{3.50}$$

When the throat radius, r_{th}, is determined it is possible to calculate the exit flow angle. First the throat flow angle has to be determined. This is done, as cited in [2], by slightly modifying the sine rule, specified earlier.

$$\sin \alpha_{th} = \frac{b_{th} o}{s_6 b_6} \tag{3.51}$$

Then the exit flow angle is determined according to.

$$\tan \alpha_6 = \frac{r_6}{r_{th}} \tan \alpha_{th} \tag{3.52}$$

Finally it is possible to calculate the deviation angle, δ_6. Deviation results from the fact that the flow does not follow the blade at the trailing edge, much like incidence for the leading edge. Baines, [12], explains the deviation comes from an underturning caused by the fact that the flow is diffusing from the throat to the trailing edge but it also exposed to a sudden expansion caused by the finite trailing edge thickness. Baines also shows how the deviation depends on nozzle exit mach number, the deviation tends to be a bit higher for high mach number. He also mentions how difficult it is to predict the deviation and gives an example of how the sine rule, equation (3.51), predicts the flow angle rather poorly for nozzles of radial turbines. Instead Baines proposes another model, [3]

$$\text{For M} < 0.3 : \quad \alpha_4 = a_0 + a_1 \cos^{-1}(o/s) \tag{3.53}$$

$$\text{For M} > 0.3 : \quad \alpha_4 = a_0 + a_1 \cos^{-1}(o/s) + a_2(M - 0.3) \tag{3.54}$$

The deviation is given by.

$$\delta_6 = \beta_6 - \alpha_6 \tag{3.55}$$

The flow path length, needed to determine the profile loss, can be integrated using the following expression

$$L = \int_0^m \frac{dm}{\sin \beta} \tag{3.56}$$

The flow area at every station is determined according to.

$$A = b(2\pi r \sin \beta - t N_N) \tag{3.57}$$

At the inlet station to every section all flow data can be calculated using the upstream flow angle and a mass balance. The flow data at the mid station of each section can also be calculated using a mass balance and assuming that $\alpha = \beta$. At the exit station the losses need to be taken into account.

The profile loss is approximated using the assumptions in the sub chapter about boundary layer. To approximate the incidence loss Aungier uses a relationship which includes a parameter called "optimum incidence angle", i^*. It is defined below.

$$i^* = \sqrt{\frac{L}{s_6}} \left(3.6 \sqrt{\frac{10 t_5}{L}} + \frac{|\beta_6 - \beta_4|}{3.4} \right) - \frac{|\beta_6 - \beta_4|}{2} \tag{3.58}$$

This relationship was originally developed by Herrig et al. [9]. The corresponding optimal flow angle is defined as.

$$\alpha^* = \beta_4 - i^* \, sign(\beta_6 - \beta_4) \tag{3.59}$$

The incidence loss can now be calculated.

$$Y_{inc} = \sin^2(\alpha_4 - \alpha^*) \frac{p_{04} - p_4}{p_{06} - p_6} \tag{3.60}$$

Baines also derives an expression which correlates the enthalpy loss over the nozzle blade, [3].

$$\xi = \frac{0.05}{Re_b^{0.2}} \left(\frac{\tan^2 \beta_6}{s/c} + \frac{o}{b} \right) \tag{3.61}$$

It can be noted that Baines correlation is much easier to apply.

It is mentioned in section 3.2 that for nozzle and impeller blades not only end walls have boundary layers which need to be taken into account when estimating the losses. There are also boundary layers building up on the blade surfaces. A simple blade loading diagram is used to approximate the velocity distribution on the pressure surface and the suction surface. An example of such a diagram is presented in figure 3.9.
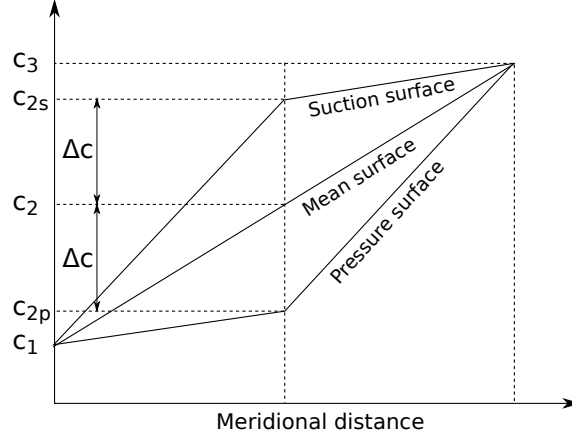

Figure 3.9.: Simple blade loading diagram used to approximate the surface distribution on the pressure surface and the suction surface. Figure adapted from [2].

The velocity difference, Δc, in figure 3.9 is approximated according to the following relationship.

$$\Delta c = \frac{2\pi(r_6 c_{6\theta} - r_4 c_{4\theta})}{L N_N} \tag{3.62}$$

It is possible for the flow to be choked and a check needs to be performed to control whether this is the case or not. The throat is the station at which the flow will choke first. Consequently the check will be performed at this station. The mass flow which is associated with a choked flow is.

$$\dot{m}^* = N_N \, b_{th} \, o \, (1 - \Delta)\rho^* c^* \tag{3.63}$$

In this equation, Δ is taken from equation (3.32). The static pressure which is desired under supersonic conditions is less than the static pressure at sonic conditions. This ultimately requires the calculation process to make additional iterations. An isentropic expansion from the choked solution will be assumed to yield the right static pressure. This however, is only possible as long as the static pressure does not yield a meridional velocity greater than the sonic velocity.

$$c_{6m} = \frac{\dot{m}}{(1 - \Delta)2\pi r_6 b_6 \rho_6} \leqslant a_6 \tag{3.64}$$

When $c_{6m} > a_6$ a shock wave might occur adding losses. To include these losses they have to be modeled.

It is possible to use variable nozzle blades, which often is called a "VGT"-arrangement. In this arrangement the nozzle blades can be turned to hold up a constant pressure level at the inlet to the nozzle blades. The fact that the blades are turned inevitable means that a clearance at the tip and bottom will arise. Baines shows that this clearance becomes significant when the blade width becomes small and that the loss which arises from it must be taken into account [12]. The losses arise due to the fact that the leakage flow is not turned to the same degrees as the flow inside the nozzle row which can cause large incidence at the impeller tip. Qiu et. al. developed a mean-line method to predict the losses which arise from the clearance [16]. Their conclusion is the same as Baines's with the addition that with a smaller nozzle opening, the clearance effect decreases and that the presence of a clearance increases the choking limit of the nozzle.

The Impeller

The performance analysis of the impeller is far more difficult and complex than those of the other components. The fluid is in general turned 90 degrees and this generates hub-to-shroud flow profile gradients which are difficult to model. The geometry is specified at the inlet, the mid passage, the outlet and the throat. The geometry variables are presented in table 3.4. The geometry can be seen in figure 3.10 and in figure 3.11.
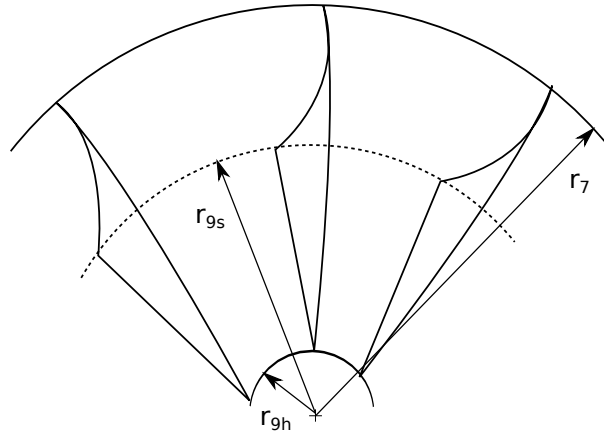

Figure 3.10.: The geometry of the impeller vanes.

There is a greater amount of different losses which have to be taken into consideration besides the ones described for the volute and the nozzle row. Aungier defines six loss
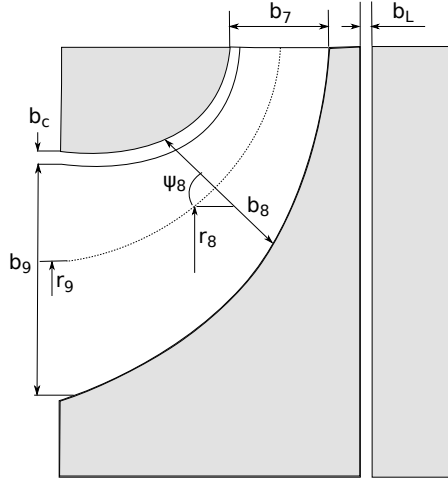
Figure 3.11.: The impeller geometry with notations. Figure adapted from [2].

Table 3.4.: The geometry needed to run the performance analysis.

Inlet radius	r_7	Mid passage radius	r_8	Outlet radius	r_9
Inlet width	b_7	Mid passage width	b_8	Outlet width	b_9
Inlet axial coord.	z_7	Mid passage axial coord.	z_8	Outlet axial coord.	z_9
Inlet tangent angle	ϕ_7	Mid tangent angle	ϕ_8	Outlet tangent angle	ϕ_8
Inlet blade angle	β_7	Mid blade angle	β_8	Outlet blade angle	β_9
Inlet blade thickness	t_7	Mid blade thickness	t_8	Outlet blade thickness	t_9
Throat blade to blade width	o	Throat passage width	b_{th}	Number of blades	N_R
Clearance	b_c	Clearance	b_L	Surface finish	e_{rms}

sources.

$$Y = Y_p + Y_{inc} + Y_{BL} + Y_{HS} + Y_{CL} + Y_Q \qquad (3.65)$$

The profile loss, Y_p, derived in chapter 3.2, is determined in a similar manner as the one for the nozzle blades. While the velocities used in expression for the nozzle blades profile loss are absolute, relative velocities are used when calculating the profile loss on the impeller. The meridional path length can be approximated using a third-order polynomial that matches the end-point coordinates and slopes. The is according to Aungier an accurate approximation. The mean surface curvature is then given by.

$$\kappa_m = \frac{|\phi_9 - \phi_7|}{m_9} \qquad (3.66)$$

The flow path length is given by.

$$L = \int_0^m \frac{dm}{\sin\beta} \tag{3.67}$$

The sub sonic flow angle is determined according to.

$$r_{th} = r_9 - \frac{o^2 \sin\phi_9}{2s_9} \tag{3.68}$$

$$\sin\alpha'_{th} = \frac{b_{th}o}{s_9 b_9} \tag{3.69}$$

$$\tan\alpha'_9 = \frac{r_9}{r_{th}}\tan\alpha'_{th} \tag{3.70}$$

The incidence loss can be determined using a relationship derived by Carmichael [6], it is recited in [2] and the results in [2] are presented here.

$$c^*_{7\theta} = \sigma(U_7 - c_{7m})\cot\beta_7 \tag{3.71}$$

$$\cot\alpha^*_7 = \frac{c_{7m}}{c^*_{7\theta}} \tag{3.72}$$

$$Y_{inc} = \sin^2(\alpha_7 - \alpha^*_7)\frac{p'_{07} - p_7}{p'_{09} - p_9} \tag{3.73}$$

In the expressions above, $c^*_{7\theta}$ and α^*_7 are the ideal inlet tangential velocity and ideal inlet flow angle respectively. The slip factor can be modeled according to Aungier's expression from [2]. It is a modification to Wiesner's model.

$$\sigma = |\sin\phi_7|\frac{\sqrt{\sin\beta_7}}{N^{0.7}} \tag{3.74}$$

Aungier argues that the expression yielding the slip factor above needs correction if the solidity becomes too low. The expression above can be used until the radius ratio r_9/r_7 exceeds a value of $r_9/r_7 > (r_9/r_7)_{lim}$.

$$(r_9/r_7)_{lim} = \frac{\sigma - \sigma_0}{1 - \sigma_0} \tag{3.75}$$

$$\sigma_0 = \sin(19° + \beta_7/5) \tag{3.76}$$

When this value is exceeded, the slip factor is calculated according to.

$$\sigma_{corrected} = \sigma(1 - \xi) \tag{3.77}$$

$$\xi = \left(\frac{r_9/r_7 - (r_9/r_7)_{lim}}{1 - (r_9/r_7)_{lim}}\right)^{\sqrt{\beta_7/10}} \tag{3.78}$$

Clearance losses emerge from the fact that the flow does not follow the blade and hence does not tribute any work. Aungier proposes that this loss be modeled using a pressure difference over the clearance gap.

$$\Delta p \left(\rho_m (rb)_m L N_N \right) = \dot{m} |r_7 c_{7\theta} - r_9 c_{9\theta}| \tag{3.79}$$

ρ_m and $(rb)_m$ is approximated using the relationship in equation (3.16). The velocity of the flow across the clearance gap must be determined and Aungier uses the following relationship.

$$u_{CL} = \sqrt{\frac{2\Delta p}{\rho_m}} \tag{3.80}$$

Then the mass flow across the clearance can be approximated.

$$\dot{m}_{CL} = 0.816 \rho_m u_{CL} N_R \delta_c \tag{3.81}$$

Finally the clearance loss is given by.

$$Y_{CL} = \frac{\dot{m}_{CL} \Delta p}{\dot{m}(p'_{09} - p_9)} \tag{3.82}$$

The losses which arise from the blade loading and hub-to-shroud loading must be taken into account. Aungier derives relationship for both losses which are presented here.

$$Y_{BL} = \frac{1}{24} \left[\frac{\Delta w}{w_9} \right]^2 \tag{3.83}$$

$$Y_{HS} = \frac{1}{6} \left[\frac{\kappa_m b_9 w_8}{w_9 \sin \alpha_9} \right]^2 \tag{3.84}$$

It has been mentioned that the total enthalpy is kept constant across the nozzle row and the volute. It is possible to use a similar relationship across the impeller. However, the parameter which is constant is the rothalpy. The rothalpy is defined as.

$$I = h_{07} - \omega r_7 c_{7\theta} \tag{3.85}$$

The disk friction loss can be included in the expression for the rothalpy.

$$I = h_{07} + \Delta H_{DF} - \omega r_7 c_{7\theta} \tag{3.86}$$

The disk friction loss, ΔH_{DF} can be modeled and Aungier presents one example [2]. The exit relative total enthalpy can then be determined.

$$h'_{09} = I + \frac{1}{2} (\omega r_9)^2 \tag{3.87}$$

The various losses can now be summed up to yield the total loss coefficient.

$$Y = Y_p + Y_{inc} + Y_{BL} + Y_{HS} + Y_{CL} + Y_Q \tag{3.88}$$

The moisture loss, Y_Q, takes into account that the fluid might condensate during the expansion. In that case the part of the fluid which condensates will not contribute to the work.

Finally the total relative pressure is given by.

$$p'_{09} = \frac{p'_{09,ideal} + Y_{p9}}{1 + Y} \qquad (3.89)$$

Where $p'_{09,ideal}$ is the ideal total relative pressure and can be determined using the exit total relative enthalpy and the entropy.

Baines takes on a slightly different approach. He categorizes the losses into following groups. Incidence loss, passage loss, trailing edge loss, tip clearance loss, shock loss (due to supersonic expansion) and windage loss. Correlations for the different losses can be found in [12].

Finally the exit static enthalpy together with a mass balance and the equation of state yield all the flow variables. The mass balance at the impeller exit is performed according to.

$$\dot{m} = (1 - \Delta) 2\pi r_9 b_9 \rho_9 w_9 \sin \alpha'_9 \qquad (3.90)$$

Where Δ is the blockage arising from the boundary layer on the end walls. Similarly to the nozzle blades, the impeller must be checked to see if a choke is present or not. The choking mass flow is given by.

$$\dot{m}_* = N_R b_{th} o (1 - \Delta) \rho_* w_* \qquad (3.91)$$

In the case of choking an isentropic expansion from the throat to the impeller exit yields all flow variables. A check must be done to make sure that the meridional exit velocity does not exceed the sonic speed.

The Diffusor

The performance analysis of the diffusor presented here is a simple analysis. More detailed analyses can be found in the literature regarding exhaust diffusor. The analysis described in this subsection is taken from Aungier, [2]. He describes it as a direct analysis which often can be more convenient in cases where the total-to-static pressure ratio is defined rather than the mass flow. The geometry which is needed to perform the analysis is presented in figure 3.12 and in table 3.5.
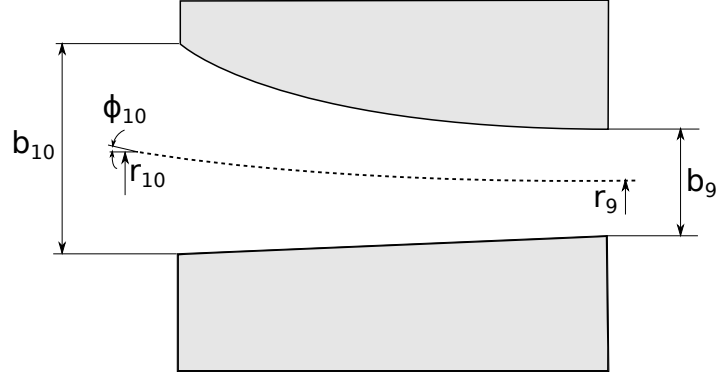
Figure 3.12.: The geometry used for the performance analysis of the diffusor.

Table 3.5.: The geometry needed for the performance analysis.

	Inlet	Exit
Radius	r_9	r_{10}
Axial coordinate	z_9	z_{10}
Slope angle	ϕ_9	ϕ_{10}

Initially the linear distance and the slope difference is approximated.

$$d = \sqrt{(z_{10} - z_9)^2 + (r_{10} - r_9)^2} \tag{3.92}$$

$$\Delta\phi = |\phi_9 - \phi_{10}| \tag{3.93}$$

Aungier defines the flow path length according to.

$$L = \frac{d\Delta\phi}{2\sin(\frac{\Delta\phi}{2})} : \qquad \Delta\phi > 0 \tag{3.94}$$

$$L = d : \qquad \Delta\phi \leqslant 0 \tag{3.95}$$

Unlike the other components of the radial turbine, the flow is decelerating in the diffusor. The resulting boundary layers are much thicker than in an accelerating flow. This analysis serves to measure the thickness of the boundary layers at the exit, much as the boundary layer analysis in chapter 3.2. The divergence angle, mentioned in the section describing preliminary diffusor design, has an impact on the blockage and is given by.

$$2\theta_c = 2\tan^{-1}\left(b_9 \frac{A_{10}/A_9 - 1}{2L}\right) \tag{3.96}$$

The exit blockage is according to Aungier, given by.

$$\Delta_{10} = \frac{\{K_1 + K_2(D-1)\} L A_9}{A_{10} b_9} \tag{3.97}$$

$$D = \frac{(\sqrt{p_{vr}} + 1)^2}{4} \tag{3.98}$$

$$p_{vr} = \frac{p_{09} - p_9}{p_{09} - p_{10,ideal}} \tag{3.99}$$

In equation (3.97), p_{vr} is the ideal velocity-pressure ratio and D is the diffusion factor.

The Vaneless Space

The radial turbine consists of one or two vaneless spaces. One after the volute and possibly one after the nozzle blades. The performance analysis presented here is rather simple. The vaneless space is divided into two sections yielding three stations. The geometry which is needed is presented in table 3.6.

Table 3.6.: The geometry needed for the performance analysis.

	Inlet	Mid	Exit
Radius	r_1	r_2	r_3
Axial Coordinate	z_1	z_2	z_3
Passage width	b_1	b_2	b_3

A simple integration of the coordinates yields the meridional coordinates.

$$m = \int \sqrt{dz^2 + dr^2} \tag{3.100}$$

The passage areas for the different stations are calculated according to.

$$A = 2\pi r b \tag{3.101}$$

The inlet flow conditions are taken from the performance analysis of the upstream component. The angular momentum is assumed to be conserved and the tangential velocity of the downstream station is given by.

$$c_\theta = c_{upstream,\theta} \frac{r_{upstream}}{r} \tag{3.102}$$

Aungier defines an entrance loss according to.

$$Y_{in} = \left(\left[\frac{A_1}{A_{upstream}} - 1 \right] \sin \alpha_1 \right)^2 \frac{p_{01} - p_1}{p_{03} - p_3} \tag{3.103}$$

The total loss coefficient is given by.

$$Y = Y_p + Y_{in} = \frac{p_{0,\text{upstream}} - p_{03}}{p_{03} - p_3} \qquad (3.104)$$

Where Y_p is the profile loss coefficient. The flow conditions are given by a mass balance together with the static enthalpy and the equation of state. Finally a check must be performed to make sure that the meridional velocity does not exceed the sonic speed.

4. Off-Design Performance Analyses

"TurbAero" uses a program called "RIFT" to conduct off-design analyses. With the help of "RIFT", two radial turbines have been analyzed. The results from "RIFT" are then compared to data from experimental testings to investigate the ability of "RIFT" to predict off-design performance of radial turbines. The turbines and test data are provided by Volvo Powertrain AB and the chapter is divided into two sections containing the different simulations of the different turbines. The governing equations which are implemented in "RIFT" have been introduced in chapter 3.

"RIFT" uses three stations of every component of the radial turbine (i.e. one for the volute, nozzle, rotor and diffusor). At every station the geometry is specified on a mean-line basis, (e.g. the radius, axial coordinate, blade angle and width are given). The geometry can be inserted manually but that would inevitable lead to errors. Instead "RIGPAC" is used to model the geometry of the nozzles and rotors. The geometry is imported into "RIGPAC", this is done in a different way depending on whether it is the nozzle or the rotor which is modeled. When a rotor is modeled the geometry is specified for the hub and shroud contours. A series of points connecting the two contours are defined using radial and axial coordinates. The blade angle and thickness is also specified at every point. The nozzle blades are modeled using the x-, y- and z- coordinates for the suction and pressure surfaces respectively. From "RIGPAC" the desired geometry is exported to "RIFT".

The geometry of the volute is modeled using a program called "VOLDES". The outlet radius, width and flow angle are specified. The resulting geometry is exported to "RIFT". The vaneless spaces' geometry are specified directly in "RIFT". The inlet radius, axial coordinate and width are taken as the exit equivalents from the upstream component. The corresponding procedure is applied for the outlet, however, with the downstream component's inlet radius, axial coordinate and width.

It is possible to use different sets of input parameters when performing simulations in "RIFT". The inlet total pressure and temperature together with the shaft speed must be specified. Then it is possible to specify either the mass flow, total-to-static pressure or the static pressure.
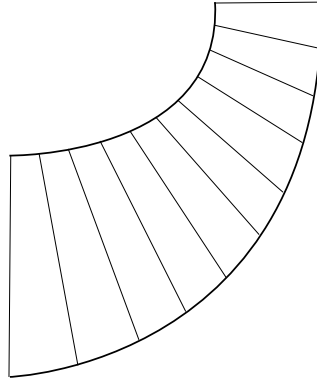
Figure 4.1.: The geometry of the modeled rotor is specified on the hub and shroud contours. A series of points connecting the two contours are defined using radial and axial coordinates.

4.1. The first radial turbine

The tests by Volvo Powertrain AB were performed in a so called "cold-rig". The turbine is designed to run at a high inlet total temperature, however, when Volvo run their tests the inlet total temperature was held at 373 K. Additionally the turbine was scaled by a factor of 0.7. In light of this, two different analyses were performed. One where the turbine was scaled and operating at flow conditions similar to those at which the tests were made and one where the turbine was not scaled and the flow conditions were similar to those at which the turbine was designed to operate at. This was done to evaluate if it made any difference to the results.

The test results was provided by Volvo Powertrain AB. Only the expansion ratios were given and, consequently, it was necessary to calculate the inlet pressures from these ratios. The speed and mass flow are given as corrected mass flow and corrected speed respectively. They were converted to give the appropriate mass flow and speed using equation (3.5).

4.1.1. Simulations on the original turbine

The first simulation used the original geometry and inlet conditions. An attempt was made to resemble the actual gas which is supposed to flow through the turbine, the mole fractions of this gas are shown in table 4.1. The geometry was given as coordinates and imported to program "RIGPAC" in "TurbAero". From "RIGPAC" the mean-line geometry was exported to "RIFT". No diffusor was used and a volute was created, using "VOLDES" in "TurbAero", to guide the flow onto the nozzle blades with as little

incidence as possible. A surface roughness of 64 μm was used for all components. An axial clearance of 0.5 mm was used between the impeller and the disk. A radial clearance of 0.5 mm was used for the impeller.

Table 4.1.: The simulations with the original radial turbine were attempting to resemble the real inlet flow conditions. The mole fractions of the gas used in "RIFT" are presented in this table.

Carbon dioxide, CO_2	0.12
Nitrogen, N_2	0.55
Oxygen, O_2	0.23
Water, H_2O	0.10

In the performance analyses the inlet total temperature and the inlet total pressure were held constant. The rotational speed and the total-to-static expansion ratio were then altered to generate the performance maps. It was explained in chapter two that the expansion ratio and mass flow could not be specified at the same time. In the light of this it was decided to specify the expansion ratio and compare the mass flow to the mass flow from the experimental tests and thus see if they converged. The input variables are summarized in table 4.2.

Table 4.2.: The simulations, on the original radial turbine, were performed with a constant inlet total temperature and pressure. The total-to-static expansion ratio and shaft speed were altered. The mass flow was used as a convergence parameter.

Inlet total temperature, T_{01}	Hot
Inlet total pressure, p_{01}	High
Expansion ratio, p_{01}/p_9	Varying
Rotational speed, N	Varying
Mass flow, $\dot{m}$	Calculated

The efficiency were measured in two different ways. $\eta_{TT,m}$ corresponds to torque measured efficiency and $\eta_{TT,T}$ corresponds to temperature measured efficiency. Which one that has best compliance is hard to determine. The error between the experimental results and simulation results is demonstrated in figures 4.2 and 4.3. It was decided to see if the simulated turbine's geometry in "RIFT" corresponded to the tested turbine's. Since the simulations used the total-to-static expansion ratio as an input variable, it was decided to compare the simulated mass flow with the mass flow measured in the test rig. They should be consistent with each other. This comparison can be viewed in figure 4.4 which shows the mass flow versus total-to-static expansion ratio with different speed lines.
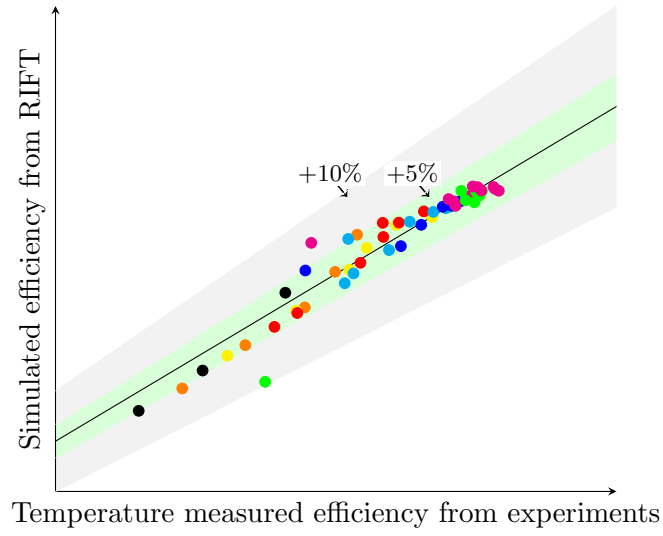
Figure 4.2.: The error from comparing the temperature measured efficiency and the simulated efficiency. The fifteen and five percent error lines are shown. Respective minus five and minus fifteen can be imagined.
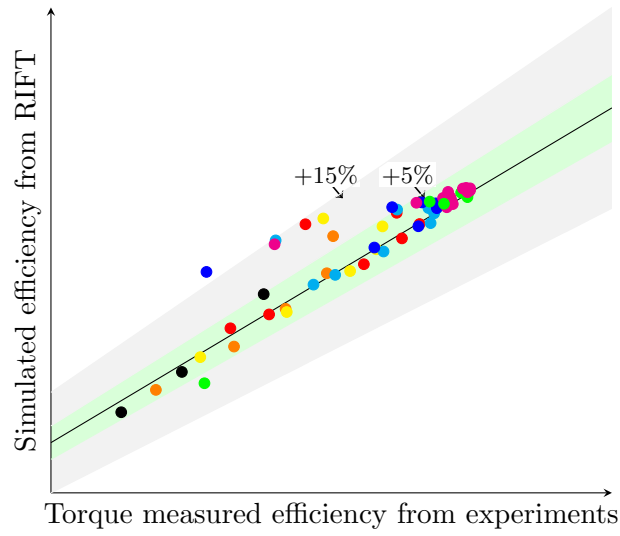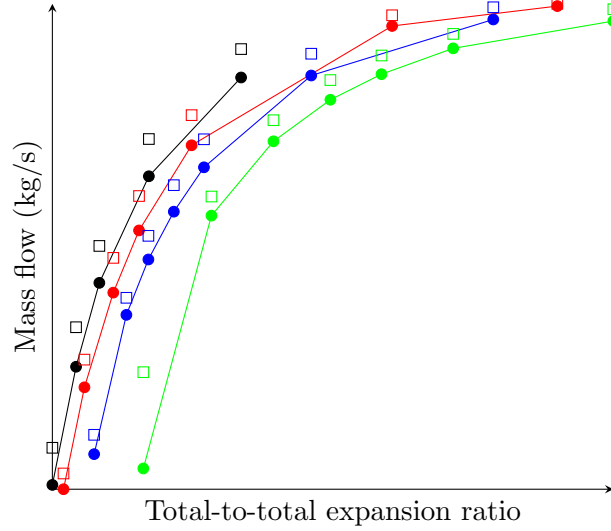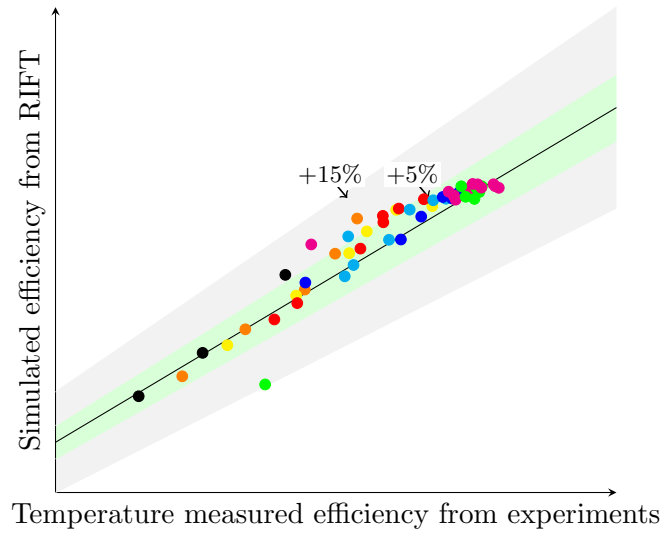

Figure 4.3.: The error from comparing the torque measured efficiency and the simulated efficiency. The fifteen and five percent error lines are shown. Respective minus five and minus fifteen can be imagined.

Figure 4.4.: The mass flow as a function of total-to-total expansion ratio with different dimensionless shaft speeds. The circles represent the simulation results and the squares represent the experimental results.

4.1.2. Simulations on the tested turbine

The second part of simulations was performed on the tested turbine. "Tested" in the meaning that it refers to the scaled turbine. The tests in the rig were performed with air as fluid and as a consequence so were the simulations. The inlet total temperature and the outlet static pressure was fixed at $373\,\mathrm{K}$ and $1.07\,\mathrm{bar}$ respectively. The inlet total pressure and the rotational speed were then altered while the mass flow was calculated to generate the convergence described previously. The input flow variables are summarized in table 4.3. The geometry for the original turbine where scaled by a factor of 0.7 and then imported into program "RIGPAC". From "RIGPAC" the mean-line geometry was exported to "RIFT". No diffusor was used and a volute was created to guide the flow onto the nozzle blades with as little incidence as possible. A surface roughness of 64 μm was used for all components. An axial clearance of 0.5 mm was used between the impeller and the disk and a radial clearance of 0.5 mm was used for the impeller.

The results are presented in the same manner as for the original turbine discussed previously. Figures 4.5 and 4.6 show the error between the experimental results and simulation results. It was decided to see if the simulated turbine's geometry in "RIFT" corresponded to the tested turbine's. Since the simulations used the total-to-static expansion ratio as an input variable, it was decided to compare the simulated mass flow with the mass flow measured in the test rig. They should be consistent with each other. This comparison can be viewed in figure 4.7, which shows the mass flow versus total-to-total expansion

Table 4.3.: The simulations, on the scaled radial turbine, were performed with a constant outlet static pressure and inlet total temperature. The inlet total pressure and shaft speed were altered. The mass flow was used as a convergence parameter.

Inlet total temperature, T_{01}	$373\,\mathrm{K}$
Inlet total pressure, p_{01}	Varying
Outlet static pressure, p_9	$1.07\,\mathrm{bar}$
Rotational speed, N	Varying
Mass flow, $\dot{m}$	Calculated

ratio with different dimensionless speed lines.

Figure 4.5.: The error from comparing the temperature measured and simulated total-to-total efficiency. The fifteen and five percent error lines are shown. Respective minus five and minus fifteen can be imagined.
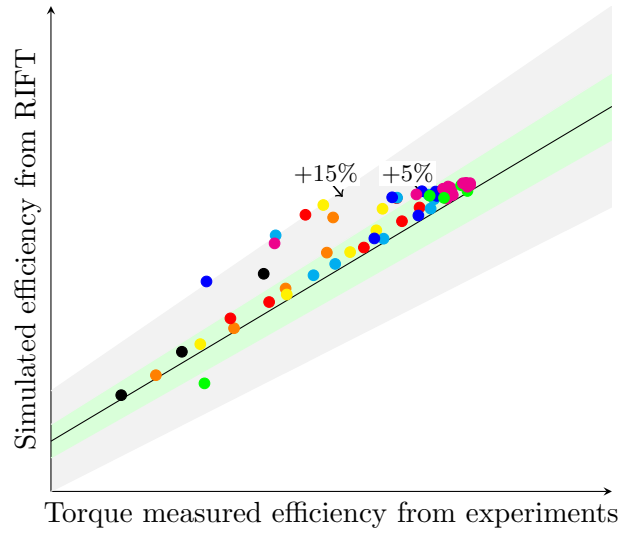
Figure 4.6.: The error from comparing the torque measured and simulated total-to-total efficiency. The fifteen and five percent error lines are shown. Respective minus five and minus fifteen can be imagined.
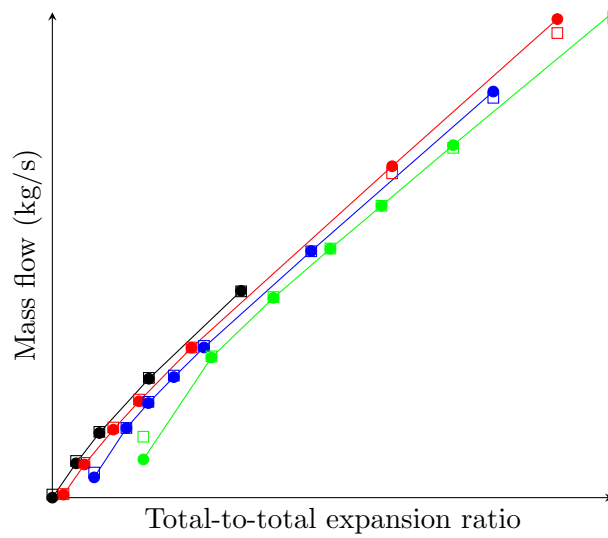

Figure 4.7.: The mass flow as a function of total-to-total expansion ratio with different dimensionless shaft speeds. The circles represent the simulation results and the squares represent the experimental results.

4.1.3. Summary

Off-design performance of the first radial turbine have been simulated using "RIFT". When Volvo performed tests on this turbine, they used a scaled prototype and the test were performed in a cold rig. To evaluate the influence of that and what difference it may bring to the results, the turbine was modeled and the performance was simulated in "RIFT" for two cases. One in which the original turbine was modeled and the analyses used the imaginary input data, and one in which the turbine and input data were modeled according to the prototype used in the tests. The results from the cold rig were comprehensive which helped in modeling the input data to the simulation analyses.

The results show relatively good agreement when comparing the total-to-total efficiency for both cases. Depending on which total-to-total efficiency is used in the comparison, the torque- or the temperature measured, small differences can be seen. The torque measured efficiency shows rather large difference for small expansion ratios, this can be seen for both cases.

It is of great importance when evaluating the results that the geometry used in the simulations is consistent with the one used in the rig. With such a small device, which this radial turbine is, even small deviations from the original design is going to influence the results. The mass flow is mainly controlled by the stator throat, hence great care should be taken when modeling it. The geometry which was given as input to this simulation was the imaginary geometry and it is possible that when the turbine was manufactured, due to tolerances and the fact that the geometry is modeled in different CAD applications, it did not result in the same geometry. A deviating geometry will not only lead to that the mass flow is wrongly predicted, but the pressure loss and thus the efficiency will not be accurately determined either. Thus the comparison in mass flow is a good measurement on how well the modeled geometry complies with the geometry used in the rig and consequently how well the losses can be predicted. The mass flow presented in figures 4.4 and 4.7 show good agreement for the case when the scaled turbine was modeled. However, the same cannot be said for the case with the original turbine. An explanation may come from the fact the mass flow and shaft speed are calculated from the dimensionless mass flow and shaft speed using equation (3.3) and it does not take which fluid is used into account.

The surface roughness was not given together with the geometry and had to be estimated. It is a parameter which is hard to determine and which greatly influence the prediction of the losses. This was discovered early in the simulations and it was decided to specify the surface roughness as constant in all components. In retrospect, it can be thought that the estimated surface roughness was a bit high which probably led to an underestimated efficiency. The efficiency was, however, probably also overestimated due to the fact that the tip of the impeller is scalloped. E.A. Baskharone presents a graph, figure 4.8, which can be used to estimate the losses due to scalloping of the impeller tip, [5]. From this

graph and the geometry of the impeller it is possible to predict how much the scalloping will influence the performance.
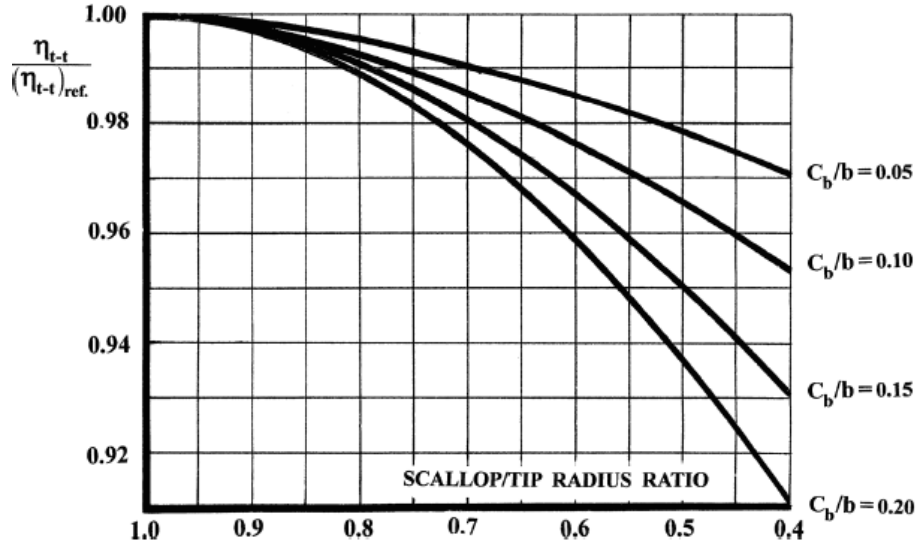

Figure 4.8.: The use of scalloping of the impeller tip generates losses. This graph, presented by E.A. Baskharone, can be used to predict them, [5], and shows the relative efficiency as a function of the portion of scalloping. The figure is taken from [5].

When analyzing the results one has to bear in mind that "RIFT" uses a meanline modeling of the losses and it would be naive to think that it could predict them in a way which would be possible with "CFD". It should also be clear that different measurement errors may be included into the test results. With that in mind the results show very good agreement with the results from the test rig.

The simulation results from the case which tried to resemble the conditions from the cold rig showed best agreement, according to flow and because of that, future simulations will be performed in the same manner.

4.2. The second radial turbine

Volvo have performed tests on the radial turbine in their cold rig. The tests were performed with air as fluid and a constant inlet total temperature of 373 K. The rotational shaft speed were altered together with the total-to-total expansion ratio in order to generate performance maps. It is possible to give the total-to-static expansion ratio, the mass flow and the static exit pressure as input variables in "RIFT" but since none of those are available from the test results a total-to-static expansion ratio was guessed and iterated until the simulated total-to-total expansion ratio converged with the one from the tests.

4.2.1. Simulations

The simulations in "RIFT" were performed with the geometry, generated in a similar fashion as previously described in chapter 4.1. The inlet total temperature was held constant at 373 K and the outlet total pressure was held constant at 1.05 bar. The inlet total pressure was then calculated using the total-to-total expansion ratio (taken from the test results) and the outlet total pressure. The total-to-total expansion ratio varied and consequently also did the inlet total pressure. The simulations were performed to converge on the total-to-total expansion ratio as discussed previously. The same surface finish was used as for the first radial turbine presented in chapter 4.1, namely 64 μm. When performing the first couple of simulations it was observed that the simulated mass flow did not match the mass flow measured in the rig. It was concluded that the nozzle throat of the modeled geometry did not match the nozzle throat of the tested turbine. A simple fix to this problem was applied, namely to change the nozzle throat until convergence of the mass flow was achieved at the design point. The geometry was then locked and all simulation performed without changing it.

Table 4.4.: **The simulations on the second turbine were performed with a constant inlet total temperature and outlet total pressure. The inlet total pressure and shaft speed were altered. Each simulation used a number of iteration to converged on the specified total-to-total expansion ratio. The mass flow and total-to-total efficiency were calculated.**

Inlet total temperature, T_{01}	373 K
Outlet total pressure, p_{09}	1.05 bar
Inlet total pressure, p_{01}	Varying
Rotational speed, N	Varying
Expansion ratio, p_{01}/p_{09}	Specified
Mass flow, $\dot{m}$	Calculated
Efficiency, η_{TT}	Calculated

Figure 4.9 shows the error between the experimental results and simulated results. It was decided to see if the simulated turbine's geometry in "RIFT" corresponded to the tested turbine's. Since the simulations used the total-to-total expansion ratio as an input variable, it was decided to compare the simulated mass flow with the mass flow measured in the test rig. They should be consistent with each other. This comparison can be viewed in figure 4.10 which show the mass flow versus total-to-total expansion ratio with different dimensionless shaft speed lines.
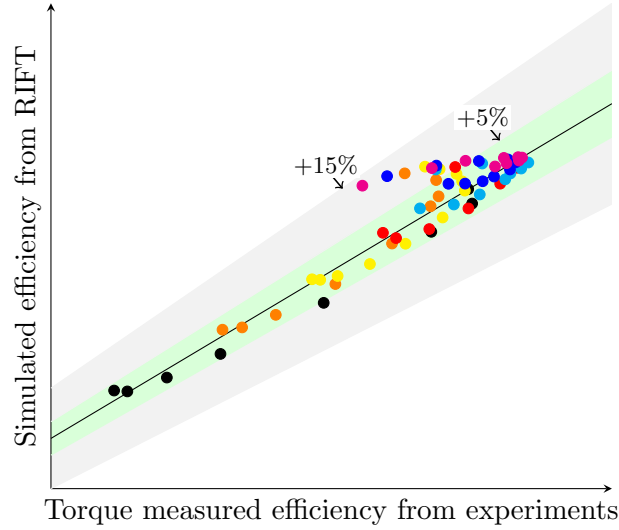
Figure 4.9.: **The error from comparing the torque measured and simulated total-to-total efficiency. The fifteen and five percent error lines are shown. Respective minus five and minus fifteen can be imagined.**

4.2.2. Summary

Off-design performance of the second radial turbine has been simulated using "RIFT". The tests, performed by Volvo, where conducted in a cold rig. It could be seen, earlier, from the results from the simulations of the first radial turbine that best agreement where met when the simulated geometry and flow conditions resembled those which prevail during the tests. In light of this it was decided to simulate the performance of the second turbine in a similar manner.

The results from the simulations can be seen in figures 4.9 and 4.10 which show the total-to-total efficiency and mass flow as a function of the total-to-total expansion ratio with different dimensionless shaft speed lines respectively. The total-to-total efficiency show good agreement except for small expansion ratio. However, since the efficiency was calculated using torque measurement (from the test results), this trend was rather
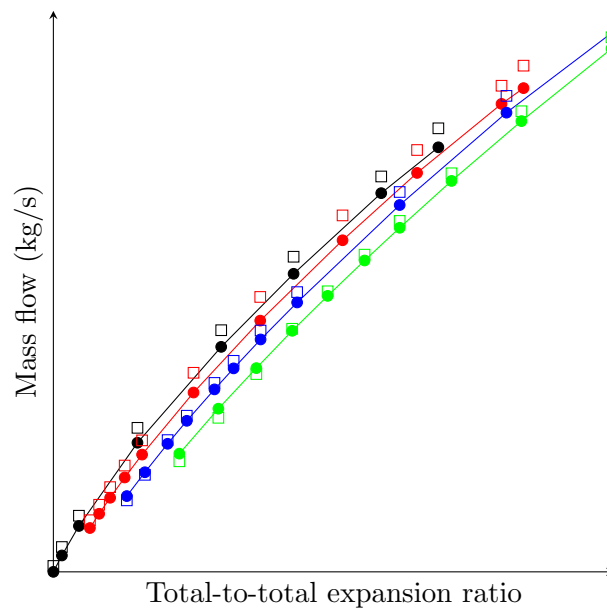
Figure 4.10.: The mass flow is presented as a function of total-to-total expansion ratio with different dimensionless shaft speed lines. The circles represent the simulation results and the squares represent the experimental results.

expected (remembering the same pattern from the first turbine).

The comparison of the simulated mass flow and the mass flow from the rig show very good agreement which indicates that the geometries matched. As mentioned earlier the nozzle throat was changed before the simulations from the one calculated by "RIGPAC". It should be understood that different sources of errors may arise along the way from design to manufacturing. It is possible that the nozzle geometry changed from the one at the sketch table to the final manufactured and tested version.

5. Design Of A Radial Turbine

In the previous chapter, performance analyses on a mean-line basis were conducted on two turbines provided by Volvo Powertrain AB. It was shown that the program tool used, "TurbAero", was able to match the experimental data in a relatively good manner. In this chapter, "TurbAero" is further used with the aim to aerodynamically design a radial turbine. It can be of convenience for the reader of this report to get familiarized with the programs and procedures which are used and therefore a short introduction will be provided next.

TurbAero was introduced in chapter four, however, a big part of the program package was not presented. "TurbAero" is a complete design system for radial and axial turbines. In this work, however, only those programs used when operating with radial turbines are employed. The working procedure when designing a radial turbine and executing performance analyses on existing radial turbines differ.

When designing a radial turbine the programs shown in figure 5.1 are employed. In this figure also the working procedure is demonstrated. Before anything can be done the operating fluid needs to be specified. This is done in the program called "RKMOD". The design process is then initiated in the program called "RIFTSIZE". "RIFTSIZE" develops "preliminary stage designs from performance specifications and empirical correlations, with minimal input by the user"[TurbAero manual].
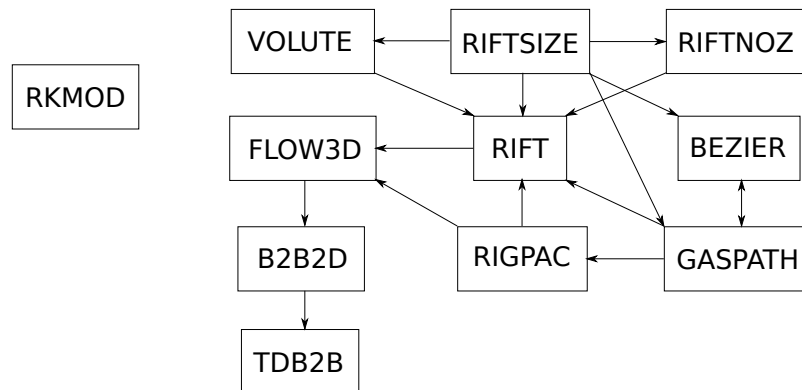

Figure 5.1.: The programs used in TurbAero and the iteration process when designing a turbine.

The preliminary design performed in "RIFTSIZE" can be updated to a detailed design. This can be seen in figure 5.1. Input files to a variety of programs can be exported from "RIFTSIZE". "VOLUTE" is a program which sizes the volute. "RIFTNOZ" is an equivalent program which sizes the nozzle. "BEZIER", "GASPATH" and "RIGPAC" are all programs which develop the geometry of the radial turbine. "RIFT" is a mean-line performance program which can be used to generate off-design maps. From "RIFT" it is possible to export an input file with flow conditions to a program called "FLOW3D". "FLOW3D" uses a quasi-three-dimensional solver which supports end-wall and blade surface boundary layer calculations. The geometry can be supplied either from "GAS-PATH" or "RIGPAC". In "FLOW3D" flow calculations are performed and the output includes preliminary blade loading charts. The calculations performed in "FLOW3D" can be updated in either "B2B2D" or "TDB2B". They are program which perform blade-to-blade analyses. "B2B2D" should be used when subsonic or slightly transonic conditions prevail. This is because it uses a potential flow solver. When supersonic conditions prevail the time-marching solver in program "TDB2B" is much better suited. The computational time required for "TDB2B" is a bit longer than for "B2B2D".
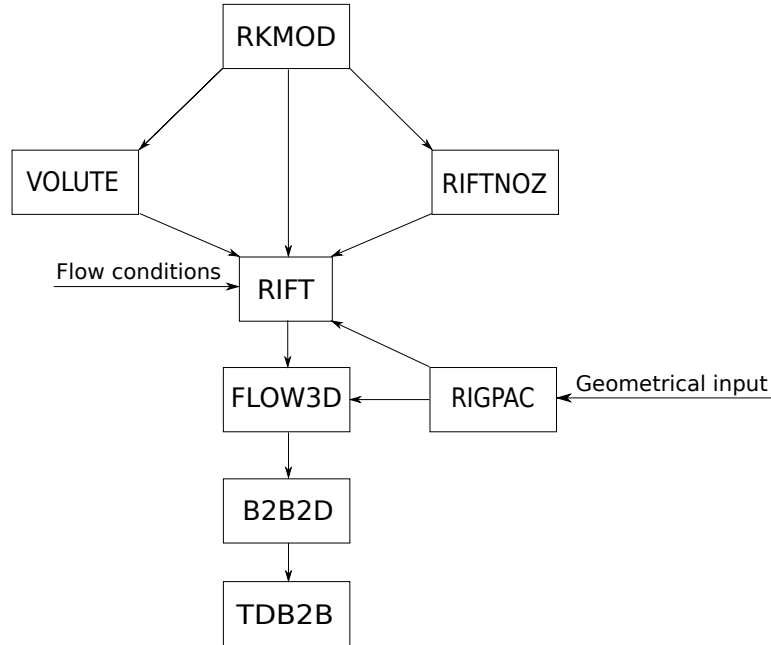

Figure 5.2.: The programs used in TurbAero and the iteration process when conducting performance analyses on radial turbines.

The working procedure when conducting performance analyses on existing radial turbines is a bit different from that of designing. The procedure was introduced in chapter four, however, a more in-depth view is given here. The programs used and in what manner they are used in is demonstrated in figure 5.2. The working fluid is composed and chosen in program "RKMOD". The geometry of the turbine is employed in pro-

gram "RIGPAC". All the geometry variables can either be inserted manually or imported using a simple text file. The geometry is then exported to programs "RIFT" and "FLOW3D". The flow conditions are specified in "RIFT". Together with the geometry imported from "RIGPAC" it is possible to simulate mean-line performance analyses in "RIFT". In this way full off-design maps can be constructed. If one operating point is chosen, further performance evaluation can be performed in program "FLOW3D". The geometry is imported from "RIGPAC" and it is possible to achieve preliminary blade loading plots. These blade loading plots can then be updated in either program "B2B2D" or program "TDB2B". The program chosen is depending on the component mach-number value.

To have any qualitative meaning, this study needed to take on some delimitation. It was decided that to define the design point, the input data from the second radial turbine, described previously, should be used.

From tests of the second radial turbine it was concluded that the turbine was too large. It was decided, therefore, to make an effort to let the new design be smaller.

Initially a preliminary design resulting from a mean-line analysis is conducted. This preliminary design is then analyzed with one- and two-dimensional tools. As mentioned before the preliminary design would most certainly have to be updated in a detailed design making the design procedure iterative.

5.1. Preliminary design

Design in RIFTSIZE

The preliminary design starts in the program "RIFTSIZE". Since the only parameter which is not specified is the speed, the geometry of the impeller tip will depend solely on it. It was mentioned earlier that either the rotational speed or the specific speed can be used and that they are functions of each other. In this case the specific speed is chosen to specify the geometry of the impeller tip. According to Aungier [2], the specific speed should be in the range of 0.45-0.75. The highest possible efficiency to be attained in "RIFTSIZE" is achieved with a specific speed of 0.55. This gives a total to static efficiency of 0.87. Unfortunately the radius of the impeller tip is then estimated to 66.4 mm. To achieve a reasonable radius, which in this case means lower, it is necessary to increase the specific speed to 0.77. This gives a lower radius of the impeller tip.

The next step in the preliminary design is to size the impeller. In this case the default settings are chosen. They are summarized in table 5.1 and derived in the appendix. It

should be noted that the angles are taken with respect to tangent.

Table 5.1.: The specifications for the rotor sizing.

Inlet blade angle	84.73°
Inlet absolute flow angle	19.22°
Inlet blade thickness	2.0 mm
Exit blade thickness	1.0 mm
Exit hub radius	9.40 mm
Exit shroud radius	37.50 mm
Rotor axial length	42.10 mm
Number of blades	#

A selection of results from the impeller sizing is presented in table 5.2. It can be seen from the results that the incidence angle is equal to the ideal incidence angle. This is not a coincidence as the default setting in "RIFTSIZE" is to achieve this. The squareness is a bit high but according to Balje [4] it should not cause any problems. The ratio of exit meridional velocity to inlet blade speed, c_{9m}/U_7 is within the range which Balje has specified. The ratio of exit to inlet meridional velocity is well within the range which Wood [18] has stated. The exit absolute mach number is estimated to 0.27 and this can be considered relatively low. This should make the preliminary impeller design a good starting point. The impeller blade angle distribution, the impeller passage area and curvature distribution and the impeller contours are shown in figures 5.3, 5.4 and 5.5. The blade angles determines the velocity levels and they should be carefully examined. The curvature is qualitatively measured using the parameter, b/R_c, which is the ratio of width over radius of curvature. This parameter should not exceed unity and it can be said that it measures the degree of distortion which can be expected [2].

Table 5.2.: A selection of results from the rotor sizing.

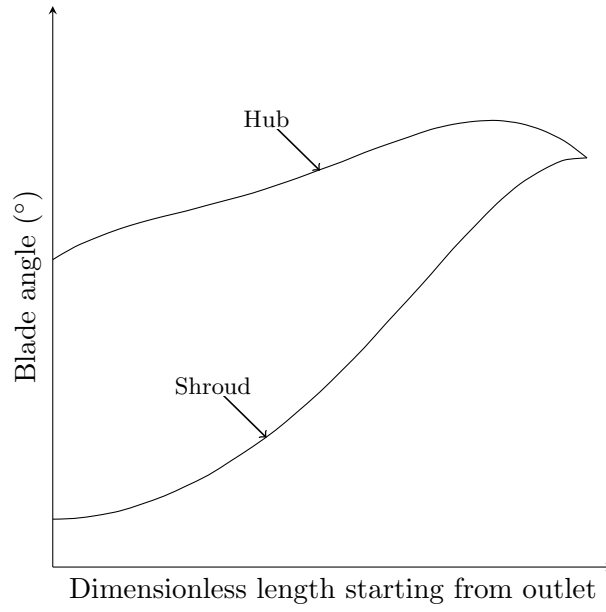|	
Incidence angle	20.28°
Ideal incidence angle	20.28°
Squareness, r_{9s}/r_7	0.7351
c_{9m}/U_7	0.3807
c_{9m}/c_{7m}	1.298
c_{7m}/U_7	0.2934
Impeller static isentropic efficiency	0.8235
Impeller total isentropic efficiency	0.8852

Figure 5.3.: The impeller blade angle distribution as a function of dimensionless length of the preliminary design.
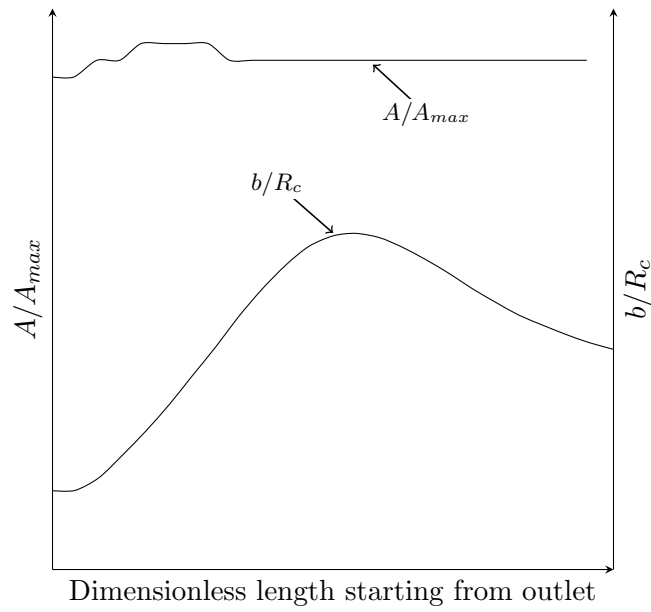

Figure 5.4.: The impeller passage area and curvature distribution of the preliminary design.
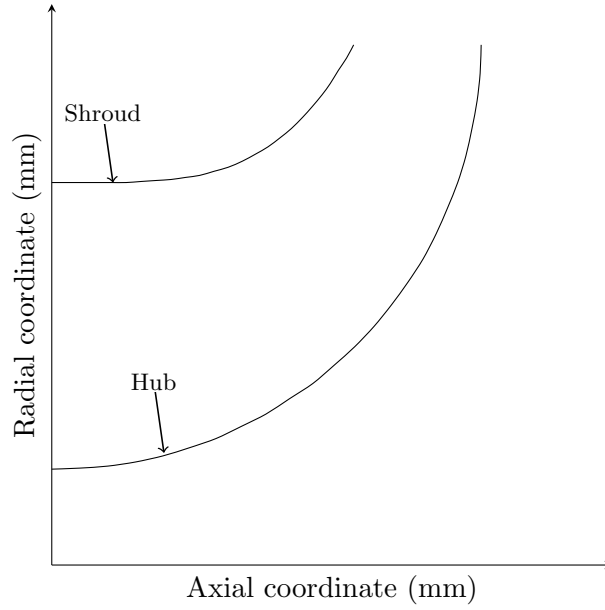
Figure 5.5.: The impeller contour plots of the preliminary design.

When the impeller has been sized, the aim is directed to the nozzle row. The nozzle row is sized with default settings except for the nozzle exit radius to impeller inlet radius ratio and the location of maximum camber. The radius ratio is lowered to make the overall size of the turbine smaller. The location of maximum camber is moved closer to the trailing edge to achieve a more even distribution of camberline blade angle. The specifications for the nozzle sizing are summarized in table 5.3 and they are derived in the appendix.

Table 5.3.: The specifications for the nozzle sizing.

Nozzle exit radius to rotor inlet radius, r_6/r_7	1.1
Camber angle, θ	0°
Location of maximum camber, a/c	0.65
Leading edge thickness to chord, t_4/c	0.025
Trailing edge thickness to chord, t_6/c	0.012
Maximum thickness to chord, t_{max}/c	0.06
Location of maximum thickness, d/c	0.4
Exit blade pitch to chord, s_6/c	0.75
Number of blades, N_N	#

A selection of results from the nozzle sizing is presented in table 5.4 (all angles are taken with respect to tangent). The nozzle-impeller interspace is compared to the correlation of

Wanabe et al and for the preliminary design it is 2.32 which is close to their suggested 2.0. The incidence angle is fairly small and should be satisfactory. The preliminary loading of 1.06 is according to Aungier, satisfactory. The nozzle camberline angle distribution and a cascade plot of the two nozzle blades can be seen in figures 5.6 and 5.7.

Table 5.4.: A selection of results from the nozzle sizing.

Inlet radius, r_4	65.3 mm
Exit radius, r_6	56.1 mm
Incidence angle	-0.4705°
Deviation angle	7.396°
Exit mach number, M_6	0.5492
Leading edge blade angle, β_4	33.13°
Trailing edge blade angle, β_6	12.6°
Nozzle radius ratio, r_4/r_6	1.165
Preliminary loading, $\Delta c/c$	1.06
Blade chord, c	23.5 mm
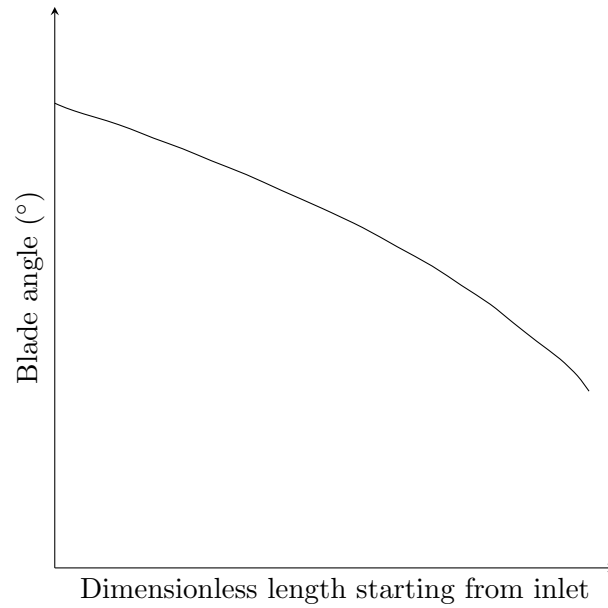
Figure 5.6.: The nozzle blades camberline angle distribution of the preliminary design.
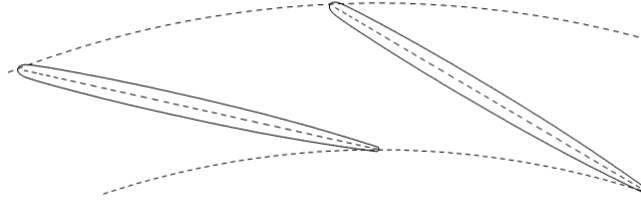
Figure 5.7.: The cascade plot of two nozzle blades of the preliminary design.

Finally the volute and diffusor are sized. It is necessary to achieve a smaller radius of the volute than the one of the second turbine to make the whole turbine smaller. This is accomplished with an external volute of elliptical size. The aspect ratio, A/B, is set to 1.15. The preliminary exhaust diffusor uses an area ratio of 1.5 giving a pressure recovery coefficient of 0.518. The mach number drops approximately 40 percent from diffusor inlet to diffusor outlet.

The gas used in the design is a mixture attempted to resemble an exhaust gas composition from a diesel engine. The mole fractions are summarized in table 5.5.

Table 5.5.: The mole fractions of the gas used.

Carbon dioxide, CO_2	0.12
Nitrogen, N_2	0.55
Oxygen, O_2	0.23
Water, H_2O	0.10

1-D performance analysis in RIFT

The preliminary design produced in the previous subsection is evaluated using the program "RIFT" which is a mean-line performance analysis tool. The results are presented as figures, 5.8 and 5.9 showing the stage total-to-total efficiency and the mass flow. To be able to make a qualitative comparison with the second turbine the same corrected speeds are used and no diffusor was incorporated.
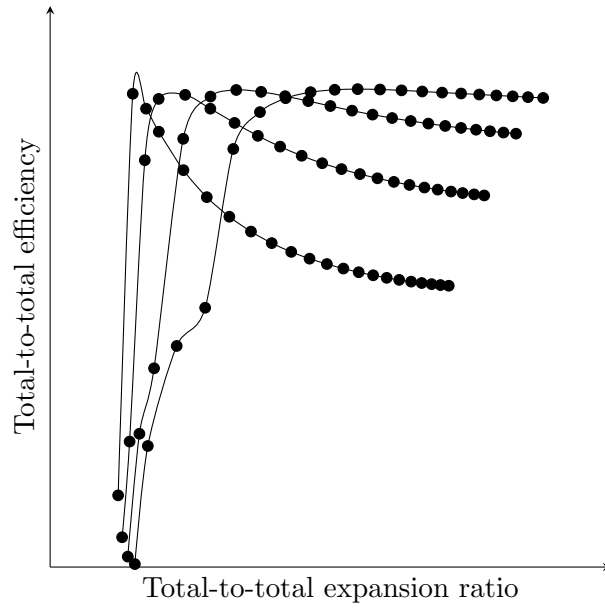
Figure 5.8.: Total-to-total efficiency as a function of total-to-total expansion ratio with different shaft speed lines.
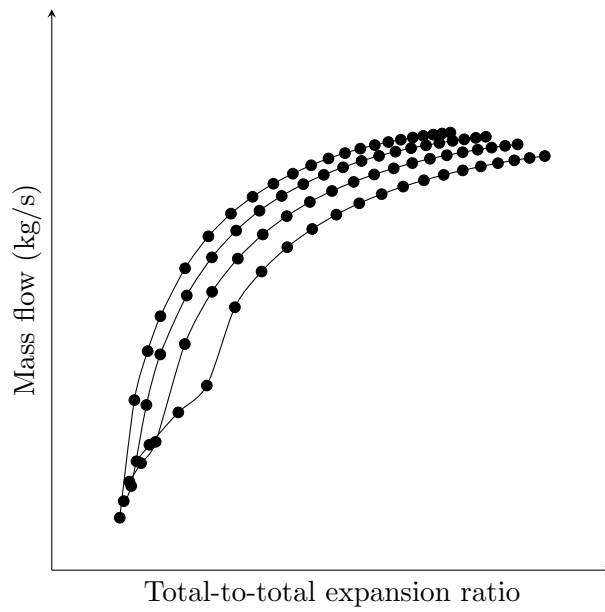

Figure 5.9.: Mass flow as a function of total-to-total expansion ratio with different shaft speed lines.

2-D blade to blade analysis

The preliminary design is thereafter analyzed in a blade-to-blade flow solver. The analyses are performed at the design point, one for the nozzle and one for the impeller.
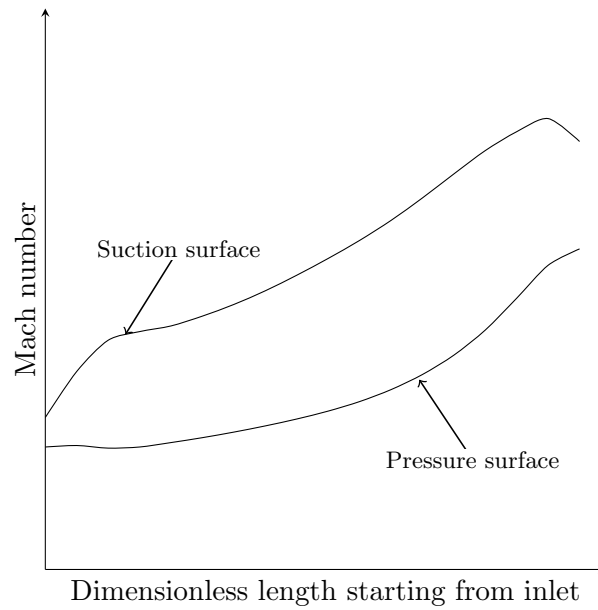
The blade loading diagram of the nozzle blade-to-blade analysis is presented in figure 5.10. The blade loading diagram from the rotor blade-to-blade analysis is presented in figure 5.11 and shows the mach number distribution on the hub and shroud contours' suction and pressure surfaces respectively.

Figure 5.10.: The blade loading diagram of the nozzle blade-to-blade analysis.
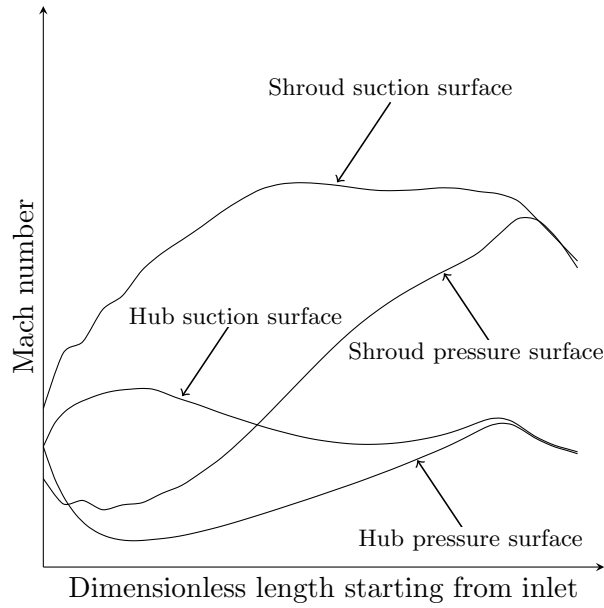
Figure 5.11.: The blade loading diagram of the rotor blade-to-blade analysis. The figure shows the mach number distribution of the hub and shroud suction and pressure surfaces respectively.

5.2. Detailed design

The preliminary design presented above showed satisfactory off-design performance but the blade loading diagram indicated a poor impeller shroud contour. In the detailed design an attempt is made to improve the design of the shroud velocity levels. It can be seen in figure 5.11 that the fluid is quickly accelerated on the suction side and then decelerated toward the trailing edge. However the fluid is also accelerated on the suction side and just before the trailing edge the flow is overturned and the blade force is reversed. It would be preferable to attain a slow to moderate acceleration on the suction surface and just before the trailing edge decelerate to meet the flow on the pressure surface and thereby minimize the deviation. An attempt was made to accomplish this by changing the camberline blade angles and the thickness distribution. These changes are presented in figures 5.12 and 5.13. It would be possible to alter the end wall contour but after reviewing the b/r_c distribution it was decided to leave it be. The flow on the hub side is not ideal but according to Aungier it is hardly possible to change this by adjusting the design. This is due to relatively low blade speeds and high blade angles. While this is true for the present case, the thickness is increased to protect the hub from centrifugal stresses and thereby ensuring the strength of the hub. The thickness of the hub contour at the trailing edge is decreased to insure a smoother transition at the exit. The hub camberline blade angles are changed to an inlet angle of 90 degrees (with respect to

tangent) to minimize the bending stresses. These changes are also demonstrated in figures 5.12 and 5.13. The blade loading diagram demonstrating the velocity on the nozzle suction and pressure surfaces shows a smooth acceleration on both these surfaces. This is decided to be satisfactory and no changes are made on the nozzle design.

The new impeller blade loading diagram is presented in figure 5.14 showing the velocity levels on the hub and shroud contours' suction and pressure surface respectively. An off-design performance analysis is also performed and a resulting comparison of the total-to-static efficiencies is presented in figure 5.17.
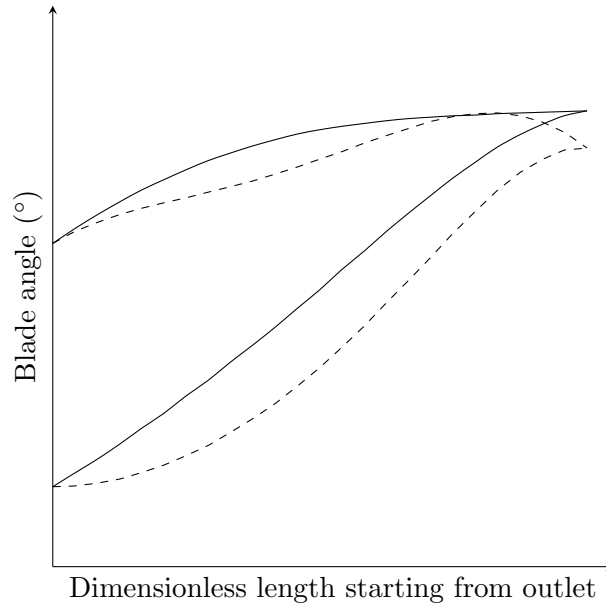

Figure 5.12.: A comparison of the blade angles for the preliminary and detailed design. The angles from the detailed design are presented with smooth lines while the angles from the preliminary design are presented with dashed lines.
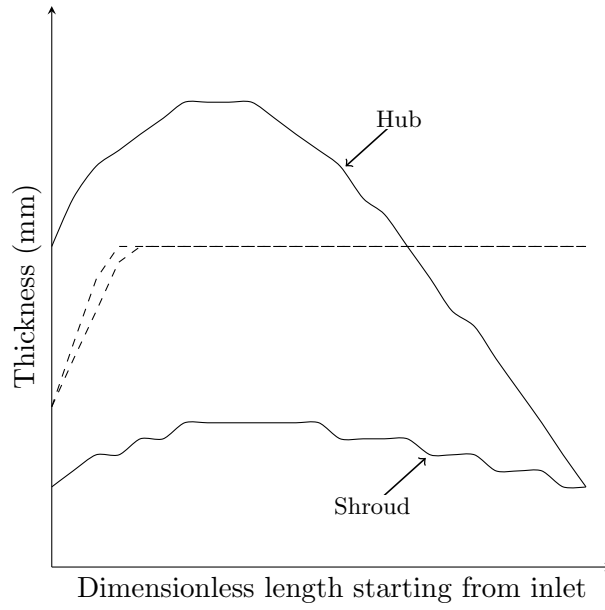
Figure 5.13.: A comparison of the thickness distribution for the preliminary and detailed design. The thickness distribution from the detailed design are presented with smooth lines while the thickness distribution from the preliminary design are presented with dashed lines.
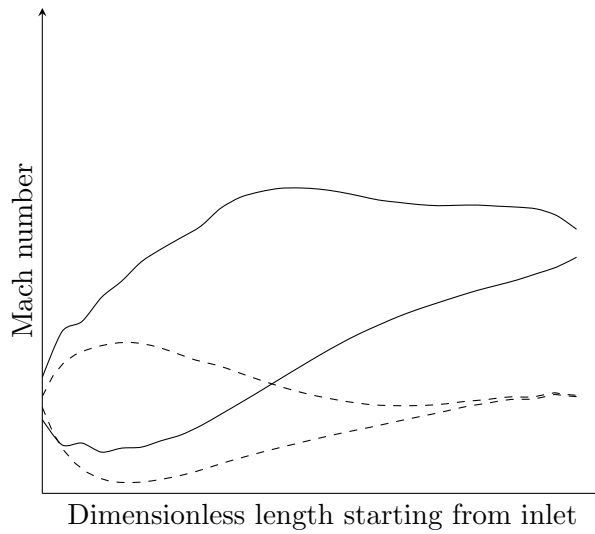

Figure 5.14.: The blade loading diagram of the rotor blade-to-blade analysis. The figure shows the mach number distribution of the hub (dashed) and shroud (smooth) suction and pressure surfaces respectively.
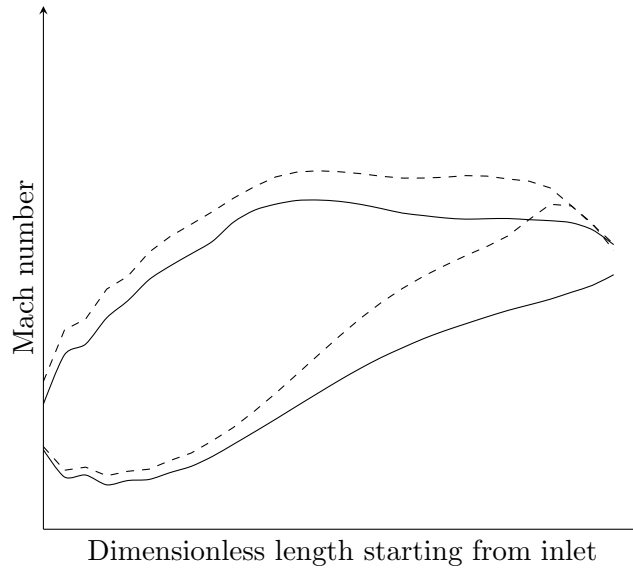
Figure 5.15.: Comparison of the preliminary and detailed design which shows the blade loading diagram for the shroud contour. Smooth lines correspond to detailed design and dashed lines to preliminary.
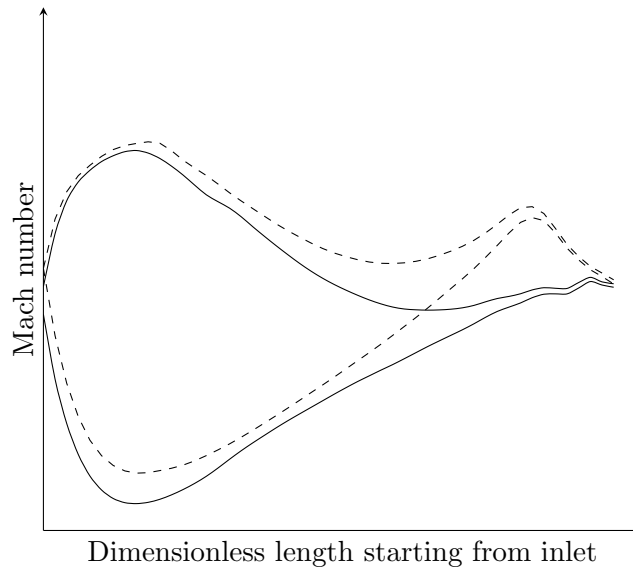

Figure 5.16.: Comparison of the preliminary and detailed design which shows the blade loading diagram for the hub contour. Smooth lines correspond to detailed design and dashed lines to preliminary.
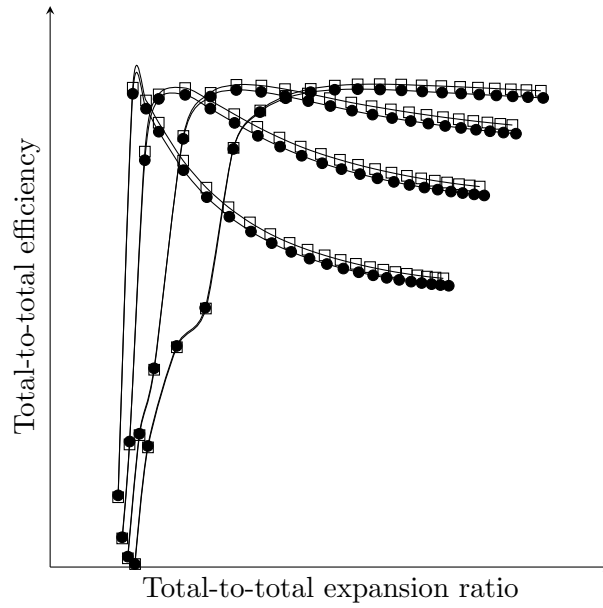
Figure 5.17.: The comparison of the total-to-total efficiency as a function of total-to-total expansion ratio for the preliminary (dots) and detailed design (squares).

5.3. Summary

In this chapter an aerodynamic design of a radial turbine is developed. This is accomplished in two steps. Initially a preliminary design is produced with the program "RIFTSIZE". The preliminary design is analyzed using a mean-line performance tool, "RIFT", and two blade-to-blade performance tools, "Q3D" and "TDB2B". Based on those analyses the design is revised resulting in a detailed design.

The preliminary design showed good off-design performance, however, from the blade-to-blade analyses it was possible to conclude that the velocity levels were not satisfactory. To remedy this, it was decided to change the blade angles and thickness distribution of the shroud and hub contours. The detailed design showed small improvement in off-design performance, however, the improvement of the velocity levels was extensive.

Finally a comparison can be made with the real second turbine. When comparing the total-to-total efficiency, it can be seen that the real turbine is slightly better. It should be clear that the effort and time which was put to develop the real turbine do not even come close to the time and effort spent on the turbine presented in this chapter. It is, therefore, possible to argue that the design tool "TurbAero" can be used to develop a good design in a relatively short amount of time with relatively small effort.

6. Conclusions

The main objective of this master thesis was to evaluate a tool for aerodynamic design and analysis. This has been conducted in two parts. The first part aimed to model the geometry and simulate the performance of two radial turbines and then compare the results with test data. In the second part an aerodynamic design of a radial turbine was developed. The results from the first part show that it is possible to simulate the performance of radial turbines using mean-line analyses (particularly with the tool used in this thesis, namely "TurbAero").

The tests, involved in the first part, were performed by Volvo and conducted in a cold rig for both turbines. Air was used as fluid in the tests and the inlet temperature was kept at $373\,\mathrm{K}$ (thereby making it "cold").

The first turbine was modeled in two cases, one in which the turbine was scaled (the turbine which Volvo performed tests on was also scaled) and all other conditions were attempted to resemble those which prevailed during the tests and one case with the original turbine and "hot" conditions. The simulations were performed in two cases to see the modeling differences that could arise. It is possible to see differences, particularly if comparing the two figures presenting the two cases' mass flows, figures 4.4 and 4.7. It was explained what influence the geometry and gas could have on the mass flow in section 4.1.3. The mass flow that can be brought through the turbine at a specific expansion ratio is mainly determined by the nozzle throat. It can be shown that for a change by one degree that the throat turns, the flow will lead to a change in mass flow by five percent [personal communication, Magnus Genrup, 2014]. This makes the flow very sensitive to changes of the throat's geometry. Best agreement in mass flow was achieved in the case which tried to resemble the conditions which prevailed during the tests (the first case). The total-to-total efficiency was measured using two different techniques in the tests, one measuring the torque on the shaft and one measuring the temperature and thereby the heat drop[1]. The results from the simulations show best agreement with the temperature measured total-to-total efficiency. The torque measured total-to-total efficiency, however, prove defective at small expansion ratios. There is no clear difference in total-to-total efficiency in the two different simulation cases, however, from the comparison in mass flow it can be concluded that it is best to perform simulations using similar conditions to the tests.

---

[1]The efficiency was then calculated using the torque and temperature.

After concluding that the modeling and simulating should be performed using similar conditions to the tests, the second turbine was modeled and simulated in this manner. The comparison in mass flow and total-to-total efficiency can be seen in figures 4.10 and 4.9. The results are similar to those of the first turbine, and shows that the good agreement, achieved for the first turbine, was not a coincidence. The total-to-total efficiency was only measured using the torque on the shaft in the tests on the second turbine, as opposed to the first turbine where the efficiency also was measured using the heat drop, and it can be seen that for small expansion ratios, there is fairly large discrepancy.

From the simulations it is concluded that there are a few parameters which have large influence on how the results from a simulation are affected. The surface roughness is hard to measure and it was estimated for the simulations. The same surface roughness was used for all components for both turbines. The first turbine's tip was scalloped, however, it is not possible to model that in "RIFT". It is assumed that the overestimating of the efficiency which this leads to is compensated by a to high surface roughness. Another feature which is often implemented in radial turbines is the usage of variable nozzle vanes. Neither this feature is possible to model in "RIFT".

The geometry which was used to model the turbines in "RIFT" was taken from the aerodynamic design. As mentioned in chapter 4.1.3 it is possible for errors to arise during either manufacturing or when the drawing is produced leading to that the simulated and tested geometry deviate from one another. The existence of measurement errors should not be underestimated and it should be clear that the results from the tests probably are not fully accurate, particularly when the turbines are run with small expansion ratios.

Finally it should be clear that, however good the results are, it would be naive to think that a mean-line analysis is able to predict the performance with the accuracy of a CFD analysis. Instead the mean-line analysis should be used as a quick way of estimating trends. With that in mind the results of this thesis are promising.

The second big objective of this thesis was to develop an aerodynamic design of a radial turbine similar to the design of the second turbine from the first part the thesis. This has been accomplished in two steps. First a preliminary design was produced. The off-design performance was simulated and a blade-to-blade analysis was performed at the turbine's design point. Based on the results from those analyses, the design was revised in a detailed design. The detailed design shows promise and it was developed with a relatively small amount of time and effort making the design tool preferable to use when designing radial turbines.

More studies should be performed to ensure the accuracy of the mean-line program, however, the results presented in this thesis are promising.

Bibliography

[1] J.D. Anderson Jr. *Fundamentals Of Aerodynamics SI.* McGraw-Hill, 2011.

[2] Ronald H Aungier. *Turbine aerodynamics: axial-flow and radial-inflow turbine design and analysis.* Amer Society of Mechanical, 2006.

[3] N Baines. Radial turbines: An integrated design approach. Technical report, Concepts NREC, 2005.

[4] O.E. Balje. *Turbomachines, A Guide to Design, Selection and Theory.* Wiley, New York., 1981.

[5] E.A. Baskharone. *Principles of Turbomachinery in Air-Breathing Engines.* Cambridge University Press, 2006.

[6] A. Carmichael. *The Aerodynamic Design of Axial-Flow and Radial-Inflow Turbines.* In Sawyer's Gas Turbine Engineering Handbook (Sawyer, J.W., editor), Gas Turbine Publications, Stamford, CT, Chapter 4., 1972.

[7] S.L. Dixon and C.A. Hall. *Fluid Mechanics and Thermodynamics of Turbomachinery.* Butterworth-Heinemann, 2010.

[8] Donald F. Young et al. *A brief introduction to fluid mechanics.* John Wiley and Sons, Inc, 2007.

[9] L.J. Herrig, J.C. Emery, and J.R. Erwin. *Systematic Two-Dimensional Cascade Tests of NACA 65-series Compressor Blades at Low Speeds.* Technical Note TN 3916, NACA, Washington, DC., 1957.

[10] S. Lieblein and W.H. Roudebush. *Theoretical Loss Relations For Low-Speed Two-Dimensional-Cascade Flow.* Technical Note TN 3662, National Advisory Committee For Aeronautics (NACA), Washington, DC., 1956.

[11] H. Maki and Y. Mori. *On the study of the flow through an impeller of mixed and inward flow radial turbines.* Bull JSME 16(91): 81-92, 1973.

[12] Hany Moustapha, Mark F Zelesky, Nicholas C Baines, and David Japikse. *Axial and radial turbines*, volume 2. Concepts NREC Wilder, VT, 2003.

[13] J. Nikuradse. *Laws of Resistance and Velocity Distributions for Turbulent Flow of Water in Smooth and Rough Pipes.* Proceedings 3rd International Congress for Applied MEchanics, Stockholm, Sweden, pp. 239-248, 1930.

[14] S. Pai. *Viscous flow theory, I-Laminar flow.* Van Nostrand, Princeton, NJ, 1956.

[15] S. Pai. *Viscous flow theory, I-Turbulent flow.* Van Nostrand, Princeton, NJ, 1957.

[16] Xuwen Qiu, Mark R. Anderson, and Nicholas C. Baines. *MEANLINE MODELING OF RADIAL INFLOW TURBINE WITH VARIABLE AREA NOZZLE.* Proceedings of ASME Turbo Expo 2009: Power for Land, Sea and Air GT2009, 2009.

[17] A. Romagnoli, C.D. Copeland, R. Martinez-Botas, M. Seiler, S. Rajoo, and A. Costall. *Current Technology of Radial-Inflow Turbines for Compressible Fluids.* Journal of Turbomachinery 135(1), paper no: Turbo-11-1184, 2011.

[18] H.J. Wood. *Current Technology of Radial-Inflow Turbines for Compressible Fluids.* Trans. ASME, Journal of Engineering for Power, pp. 72-83, 1963.

A. Preliminary Design

The work leading up to this point has mostly been performed with the program "Tur-bAero". The design process which is conducted in "TurbAero", most often starts with the program "RIFTSIZE". It has already been described how the designer will return to "RIFTSIZE" multiple times to check his or her design. In light of this, I thought it would be fitting to try to implement the equations in [2], which, according to Aungier, is the basis of "RIFTSIZE". The choice on platform fell on MATLAB$^{\circledR}$ and its build-in graphical user interface, "GUI".

The main task of the program is to, with as little input parameters as possible and as fast as possible, construct a preliminary design of a radial turbine. This will help the designer to quickly get a candidate design which will come close to meet the performance requirements.

Most of the equations are presented in chapter 3, however, the steps are not as thoroughly investigated as would be convenient if an attempt to redo this work were to be made. Because of this, I have chosen to present all the equations and steps which are conducted. This will also help in the process, in which possible errors can be corrected. The schemes which are used to numerically solve the equations that include differential terms will be presented. Also where it were required to used iteration loops, an explanation of how that was done is included.

The program goes through the following steps. Initially the impeller tip is sized. The designer can then choose to use default values, which are presented below, to construct the rotor and stator geometry, or he can change the default values according to his own preferences. Finally the volute can be designed. If the incorporation of an exhaust diffusor is preferable, it is easily accomplished by the designer. In the following sections, I will go through each part which the program are consisting of.

Impeller

To initiate the design process, the designer is asked to specify the following input parameters. The stage inlet total temperature and pressure, the stage mass flow, the stage total to static expansion ratio and the speed. Concerning the speed, he needs to choose

whether he wants to use the rotational speed or if he would like to use the concept of specific speed. Depending on which he chooses, different methodologies will be used to size the impeller tip. To make the implementations a great deal easier, I decided to use the concept of perfect gas as flow media. This does not only simplify the implementations but also makes the life a bit easier for the designer, who only needs to specify the specific heat (at constant pressure) and the ratio of the specific heats of the gas which the turbine is supposed to run with. The drawback of assuming that the gas is perfect is that the calculations are not as accurate as they would be if a more sophisticated gas model would be implemented. The control panel which meets the user is shown in figure

Figure A.1.: The design of the impeller in the radial turbine is control by certain input parameters. These are presented to the user in the impeller control panel.

With these input parameters, the impeller tip is sized using the following relations. All equations are taken from R.H. Aungier's book - "Turbine Aerodynamics - Axial-flow and radial-inflow turbine design and analysis" [2].

The static pressure at the impeller exit is calculated using the total to static expansion ratio and the total inlet pressure.

$$p_9 = \frac{p_{01}}{p_{01}/p_9} \tag{A.1}$$

Assuming that the flow through the turbine is adiabatic it can be stated that the total temperature at the impeller tip is equal to the stage inlet total temperature and since it has been assumed that the gas is perfect the total enthalpy is easily determined.

$$T_{07} = T_{01} \tag{A.2}$$

$$h_{01} = h_{07} = c_p T_{01} \tag{A.3}$$

It can be shown that for a perfect gas the following relationship holds

$$R = c_p \left(1 - \frac{1}{\gamma} \right) \tag{A.4}$$

Where, R, is the gas constant and γ is the ratio of specific heats.

$$R = \frac{R_u}{M} \quad \text{J/kg K} \tag{A.5}$$

$$\gamma = \frac{c_p}{c_v} \tag{A.6}$$

The spouting velocity is determined, using the definition which where stated in chapter 3. It is rewritten here.

$$c_{0s} = \sqrt{2\Delta h_{0,ideal}} \tag{A.7}$$

The ideal total enthalpy drop, $\Delta h_{0,ideal}$ can be calculated using an isentropic efficiency of unity.

$$\eta = \frac{h_{01} - h_{09}}{h_{01} - h_{09,s}} = \frac{c_p T_{01} - c_p T_{09}}{c_p T_{01} - c_p T_{09,s}} \tag{A.8}$$

$$\Leftrightarrow$$

$$\frac{T_{09}}{T_{01}} = \left(\frac{p_{09}}{p_{01}} \right)^{\frac{\gamma-1}{\gamma}} \Rightarrow T_{09} = T_{01} \left(\frac{p_{09}}{p_{01}} \right)^{\frac{\gamma-1}{\gamma}} \tag{A.9}$$

$$\Rightarrow \Delta h_0 = c_p(T_{01} - T_{09}) = c_p T_{01} \left[1 - \left(\frac{p_{09}}{p_{01}} \right)^{\frac{\gamma-1}{\gamma}} \right] \tag{A.10}$$

Depending on whether the designer is choosing to specify a rotational speed or a specific speed, different ways of calculating the conditions at the impeller tip have to be conducted. If he is choosing to specify a rotational speed an iterative approach has to be undertaken, however, if the choice fall on the specific speed, a direct approach is possible.

Specific speed

If the specific speed is chosen as speed variable it is possible to apply a direct calculation scheme. The total to static velocity ratio, ν_{t-s} was defined in chapter 3 as the ratio of blade speed to spouting velocity.

$$\nu_{ts} = \frac{U}{c_{0s}} \tag{A.11}$$

In Aungier's book , [2], he provides two equations which correlates the total to static velocity ratio and the total to static efficiency as functions of specific speed.

$$\nu_{ts} = 0.737 N_s^{0.2} \tag{A.12}$$

$$\eta_{ts} = 0.87 - 1.07(N_s - 0.55)^2 - 0.5(N_s - 0.55)^3 \tag{A.13}$$

The equations are plotted in figure A.2. When the total to static velocity ratio and the spouting velocity are calculated the blade tip speed is given by.

$$U_7 = \nu_{ts}\, c_{0,s} \tag{A.14}$$

The total enthalpy and temperature at the impeller outlet can be calculated using the stage inlet total enthalpy, the ideal heat drop, the total to static efficiency, given by equation (A.13) and the specific heat.

$$h_{09} = h_{01} - \Delta h_{0,ideal}\eta_{ts} \tag{A.15}$$

$$T_{09} = c_p T_{09} \tag{A.16}$$

Since I have chosen to use a perfect gas the ideal gas law can be applied. From it the density at the impeller outlet is calculated.

$$\rho_9 = \frac{p_9}{RT_9} \tag{A.17}$$

Since it is not possible to determine the static temperature, T_9, without applying some loss model the density will have to approximated using the total temperature, T_{09} instead of the static temperature. This can be said not to influence the results greatly because the absolute velocity at the impeller outlet should be kept low to yield a proper design.
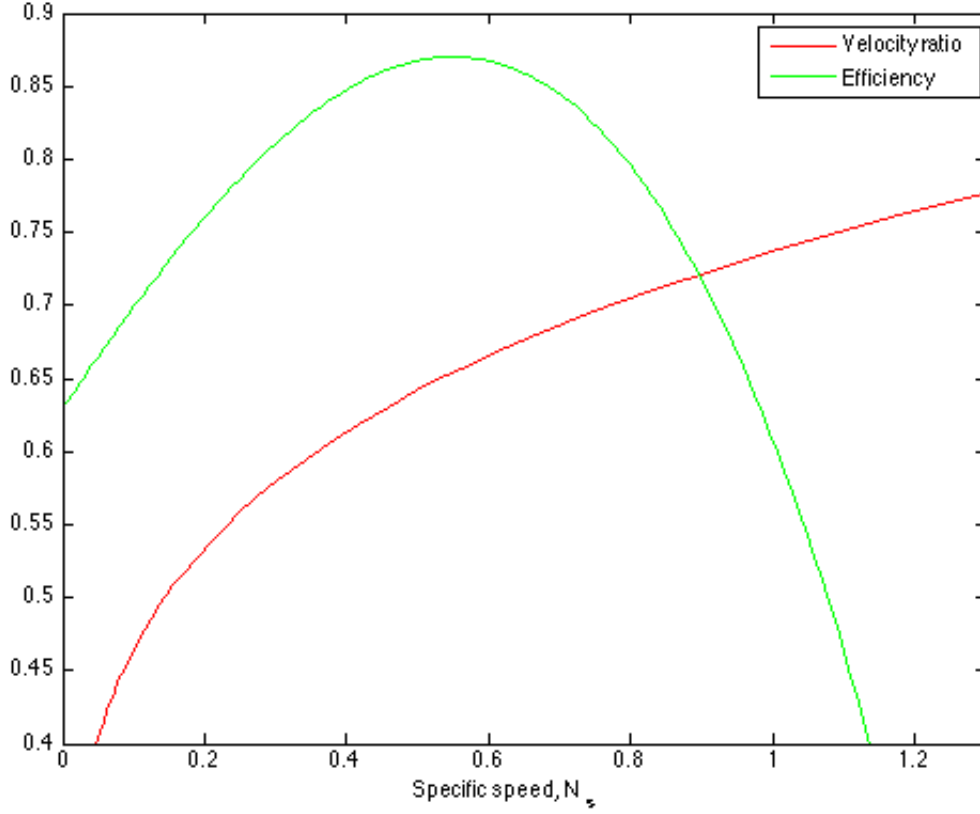
Figure A.2.: The equations, (A.12) and (A.13) are plotted against specific speed. They are used in the preliminary design process.

The density is needed to calculate the volume flow at the impeller outlet, which following the discussion outlined above will only be approximate.

$$Q_9 = \frac{\dot{m}}{\rho_9} \tag{A.18}$$

The specific speed and the rotational speed are related according to.

$$N = \frac{N_s(\Delta h_{0,ideal})^{3/4}}{Q_9^{1/2}} \tag{A.19}$$

From the rotational speed, the radius at the tip can be determined.

$$r_7 = \frac{U_7}{N} \tag{A.20}$$

Finally the total pressure and the tangential velocity at the tip are determined. To calculate the total pressure at the tip I am using the relationship found in [2].

$$\rho_{01} = \frac{p_{01}}{RT_{01}} \tag{A.21}$$

$$p_{07} = p_{01} - \rho_{01}\Delta h_{0,ideal}\frac{1 - \eta_{ts}}{4} \tag{A.22}$$

The tangential velocity at the impeller tip is approximated using the assumption that the flow at the outlet of the impeller is entirely meridional, giving: $c_{9\theta} = 0$.

$$\Delta h_0 = U_7 c_{7\theta} - U_9 c_{9\theta} = U_7 c_{7\theta} \tag{A.23}$$

$$\Rightarrow c_{7\theta} = \frac{\Delta h_0}{U_7} = \frac{\Delta h_{0,ideal}\,\eta_{ts}}{U_7} \tag{A.24}$$

Rotational speed

While the method of sizing the tip when the specific speed is used as input variable is a direct one, an iterative manner has to be conducted when the rotational speed is provided. Initially a guess of the specific speed is made. This guess will be updated until the iteration converge on the specific speed. The equations used are the following.

$$\eta_{ts} = 0.87 - 1.07(N_s - 0.55)^2 - 0.5(N_s - 0.55)^3 \tag{A.25}$$

$$h_{09} = h_{01} - \Delta h_{0,ideal}\,\eta_{ts} \tag{A.26}$$

$$T_{09} = \frac{h_{09}}{c_p} \tag{A.27}$$

$$\rho_{09} = \frac{p_9}{RT_{09}} \tag{A.28}$$

$$Q_9 = \frac{\dot{m}}{\rho_{09}} \tag{A.29}$$

$$N_s = \frac{N\sqrt{Q_9}}{\Delta h_{0,ideal}^{0.75}} \tag{A.30}$$

When the specific speed is determined the total to static velocity ratio, the tip blade speed, the tip radius, the tip total pressure and the tip tangential velocity will be calculated using equations (A.12), (A.14), (A.20), (A.21), (A.22) and (A.24). This completes the sizing of the impeller tip.

The designer will now proceed with the geometrical design of the impeller. I have, just like in "RIFTSIZE", chosen to let the user decided whether to use the default values provided by Aungier or to specifies the variables. The benefit of using the default values

as a starting point in the design is that in that it is possible to relatively quickly attain a reasonable design which later can be revised. The variables which are considered are the impeller inlet absolute flow and blade angles, the leading and trailing edge thicknesses, the hub and shroud outlet radius, the axial length of the impeller and finally the number of blades. While in "RIFTSIZE" it is possible to include splitter blades, I have chosen not to implement that detail here. Whether the designer choice fall on using the default values or not the implementation is slightly different. I will present both approaches.

Input variables according to default values

The process of providing default values to the user takes on an initial stating of almost every input variable according to correlation taken from [2], except the inlet blade angle which has to be determined in an iterative manner taking the optimal incidence angle into account. Initially the flow angle is approximated using the specific speed (all angles are taken with respect to tangent). Then the leading and trailing edge thicknesses and the hub radius at the outlet are calculated as functions of the tip radius.

$$\alpha_7 = 10.8 + 14.2N_s^2 \tag{A.31}$$

$$t_7 = 0.04r_7 \tag{A.32}$$

$$t_9 = 0.02r_7 \tag{A.33}$$

$$r_{9h} = 0.185r_7 \tag{A.34}$$

The meridional velocity at the tip can be determined using the absolute flow angle and tangential velocity. Next it is possible to calculate the absolute velocity and afterwards the other flow conditions at the tip including the static temperature, pressure and density and the corresponding mach number. The cross sectional width is needed to calculate

the exit meridional velocity and is determined using a mass balance at the tip.

$$c_{7m} = c_{7\theta} \tan \alpha_7 \tag{A.35}$$

$$c_7 = \sqrt{c_{7m}^2 + c_{7\theta}^2} \tag{A.36}$$

$$T_7 = T_{07} - \frac{c_7^2}{2c_p} \tag{A.37}$$

$$M_7 = \frac{c_7}{\sqrt{\gamma R T_7}} \tag{A.38}$$

$$p_7 = p_{07} \left(\frac{T_7}{T_{07}} \right)^{\frac{\gamma}{\gamma-1}} \tag{A.39}$$

$$\rho_7 = \frac{p_7}{R T_7} \tag{A.40}$$

$$b_7 = \frac{\dot{m}}{2\, r_7\, \pi\, c_{7m}\, \rho_7} \tag{A.41}$$

The calculation at the outlet follows a similar approach. The meridional velocity is calculated using a relationships which Aungier explains in the following way.

The exit shroud radius and axial length are selected based on maintaining a reasonable ratio of passage width-to-the flow path radius of curvature. The following procedure has been found effective in estimating values for these parameters that achieve that goal.

The following equations estimates the flow conditions at the outlet and determines the values of the axial length, the shroud radius, the width and the number of blades.

$$c_{9m} = c_{7m} \left[1 + 5 \left(\frac{b_7}{r_7} \right)^2 \right] \tag{A.42}$$

$$c_{9\theta} = 0 \Rightarrow c_9 = c_{9m} \tag{A.43}$$

$$T_9 = T_{09} - \frac{c_9^2}{2c_p} \tag{A.44}$$

$$p_{09} = p_9 \left(\frac{T_{09}}{T_9} \right)^{\frac{\gamma}{\gamma-1}} \tag{A.45}$$

$$M_9 = \frac{c_9}{\sqrt{\gamma R T_9}} \tag{A.46}$$

$$\rho_9 = \frac{p_9}{R T_9} \tag{A.47}$$

$$r_{9s} = \sqrt{r_{9h}^2 + \frac{\dot{m}}{\pi c_{9m} \rho_9}} \tag{A.48}$$

$$b_9 = r_{9s} - r_{9h} \tag{A.49}$$

$$r_9 = \frac{r_{9s} + r_{9h}}{2} \tag{A.50}$$

$$\Delta Z_R = 1.5(r_{9s} - r_{9h}) \tag{A.51}$$

$$N_R = 12 + 0.03(33° - \alpha_7)^2 \tag{A.52}$$

The inlet blade angle has to be calculate. I have chosen to let the default value of this angle be the one at which optimum incidence occur. This is the same practice which Aungier uses. The optimum incidence angle is derived from the definition of slip factor which often is mentioned when discussing centrifugal compressors. The blade angle is then derived from an iterative process which takes the metal blockage at the inlet into

account. The procedure is shown below.

$$\sigma = 1 - \frac{\sqrt{\sin \beta_7}}{N_R^{0.7}} \tag{A.53}$$

$$K_{B7} = 1 - \frac{N_r \, t_{B7}}{2 \, \pi \, r_7 \, \sin \beta_7} \tag{A.54}$$

$$c_{7\theta}^* = \sigma \left(U_7 - \frac{c_{7m} \cot \beta_7}{K_{B7}} \right) \tag{A.55}$$

$$i_7^* = \beta_7 - 90° + \tan^{-1} \left(\frac{(U_7 - c_{7\theta}^*)K_{B7}}{c_{7m}} \right) \tag{A.56}$$

$$i_7 = \beta_7 - 90° + \tan^{-1} \left(\frac{(U_7 - c_{7\theta})K_{B7}}{c_{7m}} \right) \tag{A.57}$$

The default inlet blade angle occur when the incidence angle, i, is equal to the optimum incidence angle, i^*. It is my intent to give the user of the program as much information as possible, and due to that fact the designer will be given values on the following parameters. The outlet blade speed, relative velocity, relative mach number, flow and blade angles and the pitch. At the inlet the relative velocity and the corresponding mach number are given. The throat is a very important component and the blade to blade width at throat is provided. The throat is calculated differently depending on whether the relative mach number, $M_{9,rel}$, is exceeding unity or not.

$$M_{9,rel} \leqslant 1 \quad \Rightarrow \quad o_9 = \frac{s_9 \, c_{9m}}{w_9} \tag{A.58}$$

$$M_{9,rel} > 1 \quad \Rightarrow \quad o_9 = s_9 \frac{\rho_9 c_{9m}}{\rho_* w_*} \tag{A.59}$$

In equation (A.59), ρ_* and w_*, are the density and relative velocity at sonic conditions. Finally the designer will be given information about the power and efficiency. The parameters just described are not difficult to calculate and the equations are omitted here.

Input variable according to the designer

If the designer feels that he has got adequate knowledge about how the impeller should be designed or if he would like to vary some of the parameters from the default values it is possible in this program. Naturally the calculation procedure takes a different coarse of action than the one I have used in the previous case. Initially the meridional velocity is calculated using equation (A.35), then the absolute velocity at the tip is followed using equation (A.36). Because the inlet blade angle now is specified, the parameters defined in equations (A.53)-(A.57) can be determined without having to use the iterative procedure. The equations (A.37), (A.38), (A.39), (A.40) and (A.41) can be applied to

give the static temperature, mach number, static pressure and density and width at the tip. While the outlet mean radius and width are given directly by the input parameter according to equations (A.60) and (A.61), the other flow conditions at the outlet, given by equations (A.44),(A.45),(A.47) and (A.46) together with a mass balance given by equation (A.62) yielding the outlet meridional velocity, require an iterative procedure to converge on the outlet static density.

$$r_9 = \frac{r_{9h} + r_{9s}}{2} \tag{A.60}$$

$$b_9 = r_{9s} - r_{9h} \tag{A.61}$$

$$c_{9m} = \frac{\dot{m}}{2\,\pi\,r_9\,b_9\,\rho_9} \tag{A.62}$$

$$c_{9\theta} = 0 \quad \Rightarrow \quad c_9 = c_{9m} \tag{A.63}$$

When these parameters are calculated the procedure follows the same as the one discussed in the previous section. Special care have to be taken regarding the flow conditions at the throat. This was mention above and the equations (A.58) and (A.59) are used now as well. With all the variables described thus far it is possible to construct the impeller end wall geometry, camberline and blade angles.

Impeller geometry construction

The procedure follows the one presented by Aungier in [2, p. 244-248]. Since it follows the same procedure the interested reader is referred to the original text. I am only interested in presenting the sections where numerical schemes are used. It involves three equations. One describing how the meridional distance is integrated along the impeller blade, one describing the blade angles along the hub and shroud camberline and one describing the curvature. The meridional distance is integrated using a first order discretization scheme given by.

$$dm = \sqrt{dz^2 + dr^2} \tag{A.64}$$

$$m_i - m_{i-1} = \sqrt{(z_i - z_{i-1})^2 + (r_i - r_{i-1})^2} \tag{A.65}$$

Since the inlet and outlet blade angles are given at this point, the equation yielding the blade angles are discretized following a second order finite approximation given by.

$$\cot \beta = r\,\frac{\partial \theta}{\partial m} \tag{A.66}$$

$$\cot \beta_i = r_i\,\frac{\theta_{i+1} - \theta_{i-1}}{m_{i+1} - m_{i-1}} \tag{A.67}$$

The calculation of the curvature distribution is derived from the simple equation describing curvature of any curve. The equation can be found in for example J.D. Anderson Jr. "Fundamentals Of Aerodynamics SI", [1] and is stated as.

$$\kappa = \frac{\partial \phi}{\partial s} \tag{A.68}$$

The radius of curvature is simply taken as the inverse, $R_c = 1/\kappa$. Firstly the angle is approximated using a first order finite approximation.

$$\phi_i = \tan^{-1} \frac{r_i - r_{i-1}}{z_i - z_{i-1}} \tag{A.69}$$

Then κ is approximated using a second first order finite approximation.

$$\kappa_i = \frac{\phi_i - \phi_{i-1}}{s_i - s_{i-1}} \tag{A.70}$$

The derivatives are a very unsteady when $\Delta s \to \infty$ and to solve that problem I have chosen to use a mean value of the curvature taken at intervals with steps of 3.3 percent of the total line segment.

Results

Following the calculations the designer is faced with the results in four different ways. The geometry is presented as plots and data. The plots are showing the contours, the blade angles, the passage area distribution, the curvature and the passage width distribution. It is also possible to keep the old graphs and compare them with graphs from a new calculation. General flow data and geometry are presented under "Overall results". Under "Overall results" the designer is also provided with parameters which can be used to evaluate the design. It is also possible for the user to see the specifications resulting from the default values defined above. They can be viewed under "Updated specifications". Examples of the result panels are shown in figure A.3, A.4
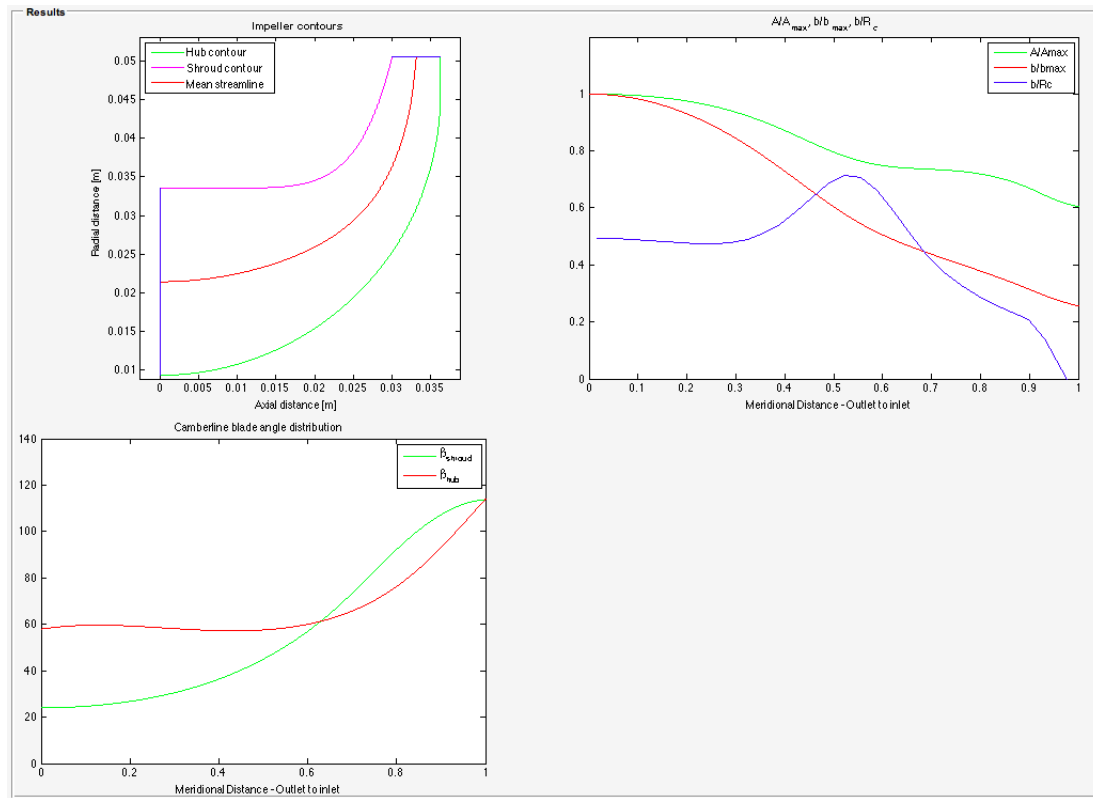
Figure A.3.: To allow the designer to evaluate the design the program provides graphical plots showing key parameters as functions of the meridional distance. The plots are showing the contours, the blade angles, the passage area distribution, the curvature and the passage width distribution.

Figure A.4.: To allow the designer to evaluate the design the program provides overall results showing flow conditions at key stations.

	Shroud					Hub			
m	z	r	theta	Beta	m	z	r	theta	Beta
0.0000	0.0000	0.0375	0.0000	27.2458	0.0000	0.0000	0.0094	0.0000	63.9813
0.0015	0.0015	0.0375	4.4877	27.3684	0.0029	0.0029	0.0095	8.3198	64.7764
0.0030	0.0030	0.0375	8.9293	27.7265	0.0057	0.0057	0.0097	16.2886	65.1609
0.0045	0.0045	0.0375	13.2828	28.3118	0.0086	0.0085	0.0102	23.9063	65.1790
0.0061	0.0061	0.0375	17.5101	29.1225	0.0115	0.0113	0.0108	31.1730	64.8937
0.0076	0.0076	0.0376	21.5776	30.1620	0.0143	0.0141	0.0117	38.0885	64.3730
0.0091	0.0091	0.0376	25.4557	31.4378	0.0172	0.0167	0.0127	44.6531	63.6866
0.0106	0.0106	0.0377	29.1191	32.9607	0.0200	0.0193	0.0139	50.8665	62.9030
0.0121	0.0121	0.0379	32.5468	34.7443	0.0229	0.0218	0.0153	56.7289	62.0876
0.0136	0.0136	0.0381	35.7219	36.8042	0.0258	0.0243	0.0168	62.2402	61.3016
0.0151	0.0151	0.0384	38.6319	39.1578	0.0286	0.0265	0.0185	67.4005	60.6014
0.0167	0.0165	0.0388	41.2682	41.8238	0.0315	0.0287	0.0204	72.2097	60.0385
0.0182	0.0180	0.0394	43.6267	44.8206	0.0344	0.0308	0.0224	76.6678	59.6607
0.0197	0.0193	0.0400	45.7075	48.1630	0.0372	0.0326	0.0246	80.7749	59.5131
0.0212	0.0207	0.0407	47.5147	51.8554	0.0401	0.0344	0.0268	84.5309	59.6404
0.0227	0.0219	0.0416	49.0569	55.8794	0.0429	0.0360	0.0292	87.9358	60.0884
0.0242	0.0231	0.0426	50.3467	60.1790	0.0458	0.0374	0.0317	90.9897	60.9067
0.0258	0.0242	0.0436	51.4010	64.6455	0.0487	0.0386	0.0343	93.6925	62.1509
0.0273	0.0252	0.0447	52.2410	69.1092	0.0515	0.0397	0.0370	96.0443	63.8843
0.0288	0.0262	0.0459	52.8920	73.3429	0.0544	0.0405	0.0397	98.0450	66.1791
0.0303	0.0271	0.0471	53.3836	77.0793	0.0573	0.0412	0.0425	99.6946	69.1156
0.0318	0.0279	0.0484	53.7496	80.0332	0.0601	0.0417	0.0453	100.9931	72.7770
0.0333	0.0287	0.0496	54.0279	81.9202	0.0630	0.0420	0.0481	101.9406	77.2385
0.0398	0.0301	0.0505	66.5522	113.7813	0.0619	0.0363	0.0505	103.4359	113.6932

Figure A.5.: To allow the designer to evaluate the design the program provides the geometry as data.

Nozzle

The nozzle geometry can be constructed once the impeller design is completed. I have chosen to minimize the number of variables which are open to the designer to vary. The control panel which the user is faced with is shown in figure A.6. The user can either choose to specify values and run the analysis directly or the user can calculate input variables which are suitable by clicking on "Calculate default input variables". The input variables are summarized and can be found in table A.1.

Table A.1.: The design of the nozzle blades in the radial turbine is controlled by certain input parameters. In this program I have chosen to minimize them, however, they are still a few which have to be specified. They are presented in this table.

Nozzle exit to rotor inlet radius ratio	r_6/r_7
Camber angle, relative to straight blade	θ
Location of maximum camber normalized by the chord length	a/c
Leading edge thickness normalized by the chord length	t_4/c
Trailing edge thickness normalized by the chord length	t_6/c
Maximum thickness normalized by the chord length	t_{max}/c
Location of maximum thickness normalized by the chord length	d/c
Trailing edge pitch normalized by the chord length	s_6/c
Number of nozzle blades	N_N

Figure A.6.: The design of the nozzle blades in the radial turbine is controlled by certain input parameters. In this program I have chosen to minimize them, however, they are still a few which have to be specified. They are presented to the user in the nozzle control panel.

The calculations are initiated with the construction of the nozzle blade camberline given by equation (A.71). This equation are then normalized by the blade chord yielding equation (A.72). After some sifts in equation (A.72) it can be written as in equation (A.73). Now equation (A.73) is solved from $x/c = 0$ to $x/c = 1$ while at every point the

solution is converged on the right y-value.

$$x^2 + \frac{c - 2a}{b}xy + \frac{(c - 2a)^2}{4b^2}y^2 - cx - \frac{c^2 - 4ac}{4b}y = 0 \qquad (A.71)$$

$$\left(\frac{x}{c}\right)^2 + \frac{1 - 2\frac{a}{c}}{\frac{b}{c}}\frac{x}{c}\frac{y}{c} + \frac{\left(1 - 2\frac{a}{c}\right)^2}{4\left(\frac{b}{c}\right)^2}\left(\frac{y}{c}\right)^2 - \frac{x}{c} - \frac{1 - 4\frac{a}{c}}{4\frac{b}{c}}\frac{y}{c} = 0 \qquad (A.72)$$

$$\frac{y}{c} = \left(\frac{x}{c}\left[1 - \frac{x}{c}\right]\right) \Big/ \left(\frac{(1 - 2(a/c))^2}{4(b/c)^2}\frac{y}{c} + \frac{1 - 2(a/c)}{b/c}\frac{x}{c} - \frac{1 - 4(a/c)}{4(b/c)}\right) \qquad (A.73)$$
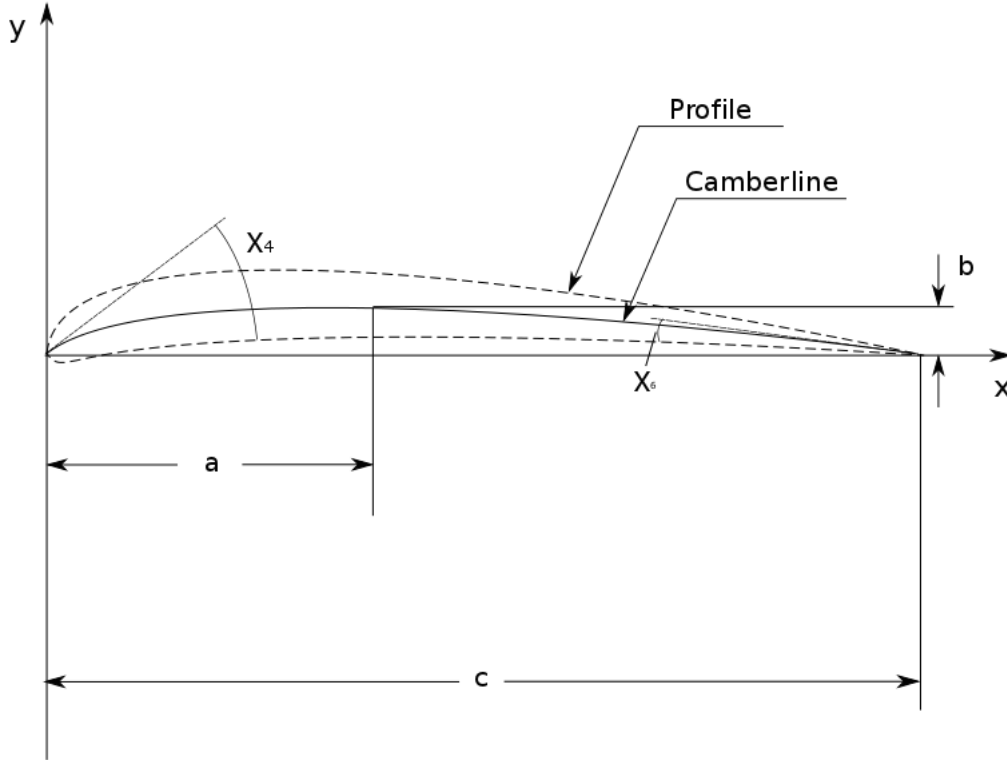

Figure A.7.: The notation and geometry used when designing the nozzle blades. Adapted from Aungier [2].

The blade geometry is completed once the suction and pressure surfaces are attained. They are constructed by adding a thickness distribution which superimposes the camberline. The equations describing the thickness can be obtained from Aungier's book, however, his equations do not yield a smooth distribution at the trailing edge and instead I have chosen to make some adjustment to his equations and normalized them by

the chord length.

$$\xi/c = \frac{x/c}{d/c}; \quad x/c \le d/c \tag{A.74}$$

$$\xi/c = \frac{1 - x/c}{1 - d/c}; \quad x/c > d/c \tag{A.75}$$

$$t_{ref}/c = t_4/c + (t_6/c - t_4/c)\, x/c \tag{A.76}$$

$$e = \sqrt{0.4 d/c}(0.03(1 - x/c)(1 - \xi/c) + 0.97) \tag{A.77}$$

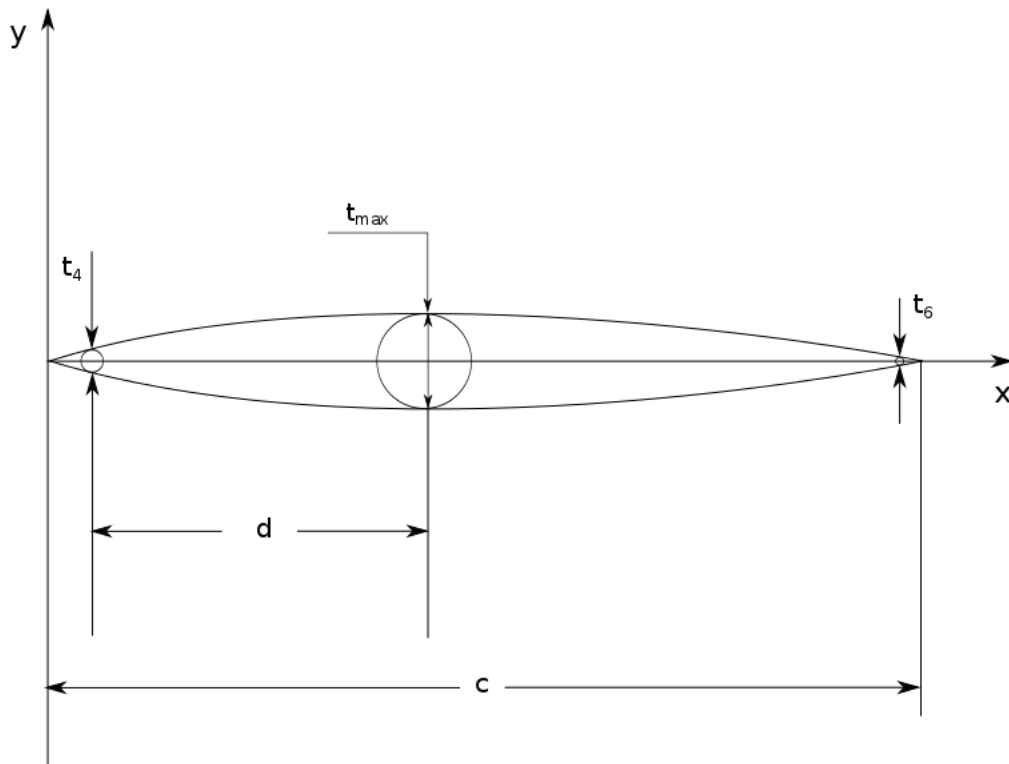$$t = t_{ref}/c + (t_{max}/c - t_{ref}/c)(\xi/c)^e \tag{A.78}$$

Figure A.8.: The thickness distribution and notation used when designing the nozzle blades. Adapted from Aungier [2].

The suction and pressure surfaces are now given by.

$$x_p/c = x_c/c + \frac{1}{2}t/c \sin\chi \tag{A.79}$$

$$y_p/c = y_c/c - \frac{1}{2}t/c \cos\chi \tag{A.80}$$

$$x_s/c = x_c/c - \frac{1}{2}t/c \sin\chi \tag{A.81}$$

$$y_s/c = y_c/c + \frac{1}{2}t/c \cos\chi \tag{A.82}$$

$$\tan\chi = \frac{\partial(y_c/c)}{\partial(x_c/c)} \tag{A.83}$$

The angle χ is calculated using a second order finite difference approximation.

$$\chi_i = \frac{y_{c,i+1}/c - y_{c,i-1}/c}{x_{c,i+1}/c - x_{c,i-1}/c} \tag{A.84}$$

It is possible to use a second order approximation and calculate at all points except the first and last point since they are calculated separately according to.

$$\chi_4 = \tan^{-1}\left(\frac{4b/c}{4a/c - 1}\right) \tag{A.85}$$

$$\chi_6 = \tan^{-1}\left(\frac{4b/c}{3 - 4a/c}\right) \tag{A.86}$$

The normalized blade is now created, however, it is described in the Cartesian coordinate system. To direct the blade towards the impeller it has to be rotated. The rotation is accomplished by a simple transformation according to.

$$x'/c = (x/c - 1)\cos\delta_6 + y/c \sin\delta_6 \tag{A.87}$$

$$y'/c = r_6/c - (x/c - 1)\sin\delta_6 + y/c \cos\delta_6 \tag{A.88}$$

$$r_6/c = \frac{s_6/c\, N_N}{2\pi} \tag{A.89}$$

$$r = \sqrt{(x'/c)^2 + (y'/c)^2} \tag{A.90}$$

$$\tan\theta = \frac{x'/c}{y'/c} \tag{A.91}$$

A second blade is constructed using equations (A.90) and (A.91) and adding an angle of $2\pi/N_N$ in equation (A.91). The angle, δ_6, is called the blade setting angle and it is defined in figure A.9. The setting angle is not known beforehand but must be found during the calculation process. This will be done by varying the setting angle until the blade to blade throat is set to give properly guidance upon the rotor blades. To be able

to approximate the proper throat width, I have to determine the flow angle at the trailing edge. I say "approximate" because there are no existing relationship which correlates the flow angle and the throat precisely, but I have chosen to use the simple sine rule. Baines shows that the sine rule does not determine the flow angle very good, especially not at high mach numbers, [12], however, since this program just aims to find a first and preliminary design it is preferable to use such a simple relation. The tangential velocity at the rotor tip is known from the rotor analysis and the ratio of the nozzle exit radius-to rotor inlet radius, r_6/r_7, is taken from the input variables. Using the relationship which states that the angular momentum is conserved it is possible to determine the tangential velocity at the trailing edge of the nozzle blades.
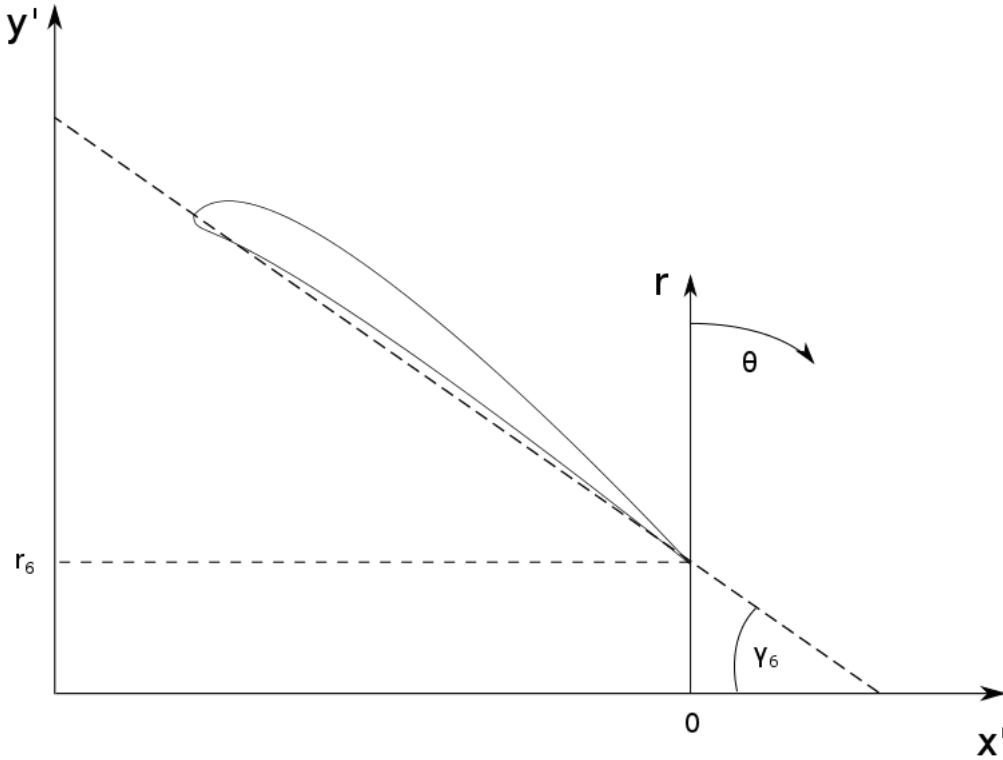

Figure A.9.: The nozzle airfoil setting angle. Adapted from Aungier [2].

$$c_{6\theta} = c_{7\theta}\frac{r_7}{r_6} \tag{A.92}$$

The flow angle can be determined if the meridional velocity is known. To calculate this velocity a mass balance will be performed. The static density at the trailing is, however, not known and it is therefore necessary to apply an iterative calculation procedure. First an initial guess of the static density is made and then the iteration begins and proceeds until the correct static density is found. I have chosen to take the static density as equal to the total density as an initial guess. This will be a relatively good guess and will, in

most cases, minimize the number of iterations to about five to six, yielding a satisfactory small numerical error. I am setting the hub to shroud width at the trailing edge to be equal to the one at the rotor inlet. This simplifies the analysis since it removes one possible input variable to be specified. Constructing the impeller design, I was using a correlation to determine the inlet total pressure of the impeller, equation (A.22), and consequently the total pressure loss as far as to the impeller tip. In this program I am assuming that this pressure loss arises entirely from the nozzle row passage and that the total pressure at the leading edge of the nozzle blades is equal to stage inlet total pressure. I am also assuming that the turbine is adiabatic and consequently the total temperature is constant and equal to the one at the stage inlet as far as to the impeller tip.

$$\text{Initial guess:} \quad \rho_6 = \frac{p_{07}}{T_{06}\,R} \tag{A.93}$$

$$c_{6m} = \frac{\dot{m}}{2\,\pi\,r_6\,b_6\,\rho_6} \tag{A.94}$$

$$c_6 = \sqrt{c_{6m}^2 + c_{6\theta}^2} \tag{A.95}$$

$$T_6 = T_{06} - \frac{c_6^2}{2\,c_p} \tag{A.96}$$

$$p_6 = p_{06}\left(\frac{T_6}{T_{06}}\right)^{\frac{\gamma}{\gamma-1}} \tag{A.97}$$

$$\rho_6 = \frac{p_6}{T_6\,R} \tag{A.98}$$

Now the exit meridional velocity is known and therefore it is possible to calculate the required throat width. I said that I would be using the sine rule and while that is still true, when the mach number exceeds unity I have chosen to use a different approach in which I am using the conservation of mass flow between the throat and exit. This brings the determination of the throat width down to two equations, shown below.

$$\tan \alpha_6 = \frac{c_{6m}}{c_{6\theta}} \tag{A.99}$$

$$M_6 = \frac{c_6}{T_6\,\gamma\,R} \tag{A.100}$$

$$o = s_6 \sin \alpha_6 \qquad M_6 \leq 1 \tag{A.101}$$

$$o = s_6\,\frac{\rho_6\,c_{6m}}{\rho_*\,a_*} \qquad M_6 > 1 \tag{A.102}$$

The density, ρ_*, and velocity, a_*, are the sonic density and speed respectively and they

are given by.

$$T_* = T_{06} \frac{2}{1 + \gamma} \tag{A.103}$$

$$p_* = p_{06} \left(\frac{T_*}{T_{06}} \right)^{\frac{\gamma}{\gamma - 1}} \tag{A.104}$$

$$\rho_* = \frac{p_*}{T_* R} \tag{A.105}$$

$$a_* = \sqrt{T_* R \gamma} \tag{A.106}$$

The equation (A.103) is derived from the following equation when the mach number is set to unity. Equation (A.107) can be found derived in for example [1].

$$\frac{T_0}{T} = 1 + \frac{\gamma - 1}{2} M^2 \tag{A.107}$$

There are some constraints regarding the calculation of the setting angle, δ_6. If the calculated setting angle is found to be below five degrees the analysis will be terminated and a message box shown making the user observant to this fault. Another message box will be shown and the analysis will be terminated if the nozzle inlet to outlet radius ratio exceed the following interval, $1.1 \leq r4/r6 \leq 1.7$. The blade angle distribution can be determined using the following relationships.

$$r \cos \delta = r_6 \cos \delta_6 \tag{A.108}$$

$$\beta = \delta - \chi \tag{A.109}$$

We are now at the point where the blade angle distribution and most of the geometry is designed. The numerical algorithms for the complete design and for the case when only the default values are calculated are the same up until now. The only difference being that when the default values are desirable all of the variable in table A.1 except the number of blades are determined by the algorithm and not by the user which is the case when the design analysis is run. The default values are set according to.

$$\frac{r_6}{r_7} = 1 + \frac{2b_7 \sin \alpha_7}{r_7} \tag{A.110}$$

$$\theta = 0° \tag{A.111}$$

$$a/c = 0.5 \tag{A.112}$$

$$t_4/c = 0.025 \tag{A.113}$$

$$t_6/c = 0.012 \tag{A.114}$$

$$t_{max}/c = 0.06 \tag{A.115}$$

$$d/c = 0.4 \tag{A.116}$$

$$s_6/c = 0.75 \tag{A.117}$$

The number of nozzle blades corresponding to default value is determined using a model in which a simple blade loading velocity is calculated. The interested reader is referred to [2] for the derivation, I will only present the resulting criteria here.

$$\frac{4\, s_6\, \sin(\beta_4 - \alpha_6)}{c\, \sin\beta_4\, \left(1 + \frac{r_6 \sin\alpha_6}{r_4 \sin\alpha_4}\right)} \leq 1 \qquad (A.118)$$

The algorithm will iterate, starting with a number of blades equal to seven, until it finds a number of blades fulfilling the criteria in equation (A.118).

The design analysis proceeds from the determination of the blade angles with the calculation of the flow conditions at the leading edge. The algorithm is designed to give an inlet flow angle corresponding to optimum incedence according to.

$$\text{ideal incidence,}\ i^* = \left(3.6\sqrt{\frac{10t_4}{L}} + \frac{|\beta_6 - \beta_4|}{3.4}\right)\sqrt{\frac{L}{s_6}} - \frac{|\beta_6 - \beta_4|}{2} \qquad (A.119)$$

$$\text{inlet flow angle,}\ \alpha_4 = \beta_4 - i^*\, \text{sign}(\beta_6 - \beta_4) \qquad (A.120)$$

I feel I should mention that before the inlet flow angle is determined all the geometry is unnormalized by a multiplication of all the geometry with the chord length. The length, L in equation (A.119) is determined from a numerical integration given by.

$$L = \int_0^m \frac{dm}{\sin\beta} = \int_0^m \frac{dr}{\sin\beta} \qquad (A.121)$$

$$L_i = L_{i-1} + \frac{r_i - r_{i-1}}{\sin\frac{\beta_i - \beta_{i-1}}{2}} \qquad (A.122)$$

It is possible to approximate dm as dr since the inlet width is taken equal to the outlet width makin $dz = 0$. The inlet area is determined according to.

$$A_4 = 2\,\pi\, r_4\, b4 \qquad (A.123)$$

Neither at the inlet will the static density be known and an iterative procedure like the one performed at the exit will be required. This summarizes the calculation algorithm. The user will be provided with a preliminary maximum velocity difference and corresponding blade loading. These parameters are given by.

$$(\Delta c)_{max} = \frac{4\,\pi\,(r_6 c_{6\theta} - r_4 c_{4\theta})}{c\, N_N} \qquad (A.124)$$

$$\text{Blade loading}: \ \frac{2\,(\Delta c)_{max}}{c_4 + c_6} \qquad (A.125)$$

Results

The user is provided with results showing the geometry, the flow conditions and parameters helping the designer to evaluate the design. An example of how the results may look like is shown in figures A.10 and A.11.

Inlet station	Outlet station	Key parameters
Total pressure, p04: 3.85 bar	Total pressure, p06: 3.74 bar	Fractional polar angle overlap, ROL: 65.41
Static pressure, p4: 3.71 bar	Static pressure, p6: 3.10 bar	DeltaCmax: 218.39 m/s
Total temperature, T04: 776.00 °K	Total temperature, T06: 776.00 °K	Preliminar blade loading: 1.06
Static temperature, T4: 768.02 °K	Static temperature, T6: 735.57 °K	Chosen vaneless space radius ratio, r6/r7: 1.10
Total enthalpy, h04: 776.00 kj/kg	Total enthalpy, h06: 776.00 kj/kg	Recommended minimum vaneless space radius ratio, r6/r7: 1.16
Static enthalpy, h4: 768.02 kj/kg	Static enthalpy, h6: 735.57 kj/kg	Nozzle radius ratio, r4/r6: 1.16
Static density, rho4: 1.69 kg/cbm	Static density, rho6: 1.48 kg/cbm	Throat, o: 5.64mm
Absolute velocity, c4: 126.31 m/s	Absolute velocity, c6: 284.38 m/s	Pitch, s6: 17.61mm
Tangential velocity, c4t: 106.26 m/s	Tangential velocity, c6t: 269.38 m/s	Incidence, i: -0.35°
Meridional velocity, c4m: 68.29 m/s	Meridional velocity, c6m: 91.12 m/s	Deviation, d: -6.16°
Absolute mach number, M4: 0.23	Absolute mach number, M6: 0.52	Flow path length, L: 23.47mm
Flow angle, alpha4: 32.73 °	Flow angle, alpha6: 18.69 °	
Radius, r4: 65.29 mm	Radius, r6: 56.04 mm	
Area, A4: 5192.20 sqmm	Area, A6: 4456.87 sqmm	
Width, b4: 12.66 mm	Width, b6: 12.66 mm	
Blade angle, beta4: 33.08 °	Blade angle, beta6: 12.53 °	

Figure A.10.: The overall results, including flow conditions and key parameters helpful to evaluate the design, from the design analysis of the nozzle blades are presented to the user.
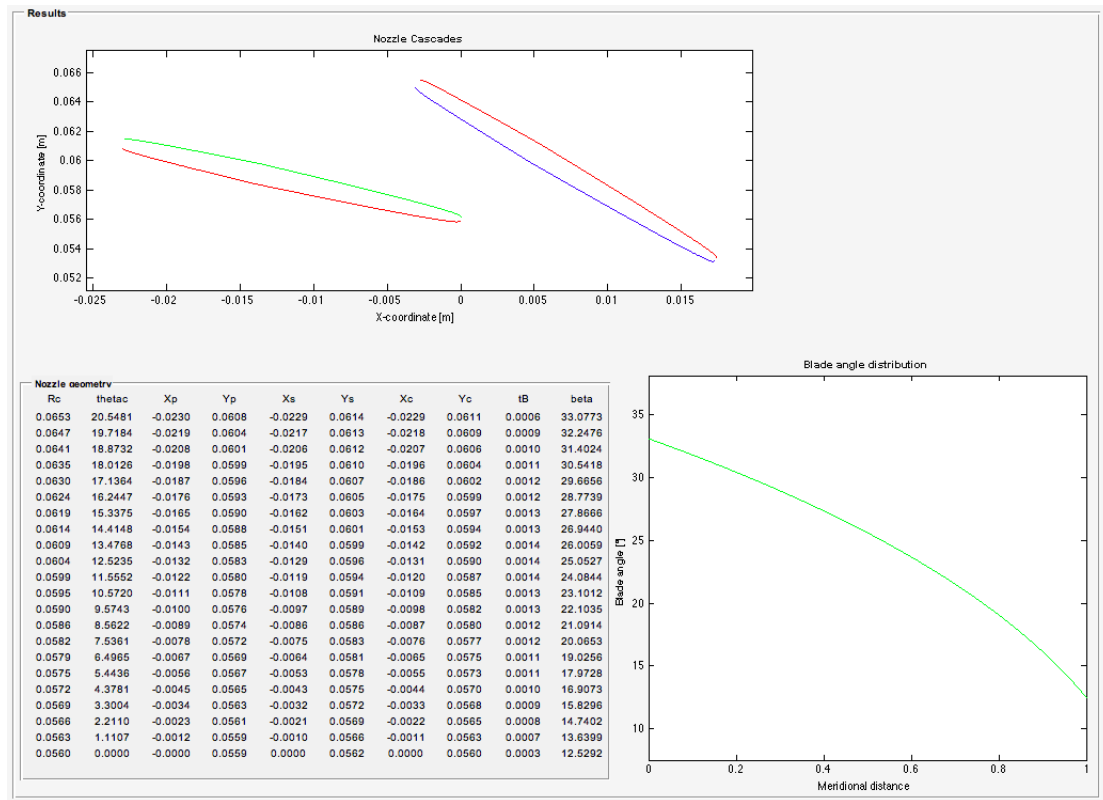
Figure A.11.: **The geometry results, including cascade plots, a plot showing the blade angle distribution and the geometry as raw data, from the design analysis of the nozzle blades are presented to the user.**

Volute

The volute is very easily to design with this program. The only parameters which are available to the designer are summarized and shown in table A.2 and in figure A.12. The user can choose to use an elliptically or rectangular shaped volute, he can also choose to use an external or internal volute, finally he must specify the aspect ratio, A/B.
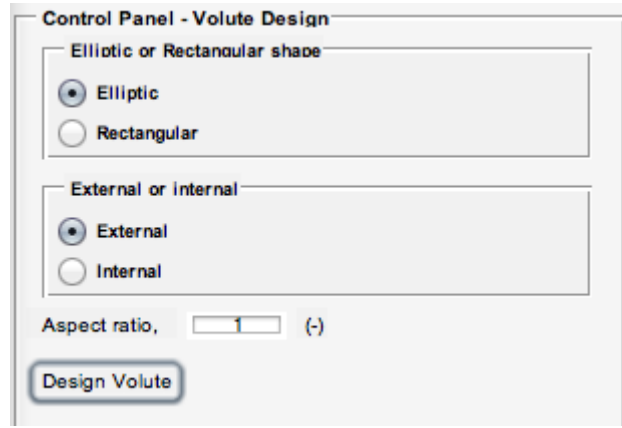
Table A.2.: **The volute is very easy to design for the user. The control panel used to vary the input variables contain three variables. They are presented in this table.**

Elliptic or rectangular shaped volute
External or internal volute
Aspect ratio, A/B

Figure A.12.: The volute is very easy to design for the user. The control panel used to vary the input variables contain three variables. They are presented in this figure
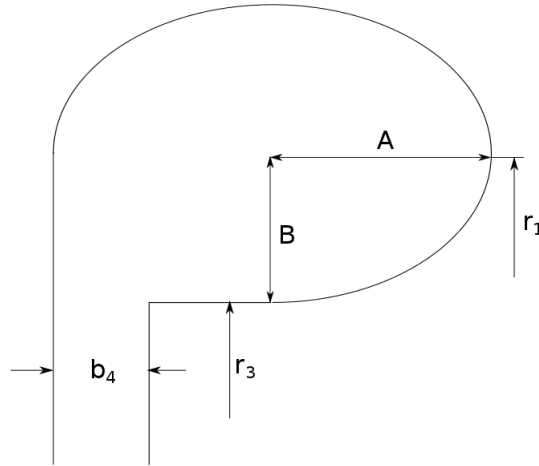

Figure A.13.: The geometry which is used to size the volute in [2]. The figure is inspired by [2]

Depending on whether the user chooses an external or internal volute the calculation algorithm takes different approaches. Both approaches, however, include these initial steps. The vaneless space between the nozzle leading edge and the volute exit is set to fulfill the following requirement.

$$r_3 = 1.05 r_4 \tag{A.126}$$

I am assuming that no pressure losses arise in the volute passage and consequently, $p_{03} = p_{01}$. Angular momentum is conserved in the vaneless passage yielding the tangen-

tial velocity at the volute exit.

$$c_{3\theta} = c_{4\theta} \frac{r_4}{r_3} \tag{A.127}$$

The outlet area is given by.
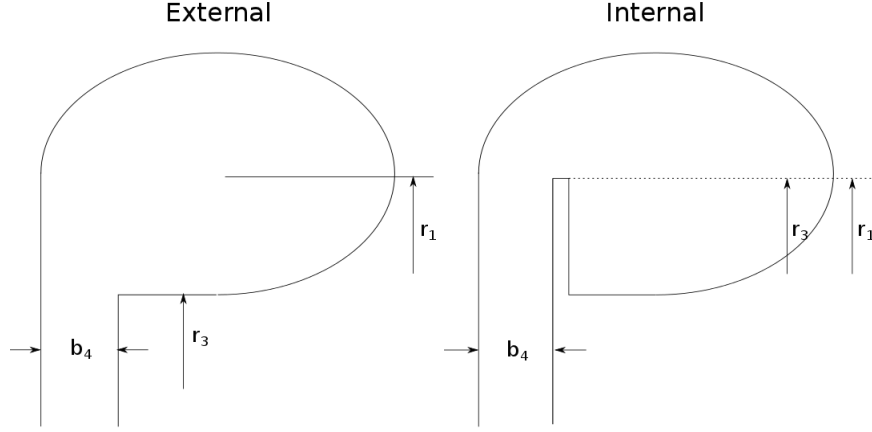
$$A_3 = 2\pi r_3 b_4 \tag{A.128}$$

Figure A.14.: The difference between an external and an internal volute shape. The figure is inspired by [2]

External volute

The algorithm calculating the external volute takes on an iterative approach. It starts with a guess of the inlet radius. It proceeds with the calculation of the inlet velocity, using angular momentum and the fact that inlet velocity is entirely tangential. When the inlet velocity is found the static temperature, pressure and density are determined. Finally the inlet area is calculated, depending on if the shape of the volute is elliptical or rectangular the expression determining the inlet area takes different forms. The area will yield the parameter, B, and then the new inlet radius can be calculated. The iterations stops when the new inlet radius is equal to the initial. The other flow conditions are

then easily determined.

$$\text{Initial guess}: \quad r_1 = r_3 \tag{A.129}$$

$$c_1 = c_{3\theta}\, \frac{r_3}{r_1} \tag{A.130}$$

$$T_1 = T_{01} - \frac{c_1^2}{2\,c_p} \tag{A.131}$$

$$p_1 = p_{01} \left(\frac{T_1}{T_{01}} \right)^{\frac{\gamma}{\gamma-1}} \tag{A.132}$$

$$\rho_1 = \frac{p_1}{T_1\,R} \tag{A.133}$$

$$A_1 = \frac{\dot{m}}{\rho_1\,c_1} \tag{A.134}$$

$$\text{Elliptic}: \quad B = \sqrt{\frac{A_1}{(\frac{3}{4}\,\pi + 1)A/B}} \tag{A.135}$$

$$\text{Rectangular}: \quad B = \sqrt{A_1\,B/A} \tag{A.136}$$

$$r_1 = r_3 + B \tag{A.137}$$

Internal volute

The iterative procedure in the algorithm calculating the external volute is not needed when the designer chooses an internal volute, instead it is possible to apply a direct approach because the inlet radius is equal to the outlet radius. The algorithm follows the same procedure as the one for the external except the expressions calculating the coefficient, B, which is given by.

$$\text{Elliptic}: B = \frac{b_3\,B/A}{2(3/4\,\pi + 1)} + \sqrt{\left(\frac{b_3\,B/A}{2(3/4\,\pi + 1)} \right)^2 + \frac{A_1\,B/A}{3/4\,\pi + 1}} \tag{A.138}$$

$$\text{Rectangular}: B = \frac{b_3}{2\,A/B} + \sqrt{\left(\frac{b_3}{2\,A/B} \right)^2 + \frac{A_1}{A/B}} \tag{A.139}$$

The results are given to the designer as shown in figure A.15.

Inlet station
Static pressure, p1: 3.81 bar
Total pressure, p01: 3.85 bar
Static temperature, T1: 773.97 °K
Total temperature, T01: 776.00 °K
Static enthalpy, h1: 773.97 kJ/kg
Total enthalpy, h01: 776.00 kJ/kg
Static density, rho1: 1.73 kg/cbm
Absolute velocity, c1: 63.71 m/s
Meridional velocity, c1m: 0.00 m/s
Tangential velocity, c1t: 63.71 m/s
Absolute mach number, M1: 0.11
Radius, r1: 108.88 mm
Area, A1: 0.0055 sqm
Coefficient, A: 0.04
Coefficient, B: 0.04

Outlet station
Static pressure, p3: 3.73 bar
Total pressure, p03: 3.85 bar
Static temperature, T3: 768.77 °K
Total temperature, T03: 776.00 °K
Static enthalpy, h3: 768.77 kJ/kg
Total enthalpy, h03: 776.00 kJ/kg
Static density, rho3: 1.70 kg/cbm
Absolute velocity, c3: 120.21 m/s
Meridional velocity, c3m: 64.88 m/s
Tangential velocity, c3t: 101.20 m/s
Absolute mach number, M3: 0.22
Flow angle, alpha3: 32.66 °
Radius, r3: 68.55 mm
Area, A3: 0.0055 sqm

Figure A.15.: The results form the volute design analysis are presented to the user.